

# **Development of 3D inkjet printing heads for high viscosity fluids**

**Petrus Jacobus Malan van Tonder**

**210125063**

**A thesis submitted in fulfilment of the requirements for the Doctoris  
Technologiae: Engineering: Electrical**



**Department: Electronic Engineering  
Faculty of Engineering and Technology  
Vaal University of Technology  
Vanderbijlpark**

**Promoter: Prof HCvZ Pienaar**

**Co-Promoter: Prof DJ de Beer**

**Date: July 2015**

## **Declaration**

I, Malan van Tonder, hereby declare that the following research information is solely my own work. This is submitted in fulfilment of the requirements for the Doctoris Technologiae: Engineering: Electrical to the Department of Electronic Engineering at the Vaal University of Technology, Vanderbijlpark. It has not been submitted before for any assessment to any educational institution.

.....

Malan van Tonder

Date: .....

## **Acknowledgements**

I hereby wish to express my gratitude to the following individuals who enabled this research and document to be completed successfully:

- Prof HCvZ Pienaar for encouragement and guidance throughout this research
- Prof DJ de Beer for encouragement and guidance throughout this research
- Telkom Centre of Excellence, TFMC, M-Tech and THRIP for funding
- Idea 2 Product Lab for printing of components used in this research
- Bertus van As, VUT Technology Station Tool Room for assisting in manufacturing of uniquely designed components used in this research
- Personnel of the Department of Electronic Engineering and Technology Station for support and encouragement

## **Dedication**

This thesis is dedicated to my parents, Pieter and Annalize van Tonder, my sister, Liezl van Tonder, and my beautiful fiancé, Jeané Bresler, for their support and encouragement during the study of this project.

## **Abstract**

Opening up local markets for worldwide competition has led to the fundamental change in the development of new products. In order for the manufacturers to stay globally competitive, they should be able to attain and sustain themselves as ‘World Class Manufacturers’. These ‘World Class Manufacturers’ should be able to:

- Deliver products in fulfilling the total satisfaction of customers.
- Provide high quality products.
- Offer short delivery time.
- Charge reasonable cost.
- Comply with all environmental concern and safety requirements.

When a design is created for a new product there is great uncertainty as to whether the new design will actually do what it is desired for. New designs often have unexpected problems, hence prototypes are part of the designing process. The prototype enables the engineers and designers to explore design alternatives, test theories and confirm performance prior to standing production of new products. Additive Manufacturing (AM) technologies enable the manufacturers to produce prototypes and products which meet the requirements mentioned above. However the disadvantage of AM technologies, is that the printing material which is required is limited to that of the supplier.

When uncommon printing materials must be used to manufacture a prototype or product, the 3D printing process stood out above the rest owing to its printing method. However the printing heads used in current commercially available 3D printers are limited to specific fluid properties, which limits new and unique powder binder combinations. Owing to the problem mentioned, the need arose to develop a more ‘rugged’ printing head (RPH) which will be able to print with different fluid properties. The RPH could then be used to print using unique and new powder-binder combinations.

The RPH was designed and constructed using the solenoid inkjet technology as reference. In order to determine the effect which the fluid properties have on the droplet formation, fourteen different glycerol-water test solutions were prepared. The fluid properties were different for each of the glycerol-water solutions. The fluid properties included the viscosity, density and surface tension of the solution. The control parameters of the RPH were theoretically calculated for each of the glycerol-water solutions and nozzle orifice diameter sizes. The control parameters of the RPH included the critical pressure and time. Using an experimental setup, droplets ejected from the RPH could be photographed in order to be analysed. It was determined that the theoretically calculated critical times could not be used in the RPH, as the pulse widths were much lower than the recommended minimum valve pulse width of the solenoid valve used.

The control parameters were then determined practically for each of the different glycerol-water solutions as well as for each nozzle orifice diameter size. The practically determined control parameters were also compared to that of the theoretically determined parameters. A mathematical model was formulated for each of the practically determined critical pressure and time parameters. Non-glycerol-water solutions were also prepared in order to determine whether the control parameters could be calculated using the practically determined mathematical models.

It was found that the practically determined mathematical models, used to calculate the control parameters, could not be used with non-glycerol-water solutions. Using the practically determined mathematical models, the drop formation process of the non-glycerol-water solutions was not optimized and satellite droplets occurred. Although the practically determined models did not work for non-glycerol-water solutions, the methods used to determine the control parameters for the glycerol-water solutions could still be used to determine the practical critical pressure and time for Newtonian solutions.

## Table of Contents

List of Figures .....	xii
List of Tables .....	xv
Glossary of abbreviations and definitions.....	xvi
Chapter 1 Introduction.....	1
1.1. Background .....	1
1.2. Rapid prototyping technologies .....	1
1.3. Justification for the research .....	3
1.4. Problem statement .....	5
1.5. Objective .....	6
1.6. Secondary objectives .....	6
1.7. Research methodology .....	7
1.7.1. Literature review .....	7
1.7.2. Experimentation .....	7
1.7.3. Design parameters.....	8
1.7.4. Construction .....	8
1.8. Contribution of the work .....	8
1.9. Delimitations .....	8
1.10. Overview of thesis .....	9
1.11. Summary.....	10
Chapter 2 Theory .....	11
2.1. Introduction .....	11
2.2. 3D Printing operation .....	11
2.3. Inkjet technology .....	12
2.3.1. Continuous inkjet (CIJ).....	13

2.3.2.	Thermal drop-on-demand (DOD) inkjet .....	14
2.3.3.	Electrostatic DOD inkjet .....	15
2.3.4.	DOD Piezoelectric inkjet .....	15
2.3.5.	Solenoid-based inkjet .....	18
2.4.	Fluid properties .....	19
2.4.1.	Viscosity .....	20
2.4.2.	Surface tension .....	23
2.4.3.	Fluid density .....	26
2.5.	Fluid mechanics .....	27
2.5.1.	Reynolds number .....	27
2.5.2.	Weber number .....	28
2.5.3.	Ohnesorge number .....	30
2.5.4.	Critical Weber number .....	32
2.6.	Control parameters .....	33
2.6.1.	Critical pressure .....	33
2.6.2.	Critical time .....	37
2.7.	Summary .....	38
Chapter 3	The more ‘rugged’ printing head .....	39
3.1.	Introduction .....	39
3.2.	Inkjet technologies .....	39
3.3.	The RPH setup .....	40
3.3.1.	VHS valve .....	42
3.3.2.	Nozzles .....	43
3.3.3.	Spike and hold unit .....	44
3.3.4.	Dual voltage power supply .....	45
3.3.5.	Differential pressure sensor and display .....	46

3.3.6.	Electronic pressure regulator .....	48
3.3.7.	Programmable logic controller .....	49
3.4.	Summary .....	50
Chapter 4	Analytical analysis .....	51
4.1.	Introduction .....	51
4.2.	Fluid solutions .....	51
4.3.	Test solutions.....	52
4.3.1.	Viscosity and density measurement.....	53
4.3.2.	Surface tension measurement.....	56
4.4.	Glycerol solution properties .....	58
4.5.	Theoretical analysis.....	61
4.6.	Summary .....	66
Chapter 5	Experimentation and results.....	67
5.1.	Introduction .....	67
5.2.	Experimental setup .....	67
5.2.1.	Macrophotography rig .....	68
5.2.2.	Camera and nozzle rig.....	70
5.2.3.	Flash delay unit .....	72
5.3.	Practical critical pressures .....	73
5.4.	Valve pulse width.....	83
5.4.1.	Minimum valve pulse width .....	83
5.4.2.	Practical critical time .....	84
5.5.	Summary .....	93
Chapter 6	Validation of results .....	94
6.1.	Introduction .....	94
6.2.	Validation of the critical pressure and time formula.....	94

6.2.1.	Practical critical pressure and time calculations .....	95
6.2.2.	Validation experimental results .....	96
6.3.	Plotting of the solutions.....	99
6.3.1.	XY matrix plotter setup .....	99
6.4.	Summary .....	102
Chapter 7	Conclusions.....	104
7.1.	Introduction .....	104
7.2.	Conclusions .....	104
7.2.1.	Construction of the RPH experimental setup.....	104
7.2.2.	Control parameters .....	104
7.2.3.	Validation of the control parameters.....	106
7.3.	Recommendations .....	106
7.4.	Patent registration.....	107
References	.....	108
Bibliography	.....	114
Annexure A	.....	119
Annexure B	.....	116
Annexure C	.....	120
Annexure D	.....	123
XY matrix plotter construction	.....	123
OpenBeam bars	.....	124
Stepper motors	.....	125
Electronical components	.....	126
Stepper driver	.....	126
Cerebot MX4cK™ board, graphical LCD and joystick	.....	127
Linear guide rails, shafts and bearings	.....	128

ABS parts .....	128
Timing belt pulleys and belts .....	129

## List of Figures

Figure 1. Subtractive and additive manufacturing .....	2
Figure 2. Different types of rapid prototyping technologies.....	2
Figure 3. 3D printer.....	12
Figure 4. Different inkjet technologies .....	13
Figure 5. CIJ technology .....	13
Figure 6. Thermal DOD inkjet.....	14
Figure 7. Single head electrostatic DOD inkjet .....	15
Figure 8. Bend mode PIT.....	16
Figure 9. Push mode PIT .....	17
Figure 10. Shear mode PIT .....	17
Figure 11. Wall displacement in the PIT operating in the shear mode.....	18
Figure 12. Solenoid-based inkjet system .....	19
Figure 13. Cross-sectional solenoid.....	19
Figure 14. Viscosity .....	20
Figure 15. Viscosity vs. temperature .....	22
Figure 16. Shear stress vs. Shear rate of non-Newtonian fluids .....	23
Figure 17. Viscosity vs. Shear rate of non-Newtonian fluids .....	23
Figure 18. Cohesive forces between the fluid molecules.....	24
Figure 19. Adhesion and cohesion forces .....	24
Figure 20. Wetting angles .....	25
Figure 21. Surface tension vs. temperature.....	25
Figure 22. Density vs. temperature and pressure .....	26
Figure 23. Difference between laminar and turbulent flow .....	28
Figure 24. Weber number vs. splashing.....	29
Figure 25. Rayleigh breakup.....	29
Figure 26. Drop on demand drop formation .....	30
Figure 27. Atomization regime .....	30
Figure 28. Effect which the Ohnesorge number has on the drop formation.....	31
Figure 29. Energetic estimation model .....	33

Figure 30. Block diagram of the RPH .....	41
Figure 31. The RPH experimental setup.....	42
Figure 32. The Lee Corporation's VHS valve .....	43
Figure 33. The Lee Corporation's micro-dispense nozzle design .....	44
Figure 34. Spike and hold unit wave forms .....	45
Figure 35. The Lee Corporation's spike and hold unit .....	45
Figure 36. Dual power supply.....	46
Figure 37. Dual power supply circuit.....	46
Figure 38. MPX5700DP pressure sensor .....	47
Figure 39. MPX5700DP pressure measuring circuit diagram .....	48
Figure 40. The MPX5700DP pressure display unit .....	48
Figure 41. Festo's electronic pressure regulator.....	49
Figure 42. PC visual interface.....	50
Figure 43. Hydroxyl group .....	52
Figure 44. Water 2D and 3D structural formula .....	53
Figure 45. Glycerol 2D and 3D structural formula.....	53
Figure 46. Anton Paar SVM 3000 viscometer.....	54
Figure 47. Stabinger measuring principle .....	54
Figure 48. Oscillating U tube method.....	55
Figure 49. Optical contact angle instrument .....	57
Figure 50. Live view of drop .....	57
Figure 51. % v/v glycerol vs. viscosity and density .....	59
Figure 52. % v/v glycerol vs. surface tension .....	60
Figure 53. Ohnesorge number vs p critical .....	64
Figure 54. Ohnesorge number vs. t critical.....	65
Figure 55. Experimental setup .....	67
Figure 56. The object-telephoto lens combination technique .....	69
Figure 57. Reproduction ratio .....	69
Figure 58. Macrophotography rig .....	70
Figure 59. Camera and nozzle rig .....	71
Figure 60. Delay unit PCB.....	72
Figure 61. Flash trigger circuit.....	73

Figure 62. 70% v/v glycerol pressure sweep with the 0.254 mm nozzle.....	75
Figure 63. Practical fluid pressures for 0.254 mm nozzle .....	77
Figure 64. Practical fluid pressures for 0.191 mm nozzle .....	78
Figure 65. Practical fluid pressures for the 0.127 mm nozzle .....	79
Figure 66. Ohnesorge number vs. practical critical pressure .....	82
Figure 67. VHS minimum pulse width .....	84
Figure 68. 35% v/v glycerol time sweep using a 0.191 mm nozzle .....	86
Figure 69. Practical critical pulse widths for the 0.127 mm nozzle.....	87
Figure 70. Practical critical pulse widths for the 0.191 mm nozzle.....	88
Figure 71. Practical critical pulse widths for the 0.254 mm nozzle.....	89
Figure 72. Ohnesorge number vs. valve pulse time.....	93
Figure 73. 65% glycerol-water solution.....	97
Figure 74. Z corp solution.....	98
Figure 75. VX 500 solution .....	98
Figure 76. VX1000 solution .....	98
Figure 77. 40% glycerol - ethanol solution.....	98
Figure 78. 50% glycerol - ethanol solution.....	98
Figure 79. 65% glycerol-ethanol solution 2D plotting results .....	99
Figure 80. Z corp 2D plotting results .....	100
Figure 81. VX 500 2D plotting results.....	101
Figure 82. VX 1000 2D plotting results.....	101
Figure 83. 40% glycerol-ethanol solution 2D plotting results .....	101
Figure 84. 50% glycerol-ethanol solution 2D plotting results .....	102
Figure 85. Isometric view of XY table .....	123
Figure 86. The XY table with the RPH system.....	124
Figure 87. OpenBeam bars.....	124
Figure 88. Hybrid stepper motor.....	126
Figure 89. DRV8825 stepper driver.....	126
Figure 90. Electronical components for XY plotter.....	127
Figure 91. Linear guide rail .....	128
Figure 92. ABS printed parts .....	129

## List of Tables

Table 1. Materials for the additive manufacturing technologies .....	4
Table 2. Effects of the Reynolds number on the flow condition. ....	28
Table 3. Different Weber number regimes .....	29
Table 4. Experimental results of Reis, Ainsely and Derby (2005) .....	32
Table 5. Comparison between the different inkjet technologies.....	39
Table 6. Fluid properties of glycerol-water solutions .....	59
Table 7. Theoretical control parameters .....	62
Table 8. 70% v/v glycerol dispensed volumes.....	76
Table 9. Practical critical fluid pressure.....	80
Table 10. Droplet diameters.....	86
Table 11. Pulse widths .....	90
Table 12. Different validation fluid solutions with their fluid properties.....	94
Table 13. Critical pressure and time for each of the validation fluid solutions using a 0.127 mm nozzle .....	95
Table 14. Critical pressure and time for each of the validation fluid solutions using a 0.191 mm nozzle .....	96
Table 15. Critical pressure and time for each of the validation fluid solutions using a 0.254 mm nozzle .....	96

# Glossary of abbreviations and definitions

## A

AM – Additive Manufacturing  
AC – Alternating Current

## C

CIJ – Continuous Inkjet  
CAD – Computer Aided Design  
CFC – Continuous Function Chart

## D

DOD – Drop on Demand  
DLP – Digital Light Processing  
DMLS – Direct Metal Laser Sintering  
°C – Degrees Celsius  
 $\eta$  – Dynamic Viscosity  
 $d$  – Diameter  
 $D_{\text{channel}}$  – Diameter of channel  
 $D_{\text{nozzle}}$  – Diameter of Nozzle  
DSLR – Digital Single-Lens Reflex

## E

EBM – Electron Beam Melting  
 $E_{\text{friction}}$  – Geometrical Pressure Loss  
 $E_{\text{kinematic}}$  – Kinetic Energy required for free-flying droplet  
 $E_{\text{surface}}$  – Energy required for free-flying droplet  
EPDM – Ethylene Propylene Diene Monomer

## F

FDM - Fused Deposition Modeling  
FC – Fuel Cell  
 $\rho$  – Fluid Density

## H

Hz – Hertz  
h – Height

## I

I2P – Idea 2 Product Lab

## K

$\text{Kg/m}^3$  – Kilogram per cubic meter

## L

LOM – Laminated Object Manufacturing

LENS – Laser Engineering Net Shaping  
LCD – Liquid Crystal Display

## M

m – Meter  
 $m$  – Mass  
mm – Millimeter  
 $\mu\text{m}$  – Micrometer  
MIT – Massachusetts Institute of Technology  
MJM – Multi-Jet Modelling  
mPa.s – Millipascal-Second  
 $\text{MW/m}^2$  – Megawatt per meter squared  
 $\mu\text{s}$  – Microseconds  
ms – Milliseconds  
ml – Milliliter  
min – Minute

## N

ns – Nanosecond

## O

Oh – Ohnesorge number  
OEM – Original Equipment Manufacturer  
OH – Hydroxyl Group  
OCA – Optical Contact Angle measurement

## P

$P_{\text{critical}}$  – Critical Pressure  
P – Pressure  
Pa – Pascal  
kPa – Kilo Pascal  
PIT – Piezoelectric Inkjet Technology  
PLC – Programmable Logic Controller  
PC – Personal Computer  
PPS – PolyPhenylene Sulphite  
PEEK – Polyether ether ketone  
 $\Delta p$  – Difference in Pressure  
PIC - Programmable Interface Controller

## Q

$Q_{\text{critical}}$  – Critical volume flow

## **R**

Re – Reynolds number

RP – Rapid Prototyping

RPH – More ‘rugged’ Printing Head

## **S**

SLA – Stereo Lithography Apparatus

SLS – Selected Laser Sintering

SLM – Selected Laser Melting

SHS – Selective Heat Sintering

SGC – Solid Ground Curing

SM – Subtractive Manufacturing

$\tau$  – Shear stress

$\sigma$  – Surface tension

## **T**

$t_{\text{critical}}$  – critical time

3D – Three Dimensional

3DP – Three Dimensional Printing

$\Theta$  – Theta

$l$  – Length

2D – Two Dimensional

## **U**

UV – Ultraviolet

UAM – Ultrasonic Consolation

## **V**

V – Voltage

v – Volume

$v_{\text{velocity}}$  – Velocity

$v_{\text{channel}}$  – Velocity through channel

$v_{\text{drop}}$  – Velocity of Droplet

$V_{\text{drop}}$  – Drop volume

VHS valve – Very High Speed Valve

$V_s$  – Supply voltage to sensor

$V_{\text{out}}$  – Output Voltage

$v/v$  – volume over volume ratio

VUT – Vaal University of Technology

## **W**

$We$  – Weber number

$We_{\text{critical}}$  – Critical Weber number

$W_{\text{pressure}}$  – Mechanical Work generated

# **Chapter 1 Introduction**

## **1.1. Background**

Opening up local markets for worldwide competition has led to the fundamental change in the development of new products. In order for the manufacturers to stay globally competitive, they should be able to attain and sustain themselves as ‘World Class Manufacturers’ (Liou, 2008:1-3). According to Liou (2008) these ‘World Class Manufacturers’ should be able to:

- Deliver products in fulfilling the total satisfaction of customers.
- Provide high quality products.
- Offer short delivery time.
- Charge reasonable cost.
- Comply with all environmental concern and safety requirements.

When a design is done for a new product there is great uncertainty as to whether the new design will actually do what it is desired for. New designs often have unexpected problems, hence prototypes are part of the designing process. The prototype enables the engineers and designers to explore design alternatives, test theories and confirm performance prior to standing production of new products. Rapid Prototyping (RP) technologies enable the manufacturers to produce prototypes and products which meet the requirements mentioned above (Liou, 2008:3-6).

## **1.2. Rapid prototyping technologies**

RP technologies use various engineering, computer control and software techniques to directly produce a physical model (prototype or product) in accordance with the geometrical data delivered from the 3-Dimensional (3D) computer drawing also known as the Computer Aided Design (CAD) model. RP technologies can be divided into two groups, namely the manufacturing process that ‘adds’ (additive manufacturing) or ‘removes’ (subtractive manufacturing) material layer-by-layer to

create the desired 3D object (Liou, 2008:9-12). The difference between the two manufacturing processes is demonstrated in Figure 1.

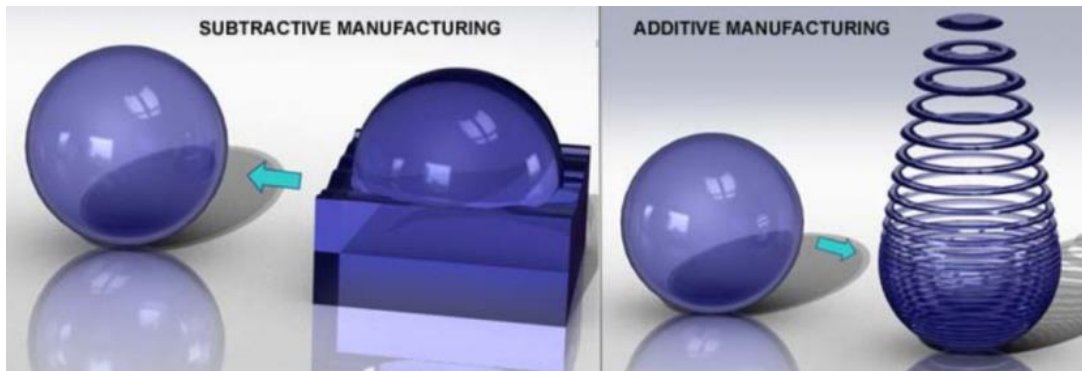


Figure 1. Subtractive and additive manufacturing (Rapid Manufacturing Association, 2011)

There are a number of AM technologies available and, according to Kruth (1991), can be divided into three different groups. These groups will depend on the state of prototyping material used before part formation. The different RP technologies are outlined in Figure 2.

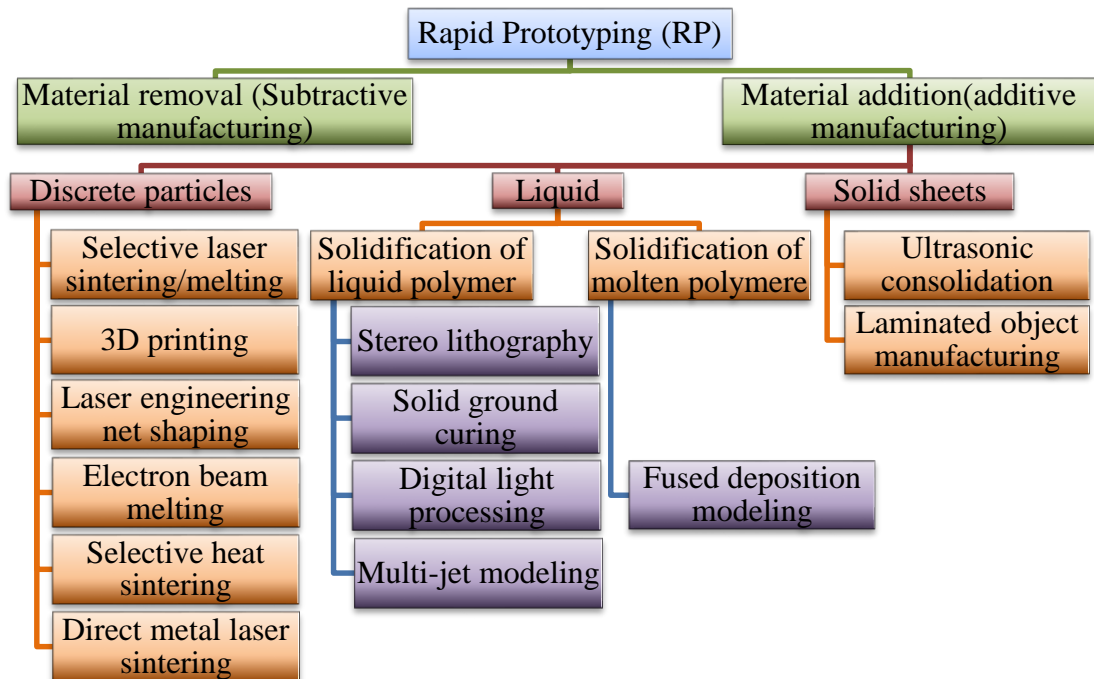


Figure 2. Different types of rapid prototyping technologies

A number of new AM technologies have been added to Kruth's (1991) original RP flow chart, as new and improved additive manufacturing technologies are constantly introduced into the market.

Liquid-based technologies entail the solidification of resin on contact with light, in the form of a laser beam or UV light, and the subsequent solidification of the molten prototype material. Processes that use powder-based (discrete particles) technologies' layers can be fused together using laser or binding agents (Kumar and Pityana, 2010). Lastly, processes which use solid sheets can be classified as sheets bonded together using laser, adhesive or ultrasonic welding (Pham and Gault, 1998).

**Please note that** in this research subtractive manufacturing will not be addressed, as it is a technique used for the removal of material and is a field on its own.

### **1.3. Justification for the research: The imperatives**

The disadvantage of AM technologies, is that the printing material which is required is limited to that of the supplier. For instance, when a prototype or product must be manufactured from graphite or bone-like materials, the supplier might not be able to supply the user with that specific material. An advantage of printing with graphite can be the manufacturing of bipolar plates for fuel cells (FCs), whereas bone can be used to manufacture medical implants. The different types of base materials available for the AM technologies discussed are shown in Table 1.

When materials, not mentioned above, must be used to print a prototype or product, the 3D printing process is different, owing to the following reasons:

- It does not melt the layers into each other but it uses binder to 'glue' the layers to each other (Chua, Leong and Lim, 2003:197). Some materials have a very high melting point or do not melt at all. For instance, graphite has a melting point of 3827 °C at a pressure of 11 Mpa (Ronchi, Beukers, Heinz, Hieraut and Selfslang, 1992).

- It uses powder and a fluid binder as its printing material. The desired material can be milled into a powder form and a suitable fluid binder can then be used to ‘glue’ the powder layers together (for example bone or graphite powder).

**Table 1. Materials for the additive manufacturing technologies (Cotteleer, Holdowsky and Mahto, 2014)**

<b>RP technology</b>	<b>Available material</b>
Stereolithography (SLA)	Liquid photopolymer, composites
Digital light processing (DLP)	Liquid photopolymers
Multi-jet modelling (MJM)	Liquid photopolymers, wax
Fused deposition modelling (FDM)	Thermoplastics
Electron beam melting (EBM)	Titanium powder, cobalt chrome powder
Selective laser sintering / melting (SLS / SLM)	Paper, plastic, metal, glass, ceramic or composite powders
Selective heat sintering (SHS)	Thermoplastic powders
Direct metal laser sintering (DMLS)	Stainless steel, cobalt chrome or nickel alloy powders
3D printing (3DP)	Ceramic, acrylic, sand, plaster or composite powders
Laminated object manufacturing (LOM)	Paper, plastic, metal, ceramics or composite laminates
Ultrasonic consolidation (UAM)	Metal and metal alloy laminates
Laser engineering net shaping (LENS)	Metal and metal alloy powders

However the main drawbacks of the 3D printing processes currently available are:

- The 3D printers have large bed sizes requiring large amounts of powder to print a small part (Chua *et al.*, 2003:194). It spreads the entire printing platform with powder even though a small area is used to print the part. This can be problematic when working with expensive and small amounts of powders.

- The fluid binder used in the 3D printers must have a low viscosity because of the inkjet technology used. For instance the Z310 printer uses HP print head technology, which uses an ink viscosity in the region of 2 mPa-s (Wei, 2007:278). To match this ink viscosity, the 3D printer manufacturers will mix various chemicals with water to match the originally used ink viscosity (Butt and Kappl, 2010:164). The real binder in the 3D printing process is in the powder and not the fluid binder. The water mixture is used to activate the binder in the powder to cause hardening (Diegel, 2012). This can be problematic when working with expensive powders and powders not supplied by the manufacturers (uncommon powders). When the binder is mixed with the powder it becomes almost impossible to extract that binder component from the original powder, if it must be used for other applications. A possible solution to this problem is if the binder is the fluid and not the powder. This is not possible with current inkjet technology used. When a glue-like fluid is used for the binder, it will increase the viscosity and will clog the printing head.
- It was observed that the lifetime of inkjet cartridges, used in the Z printer 310 3D printer, was relatively short. This increases the printing cost owing to the fact that the inkjet cartridge must be replaced quite often.

If the drawbacks discussed above are resolved, then the 3D printer can be used to print prototypes or products with uncommon materials, for example graphite can be used to print bipolar plates for FCs. The advantage of such a 3D printed bipolar plate is that fluid channels can be printed within the plate, which is not possible with the current manufacturing technology available.

#### **1.4. Problem statement**

Printing with current commercially available 3D printers is limited to the specific printing materials supplied by the original equipment manufacturer (OEM). Thus, if a prototype is printed with a commercial 3D printer it can only be printed with the material supplied by the OEM, and not with the desired engineering material.

## **1.5. Objective**

Binder components can be mixed with uncommon printing powders in order to form a powder that can be used in current 3D printers (the fluid printed by the inkjet technology is used to activate the binder within the powder). The problem with this is that it will be nearly impossible to extract the binder component from the original powder. This is a problem when working with expensive materials. A possible solution to the problem could be if the binder component is in the fluid printed by the printing head, and not in the printing powder. With the current inkjet technology used in 3D printers it is not possible to print high viscosity fluids as it is limited to that of the print head manufacturer. When printing with binders that are ‘glue-like’, their fluid properties will differ from that of the fluid properties used in the inkjet technology and will destroy/clog the print head. Glue-like fluid will have a higher viscosity compared to the original binder used. The objective of this research is to develop a more ‘rugged’ printing head (RPH) which will be able to print with different fluid properties, which include high viscosity fluids.

## **1.6. Secondary objectives**

In order to achieve the objective of this research, the following aspects must also be addressed:

- Prepare fluid solutions with different fluid properties in order to determine the effect which the fluid properties have on the drop formation process. The different fluid properties will include the viscosity, density and surface tension.
- Determine which aspects of the RPH need to be controlled in order to obtain an adequate drop formation process when using different fluids.
- Design and construct a mechanical structure to test the RPH. This mechanical structure will enable the printing head to move in the X-Y direction using pre-determined coordinates. The print head will then be used to deposit droplets onto a platform, in matrix format, to determine whether an adequate drop formation process takes place.

- Design and construct the necessary control circuitry and components for the proper control of the RPH. The RPH will then be used in 3D printing applications at a later stage.

## **1.7. Research methodology**

The research project will be addressed in the following manner:

### **1.7.1. Literature review**

Firstly, a literature study will be conducted on all of the different types of additive manufacturing technologies, which includes the materials available for each technology. An in-depth study will then be conducted on the theory and operation of the 3D printing technology. This study will include:

- the different inkjet technologies, which could be used with 3D printing,
- the different fluid properties, which have to be kept in mind when designing inkjet systems and
- the theoretical design of an inkjet system, which includes the different control parameters and calculations.

Although all these aspects will be researched, the main focus area will be the development and construction of a RPH which will be able to print with different fluid properties.

### **1.7.2. Experimentation**

The theoretically determined control parameters would be tested on the RPH. The control parameters would also be determined using a practical approach, which could then be compared against the theoretically determined control parameters. The experimental setup used to determine the practical control parameters would also be developed and constructed for the RPH.

### **1.7.3. Design parameters**

All the theoretical and practically determined data, using the experimental setup, would be taken into account for the design, and development of the RPH. Although the printing head is the main focus, some of the components would have to be developed in order to test and control the RPH.

### **1.7.4. Construction**

The project will involve a theoretical and practical design for the development of a RPH and a XY table. The XY table will be designed in such a manner that it can accommodate the RPH and that it can be converted into a 3D printer on a later stage. A 2D matrix could be plotted, using the RPH and XY table, in order to test the RPH using different fluid solutions.

## **1.8. Contribution of the work**

The contribution of this research to the AM technology is a print head that can print binders with various fluid properties for example different viscosity, surface tension, density combinations. The RPH can be used as a platform to develop new binder-powder combinations, as the printable fluid is then not limited to that of the print head manufacturer. The printability of new binder-powder combinations include: printing of bone, printing of graphite plates for FCs, printing of FC membranes, printing of prototypes with plaster, etc. The developed RPH could be used in a 3D printer. Owing to the innovative nature of the project, as well as the multi-, inter- and transdisciplinary approach, it is envisaged that the project will yield more than one patent.

## **1.9. Delimitations**

This research did not include the non-Newtonian fluids, owing to the fact that the shear rate (pressure) has an effect on fluid's properties.

## **1.10. Overview of thesis**

Chapter 2 - In this chapter the initial literature review that was done to determine the different aspects that have to be kept in mind to develop the RPH, was outlined. This study involved the different inkjet technologies, fluid properties, fluid mechanics and print head control parameters.

Chapter 3 - This chapter focused on the practical design and construction of the RPH. The main components of the RPH were also discussed. The main components included the VHS valve, nozzles, spike and hold unit, dual voltage power supply, differential pressure sensor, electronic pressure regulator and PLC.

Chapter 4 - In this chapter different glycerol-water test solutions were prepared in order to determine the effects which the fluid properties have on the drop formation process. An analytic analysis was done on all of the different solutions to determine the theoretical control parameters. These parameters included the critical time and pressure.

Chapter 5 - This chapter focused on whether the theoretical parameters can be used with the RPH. The control parameters were also determined practically using the RPH experimental setup. The practically determined control parameters included the critical time and pressure. The mathematical equations, for the practical control parameters results, were also determined.

Chapter 6 – In this chapter the formulated mathematical equations for the practically determined control parameters were validated using different fluid solutions. Various solutions were also plotted, in a 2D matrix, to determine whether the determined formulas, critical time and pressure, could be used to determine the RPH's control parameters.

Chapter 7 - Contains conclusions obtained from the development of the RPH.

### **1.11. Summary**

In this chapter the background of the need to develop a more ‘rugged’ printing head system, was given. The justification of the study along with the topic of research and research objectives and methodology were also given. In conclusion, an overview of the research was also represented.

Chapter 2 will present a literature review on all of the different aspects that have to be kept in mind to develop the RPH.

## **Chapter 2 Theory**

### **2.1. Introduction**

Printing with current commercially available 3D printers, is limited to the specific printing materials supplied by the original OEM. In order to print with uncommon powder-binder combinations not supplied by the OEM, the inkjet technology used in the 3D printer must have the same fluid properties as the original binder supplied by the manufacturer. If the fluid properties are not the same it will cause the inkjet technology used to malfunction or be destroyed. A possible solution is to develop a RPH which will be able to print with different fluid properties. In order to develop such a RPH there are a number of aspects that has to be considered. In the following chapter the operation of the 3D printer given and an in-depth study will be made of all the necessary aspects that have to be addressed for the development of the RPH.

### **2.2. 3D Printing operation**

The 3DP technology was originally developed by the Massachusetts Institute of Technology (MIT) in 1993, which licensed the technology to several companies for different applications. Z-Corporation commercialized the technology to produce machines for plaster and starch parts, while ProMetal Inc., Soligen Inc. and Therics commercialize the process respectively for metal, investment casting and pharmacology applications (Ramin, 2010:35). The Vaal University of Technology (VUT) uses various 3D printing technologies namely: Zcorp 310 and Projet® 660 Pro printer which uses plaster as a printing material, Voxeljet VX1000 silica sand printer and Voxeljet VX500 Polymethyl methacrylate (PPMA) printer. All of the 3D printing technologies work in the same manner namely: the printer spreads a layer of powder from the powder container onto the printing platform. A print is made on the powder with a fluid binder using inkjet technology, where the printing head is enabled to move in the X-Y direction. The powder is ‘glued’ together where the binder is printed. The remaining powder serves as support for the top layers. When

the printer has finished with a layer the printing platform moves down in the Z direction. Another layer of powder is spread on the printing platform in order to print the next layer. Once the process is complete, the excess powder is vacuumed and parts are lifted from the bed (Chua *et al.*, 2003:197). Figure 3 demonstrates the operation of the 3D printer.

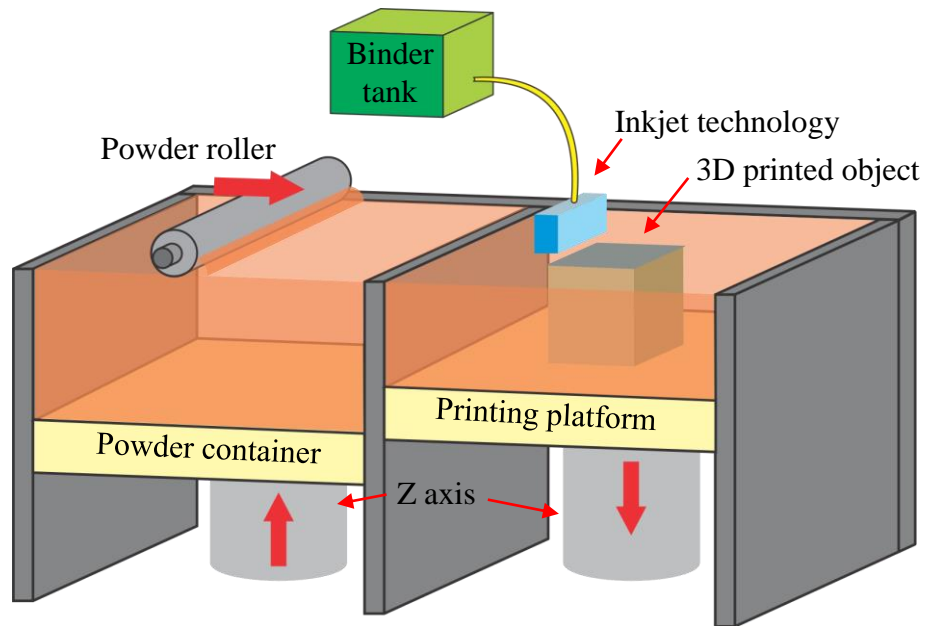


Figure 3. 3D printer

### 2.3. Inkjet technology

There is a wide range of inkjet technologies presently available. However not all of them can be used, or modified, to print with high viscosity fluids. The different inkjet technologies that have been considered for this research are demonstrated in Figure 4. Inkjet technologies can mainly be divided into two groups namely: the continuous mode inkjet technologies and drop-on-demand mode inkjet technologies. The drop-on-demand (DOD) inkjet technology can then be divided into thermal, electrostatic, piezoelectric and solenoid-based technologies. The piezoelectric is subdivided into the shear, push and bend mode (Glynne-jones, Coletti, White, Gabriel and Bramanti, 2010).

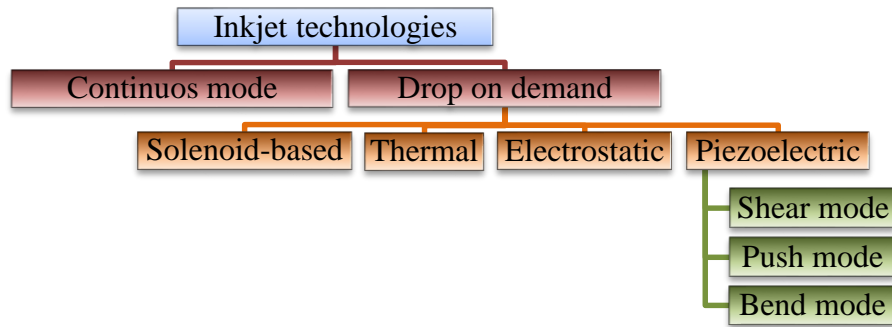


Figure 4. Different inkjet technologies

### 2.3.1. Continuous inkjet (CIJ)

In the CIJ technology, ink is forced through a small orifice, under pressure. The small orifice which forms the nozzle has a typical diameter size of between 50-80  $\mu\text{m}$ . When the ink exits the nozzle it breaks up into uniform drops; this is due to capillary waves induced onto the nozzle. These capillary waves are normally generated by electromechanical devices (Chaudhary, Redekopp and Maxworthy, 1979). The droplets formed are approximately twice the size of the orifice diameter. The ink drops travels through a charging electrode and thus acquires an electric charge. The charged drops are then directed to the catcher or to the desired location on the substrate by means of a second electrostatic field. Only a small fraction of the droplets are used to print, the majority being recycled. The technology is known as a CIJ, because of the continuous stream of ink drops, and is one of the oldest ink jet systems. The ink viscosity range for CIJ is between 2.8 and 6 mPa.s (Pimbley, 1984). The operation of the CIJ is demonstrated in Figure 5.

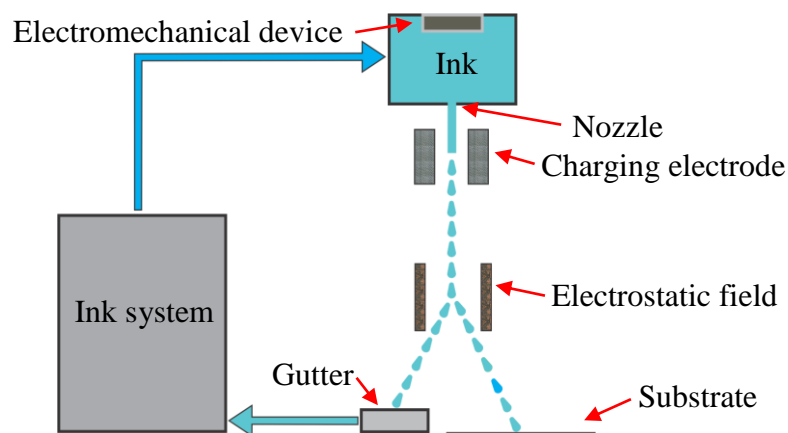


Figure 5. CIJ technology

### 2.3.2. Thermal drop-on-demand (DOD) inkjet

The main components of the thermal DOD inkjet technology are a tiny resistor and a pressure chamber with an outlet. The outlet, comprising of a nozzle, is used to control the droplet characteristics, especially to increase the velocity. When current flows through the resistor it warms up the ink inside the pressure chamber to a temperature of 340°C. Owing to the rapid heating of the ink inside the chamber bubbles start to form; this will increase the pressure inside the chamber and force the ink through the nozzle orifice. Although the ink is warmed it does not boil due to the rapid heating and cooling of the ink. As the resistor cools down the bubble collapses, resulting in a negative pressure inside the pressure chamber and more ink is drawn from the reservoir. The pressure chamber is about 0.1  $\mu\text{m}$  thick. The resistor used to warm the ink has a surface power density of 1200  $\text{MW}/\text{m}^2$ , which is more than the surface of the sun. The resistor is able to warm the ink to 1000000  $^{\circ}\text{C}$  in 1 second. Thus the electrical pulses supplied to the resistor are very short (around 0.1ms), otherwise the resistor will be destroyed. There are no movable parts in this inkjet technology which means it can operate at very high operating frequencies (Nigro and Smouse, 1999). The thermal DOD inkjet technology normally operates with ink viscosities lower than 30 mPa.s. Owing to the heating method used in this technology, unwanted chemical reactions may occur with fluid not specifically designed for this technology (Babiarz, 2006). The working of the thermal DOD inkjet technology is demonstrated in Figure 6.

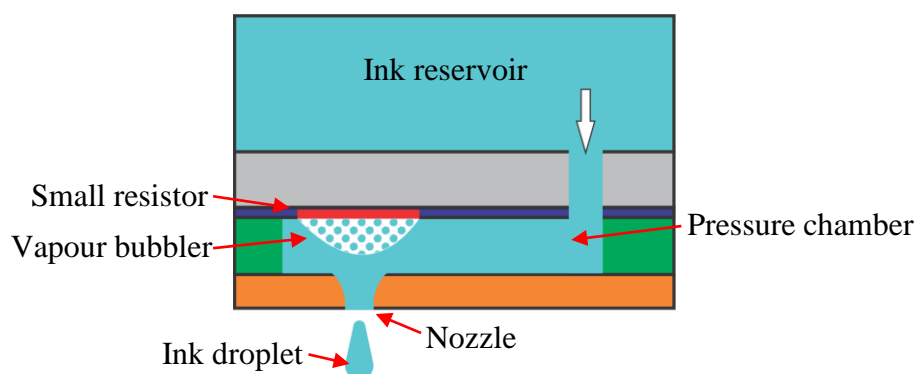


Figure 6. Thermal DOD inkjet

### 2.3.3. Electrostatic DOD inkjet

In electrostatic DOD inkjet technologies, an electrostatic force is used to guide the ink drops onto the printing substrate. The ink used in this technology plays a huge role in the ejection process, because the ink consists of electrically charged conventional pigments in non-conductive fluid. Electrical pulses are then supplied to an electrode inside the print head. An electrical force is then directly applied to the charged ink particles, by means of the electrode. The electrostatic field between the charged ink particle and the -ve electrode will cause the ink to migrate onto the print substrate. The longer the electrical pulse is applied, the more ink is ejected. The electrostatic force can shape the ink drops, as well as create a drop smaller than the ejector diameter. The print head structure is very basic; it consists of walls, flow channels and ejectors. Thus the print head is an open structure (nozzleless). The operation of a single head electrostatic DOD inkjet printer can be seen in Figure 7 (Newcombe, 2009).

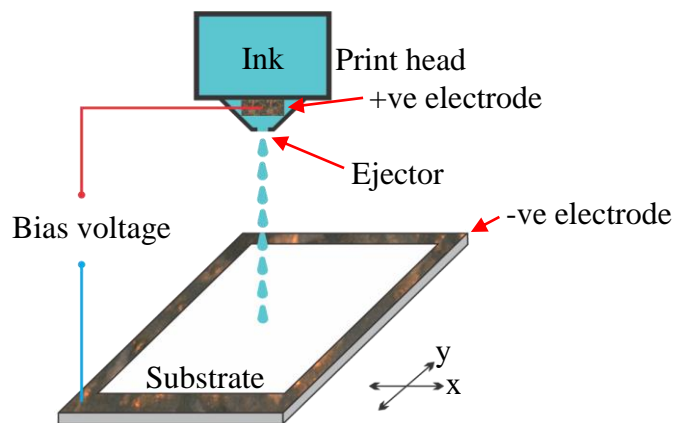


Figure 7. Single head electrostatic DOD inkjet

### 2.3.4. DOD Piezoelectric inkjet

As seen in Figure 4, the Piezoelectric Inkjet Technology (PIT) can be subdivided into three main types namely bend, push and shear mode. The PIT uses piezoelectric components to create a mechanical movement inside the ink reservoir (Caglar, 2009: 15). Usually ink viscosities lower than 30 mPa.s are used in these technologies, however specialised PITs are available for higher viscosity liquids. PITs are more chemical inert compared to thermal inkjet technologies, which is a significant

advantage over thermal inkjet technologies (Babiarz, 2006). The different PIT types will be discussed below:

#### 2.3.4.1. Bend mode

The bend mode PIT consists mainly of a pressure chamber which includes an inlet and an outlet in the form of a nozzle orifice. A conductive diaphragm forms a side of the chamber wall with a deflection plate made of piezoelectric ceramics. When a voltage is applied to the piezoelectric plate it causes it to contract. This causes the diaphragm to flex inwards, into the pressure chamber. The diaphragm motion causes an increase in the pressure inside the chamber which forces the ink through the nozzle orifice. The ink exits the nozzle, which will form a droplet. The droplet size is proportional to the voltage applied to the deflection plate, the pulse duration and diameter size of the nozzle orifice. If a higher voltage is applied to the deflection plate it will cause the diaphragm to flex more compared to that when a smaller voltage is applied. If the deflection plate flexes more the pressure inside the chamber will be more, compared to when the deflection plate flexes less (Kyser and Sears, 1976). The operation of a bend mode PIT is shown in Figure 8.

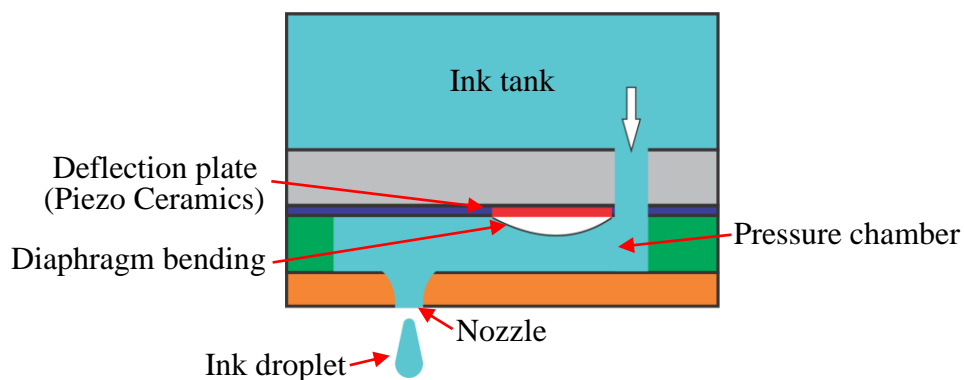


Figure 8. Bend mode PIT

#### 2.3.4.2. Push mode

The push mode PIT operates on the same principle as the bend mode PIT. The Push mode PIT mainly consists of a piezoelectric ceramic rod and a pressure chamber (the same pressure chamber as used in the bend mode PIT). A voltage placed across the piezoelectric ceramic rod will cause it to expand into the pressure chamber, which

will cause an increase in the pressure. An increase in the chamber pressure will force the ink through the nozzle orifice, which will form an ink droplet. A thin diaphragm between the piezoelectric actuator and the fluid is incorporated to prevent the undesirable interaction between the ink and actuator materials (Mikalesen, 1988).

The operation of the push mode PIT is demonstrated Figure 9.

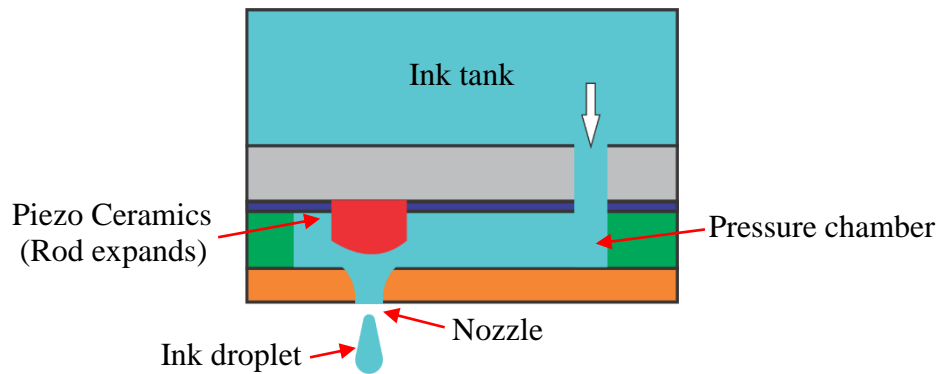


Figure 9. Push mode PIT

#### 2.3.4.3. Shear mode

The shear mode PIT mainly consists of the following components: base plate, inactive cover plate and a nozzle plate. The assembly of the shear mode PIT can be seen in Figure 10.

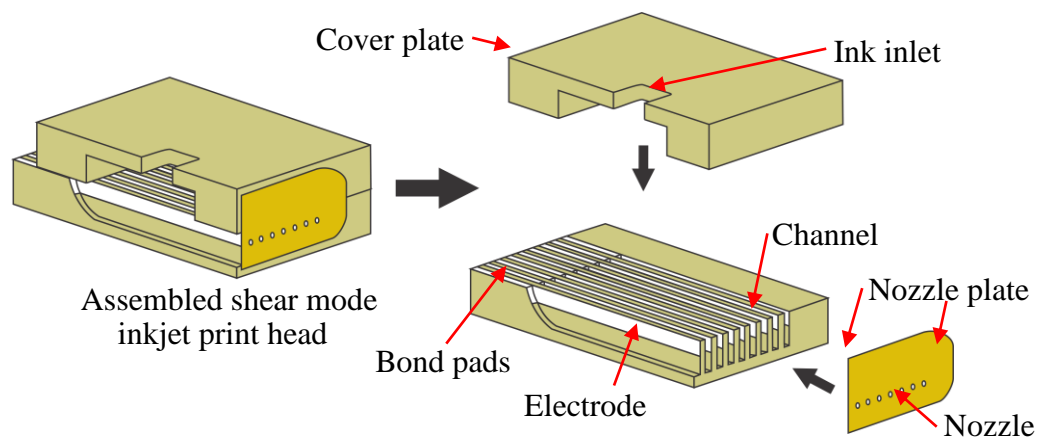
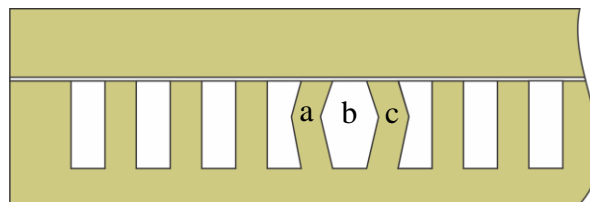


Figure 10. Shear mode PIT

As demonstrated, the base plate consists of multiple ink channels. These channels have a shallow bottom near the bond pad and become deeper in the main part. Metal

electrodes are deposited on both upper halves of the channel walls. Each of the metal electrodes is connected to a wire board area. The cover board is glued onto the base plate, and serves as a roof to the ink channels. The nozzle plate is assembled onto the front surface of the printing head (Beurer and Kretschmer, 1997). When a voltage is applied to the electrodes a field is generated perpendicular to the direction of polarization in the channel walls. This produces the shear mode displacement in the upper half of the channel wall. The lower half of the channels is forced to follow the motion of the upper half, and forms a chevron shape. The displacement of the upper half of the channel wall will cause an increase inside the ink channels and result in the ink passing through the nozzle orifice. Figure 11 demonstrates when the polarity on the channel wall a and c are the same, it causes the walls to bend outwards due to the same fields generated. When opposite polarities are connected onto channel walls a and c the walls will bend inwards and decrease in the channel volume thus increasing the pressure inside the channel which will force the ink through the nozzle orifice (Brunahl, 2003).



**Figure 11. Wall displacement in the PIT operating in the shear mode**

### **2.3.5. Solenoid-based inkjet**

Although solenoid-based inkjet technologies are mostly used in the industry, they are not well known. The solenoid-based inkjet operates in a different manner compared to traditional inkjet technologies discussed previously. There are no physical changes, e.g. piezoelectric material or thermal heating, inside the print head to induce droplet dispensing. A constant pressure is rather used as the driving force for the ink. The operation of the solenoid-based inkjet technology is demonstrated in Figure 12. The ink container is pressurised by means of an air pump, the pressure in the container would be constant. The pressure inside the tank will cause the fluid to be pressurised at the solenoid's inlet. As current passes through the coil inside the

solenoid valve a magnetic field is created. The plunger, that is keeping the orifice closed, will move towards the magnetic field. This will enable the ink to flow through the orifice to the outlet of the valve. Figure 13 shows a cross-sectional view of a solenoid valve.

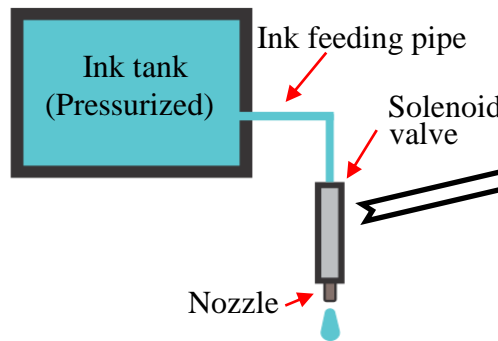


Figure 12. Solenoid-based inkjet system

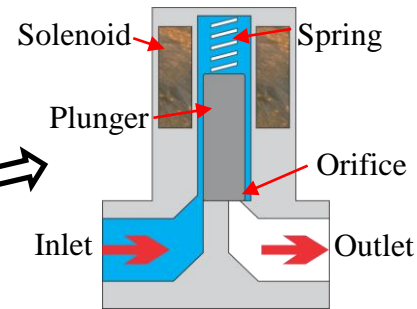


Figure 13. Cross-sectional solenoid

The outlet of the solenoid valve is then connected to a nozzle with a specific orifice diameter size. As the ink exits the nozzle, ink drops are formed. In order to obtain a single ink drop the solenoid valve is supplied with a very short electrical pulse. The main advantage of solenoid-based inkjet technology is the nozzle can easily be changed (Ozaeta, 2008:45-46). Owing to this fact the nozzle will be easy to unclog and it will be easy to experiment with different orifice sizes. No information on the workable ink property ranges could be found due to the lack of documented research.

#### 2.4. Fluid properties

The fluid used in the inkjet technology will determine its design specification, for example, the channel diameters, nozzle orifice diameter size, etc. Using fluid mechanics a fluid's behaviour can be analyzed to choose a nozzle in order to ensure an adequate drop formation. The fluid properties which must be taken into consideration when designing inkjet technologies are the fluid's viscosity, surface tension and density (Lindemann, 2006: 47-48). The different fluid properties are addressed below:

### 2.4.1. Viscosity

Viscosity can be described as the measure of a fluid's resistance to flow. This resistance becomes apparent, between the fluid particles, when the fluid starts to move. The greater the resistance, the more force is required for the fluid movement. This force is known as the shear stress (Yildirim, Solaimanian and Kennedy, 2000: 6). There are mainly two types of viscosities namely: dynamic and kinematic viscosity (Kazys and Rekuviene, 2011). Both of the viscosities are discussed below:

#### 2.4.1.1. Dynamic viscosity

Dynamic viscosity, also known as the absolute viscosity, can be explained by using Figure 14. Fluid is trapped between two horizontal plates, one stationary and the other moving at a constant velocity. The velocity of the different fluid layers will increase linearly from zero, at the stationary plate, towards the moving plate. The friction between the moving layers will result in a force resisting their relevant motion. The top fluid layer will apply an opposite moving force to the moving plate, thus an external force is needed to keep a constant velocity.

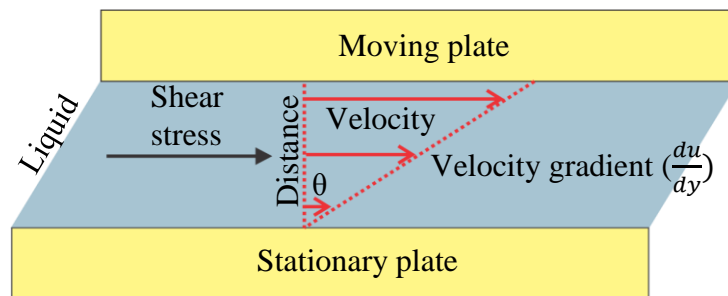


Figure 14. Viscosity

The velocity gradient defines the constant deformation of the fluid under force. A fluid with a higher fluid viscosity (thicker fluid) will cause a decrease in the angular deformation ( $\Theta$ ), whereas a fluid with a low viscosity (thinner fluid) will cause an increase in the angular deformation. Thus a fluid with a low angular deformation would flow easier compared to a fluid with a high angular deformation (Viswanath *et al.*, 2007: 1-2). Using Newton's law of friction, seen in Eq. 1, the dynamic viscosity of a fluid can be calculated (Viswanath, Ghosh, Prasad, Dutt and Rani, 2007: 1-2).

$$\tau = \eta \frac{du}{dy} \quad \text{Eq. 1}$$

Where :

$\tau$   $\equiv$  Shear stress (Pa)

$\eta$   $\equiv$  Dynamic viscosity (Pa.s)

$\frac{du}{dy}$   $\equiv$  Velocity gradient

#### 2.4.1.2. Kinematic viscosity

The kinematic viscosity is known as the ratio between the dynamic viscosity and the density of a fluid (the rate at which momentum is transferred through a fluid). The kinematic viscosity is calculated using the following equation (Kazys and Rekuviene, 2011):

$$\nu = \frac{\eta}{\rho} \quad \text{Eq. 2}$$

Where :

$\nu$   $\equiv$  Kinematic viscosity (cSt)

$\eta$   $\equiv$  Dynamic Viscosity (Pa.s)

$\rho$   $\equiv$  Liquid density (kg / m<sup>3</sup>)

#### 2.4.1.3. Newtonian and Non-Newtonian fluids

Fluids which behave according to Newton's law are called Newtonian fluids, whereas fluids that do not behave according to Newton's law are called non-Newtonian fluids. The two types of fluid are discussed below:

- **Newtonian fluids**

The viscosity of a Newtonian fluid depends on two factors namely: the fluid's composition and temperature. The effect which the temperature has on water, a Newtonian fluid, is shown in Figure 15. As demonstrated in Figure 15, a rise in the temperature of water would decrease its viscosity. Because the temperature has an effect on the viscosity, the temperature at which the viscosity was measured would always be specified (Munson and Young, 1998).

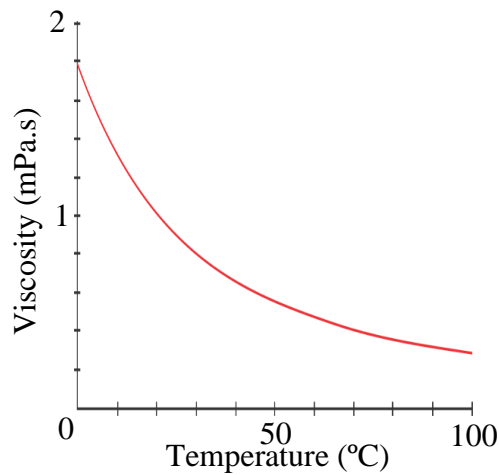


**Figure 15. Viscosity vs. temperature**

- **Non-Newtonian fluids**

For non-Newtonian fluids the plot of shear stress against shear rate will not be linear, as demonstrated in Figure 16. Thus the viscosity of the fluid will not only depend on its composition and temperature but also on the shear stress and rate, which is demonstrated in Figure 17. Not all the non-Newtonian fluids will react in the same manner to a change in the shear stress. The different types of non-Newtonian fluids are:

- Shear thickening fluids: An increase in shear stress will result in an increase of the fluid's viscosity.
- Shear thinning fluids: An increase in shear stress will result in a decrease of the fluid's viscosity.
- Rheopectic fluids: The viscosity of the fluid will decrease over time when agitated.
- Thixotropic fluids: The viscosity of the fluid will increase over time when agitated.

Water-corn starch mixtures are an example of non-Newtonian fluids. When a rapid force is applied to this mixture its viscosity will increase and more resistance will be encountered (Munson and Young, 1998). Non-Newtonian fluids will be excluded in this research, owing to the change in shear rate when the fluid flows through an orifice. The shear rate in the centre of the orifice will be lowered compared to the

wall of the orifice. The shear rate will also change according to the fluid pressure. Thus if a non-Newtonian fluid flows through an orifice its viscosity will vary depending on where in the orifice the measurements is taken (Hall, Berger and Collins, 1995: 64).

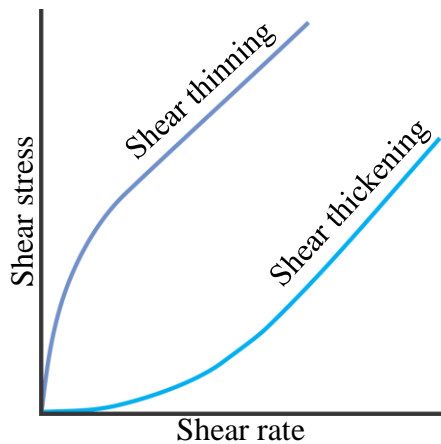


**Figure 16. Shear stress vs. Shear rate of non-Newtonian fluids**

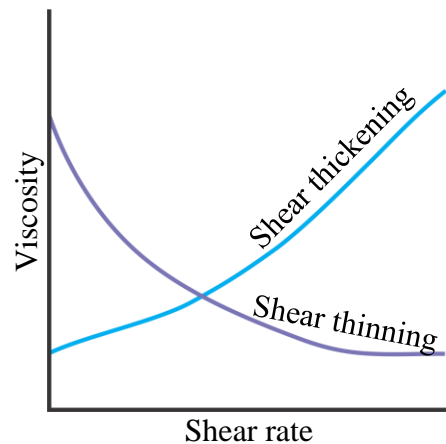


**Figure 17. Viscosity vs. Shear rate of non-Newtonian fluids**

#### 2.4.2. Surface tension

The surface tension phenomenon is caused by cohesive forces between the fluid molecules. The molecules attract each other by means of van der Waals forces or dipole interactions for polar molecules (Vowell, 2009). The molecules inside the fluid mass are surrounded by other molecules, which attract each other equally resulting in a net force of zero. However the molecules at the surface do not have molecules on all sides and are therefore pulled inwards, because of the positive or negative net force acting on to the surface module. The two forces are demonstrated in Figure 18. The inward net force is balanced by the resistance of the fluid to compress. The outer layer of the fluid forms a stretched elastic membrane. The fluid will always try to minimize the surface area, thus forming a shear. The intensity of the molecular attraction per unit length along any line in the surface is called surface tension and is defined by the Greek letter sigma ( $\sigma$ ), which is measured in N/m. Molecule A will experience zero net force due to the surrounding molecules, molecule B and C will experience a inward force and will form a shear shaped elastic membrane that will compress the fluid (Munson and Young, 1998: 26). The inward

force will cause an increase in pressure inside a drop of fluid. Thus, an increase in the fluid surface tension will result in an increase in the pressure inside a droplet. When fluid is exposed to objects a second force is experienced namely the adhesion force.

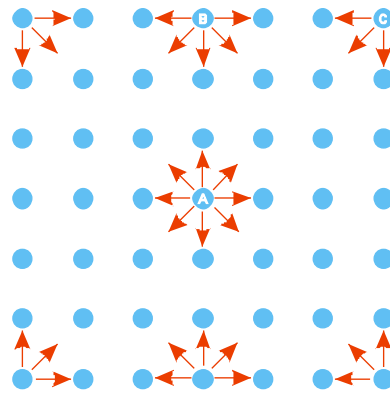


**Figure 18. Cohesive forces between the fluid molecules**

#### 2.4.2.1. Adhesion forces

Adhesion forces can be defined as the forces experienced by unlike molecules. This phenomenon can be explained by the meniscus effect, for example water inside a glass cylinder (smaller than 5 mm). The adhesion forces, between the water and the glass, overpower the cohesive forces and the water molecules will be pulled up the wall as demonstrated in Figure 19.

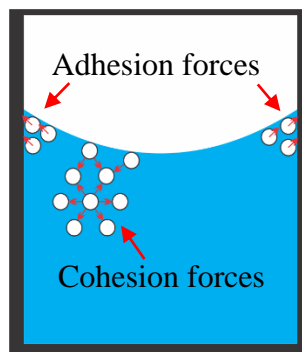


**Figure 19. Adhesion and cohesion forces**

However the height to which the molecules will be lifted depends on the diameter of the glass cylinder and the strength of the adhesion forces. A decrease in the cylinder

diameter would increase the ratio between the adhesion and cohesion forces which would result in an increase in the height to which the molecules would be lifted (Munson and Young, 1998: 27-28). When a droplet rests on a dry solid surface, a contact angle can be observed due to the cohesive force of the fluid and adhesion force between the fluid and the solid surface. Different contact angles are demonstrated in Figure 20.

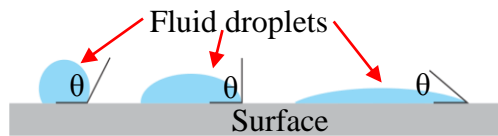


**Figure 20. Wetting angles**

For a contact angle less than  $90^\circ$  the fluid is classified as wetting. This means the fluid molecules will spread across the solid surface. However when the contact angle is greater than  $90^\circ$  the fluid is classified as non-wetting. When a fluid is wetting a surface the adhesive forces are greater than the cohesive forces (Agrawal, 2001: 26).

#### **2.4.2.2. Surface tension influencing factors**

There are two factors that will influence the surface tension of a fluid, namely the temperature and the fluid composition. An increase in a fluid's temperature will cause a decrease in its surface tension. Thus it is always necessary to specify the temperature at which the surface tension was measured. The change in surface tension of water under different temperatures is shown in Figure 21.

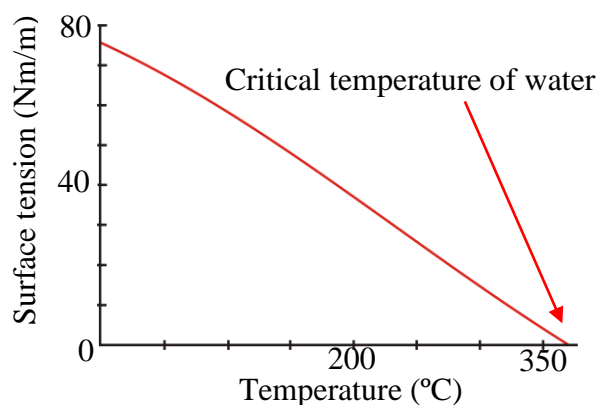


**Figure 21. Surface tension vs. temperature**

At the fluid's critical temperature the surface tension will be zero. The critical temperature is the point at which the phase boundary between fluid and gas terminates. The critical temperature of water is 374°C (Munson and Young, 1998: 26-28).

### 2.4.3. Fluid density

The density of a specific fluid can be described as the mass per unit volume and is measured in kg/m<sup>3</sup>. The following equation can be used to calculate the density of a specific fluid:

$$\rho = \frac{m}{v} \quad \text{Eq. 3}$$

Where:

$\rho$   $\equiv$  Density (kg/m<sup>3</sup>)

$m$   $\equiv$  Mass (kg)

$v$   $\equiv$  Volume (m<sup>3</sup>)

The density of a fluid mainly depends on the fluid composition, however the temperature and pressure can cause a change in the density. The temperature and pressure will only have a small effect on the fluid's density. The effect which the temperature and pressure has on the density of water is shown in Figure 22 (Munson and Young, 1998: 12).

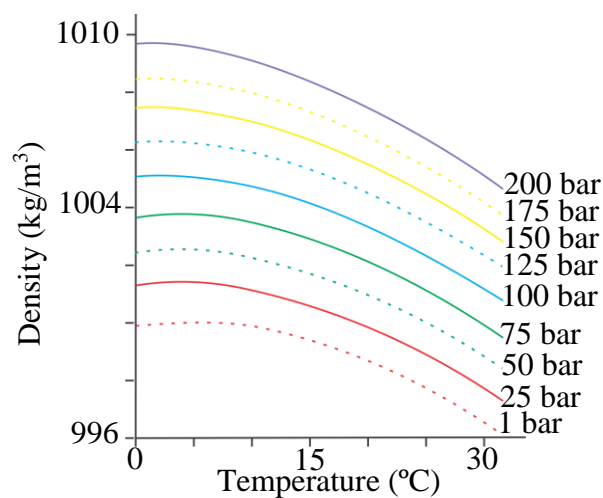


Figure 22. Density vs. temperature and pressure

## 2.5. Fluid mechanics

By using fluid mechanics the behavior of a fluid can be analyzed inside a channel or a nozzle orifice, to ensure adequate drop formation. Fluid mechanics is the study of fluid, either in motion or at rest. Fluid mechanics are used in a wide range of applications, for example, the design of jets, nozzles, pipes, turbines, fans, ships, inkjet technologies, rockets, etc. (White, 1999: 3). In fluid mechanics there are three important dimensional numbers used to analyse the fluid behaviour namely the Reynolds number, Weber number and Ohnesorge number.

### 2.5.1. Reynolds number

When a fluid flows through a cylindrical tube at a relatively low velocity the fluid layers move parallel to each other and this is known as laminar flow. However when the velocity of the fluid increases the moving parallel fluid layers convert into vortex streets, which causes turbulent flow. The difference between laminar and turbulent flow inside a cylindrical tube is shown in Figure 23. When a fluid approaches the turbulent flow condition its resistance to flow increases and would increase the force necessary to move the fluid compared to that of laminar flow conditions. The Reynolds number describes the ratio between the internal forces to the viscous forces for a given fluid. The following equation is used to calculate the Reynolds number for a given flow condition (Westerhof, Sterhiopulos and Noble, 2010: 21-22).

$$\text{Re} = \frac{\rho \cdot v_{\text{velocity}} \cdot l}{\eta} \quad \text{Eq. 4}$$

Where:

- Re   ≡   Reynolds number
- $\rho$     ≡   Fluid density (g / l)
- $v_{\text{velocity}}$  ≡   Velocity of fluid (m/s)
- $l$     ≡   Length (m)
- $\eta$     ≡   Dynamic viscosity (Pa.s)

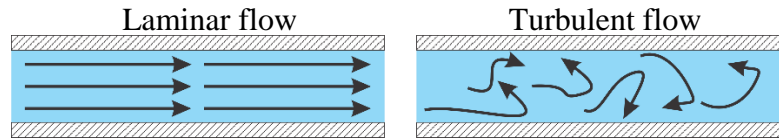


**Figure 23. Difference between laminar and turbulent flow**

The correlation between the Reynolds number and the flow conditions is demonstrated in Table 2.

**Table 2. Effects of the Reynolds number on the flow condition.**

<b>Reynolds number</b>	<b>Flow condition</b>
Re < 1	It is considered as creeping flow which is defined as laminar flow.
1 < Re < 2200	The viscous forces of the fluid are more dominant and laminar flow is revealed.
Re > 2200	The internal forces of the fluid are more dominant and turbulent flow is revealed.

### 2.5.2. Weber number

The Weber number can be defined as the ratio between the fluid's inertia (kinetic energy) and the surface tension. The Weber number for a droplet can be calculated using the following equation:

$$We = \frac{\rho \cdot d \cdot v^2}{\sigma} \quad \text{Eq. 5}$$

Where:

- $We$  ≡ Weber number
- $\rho$  ≡ Density (g / l)
- $d$  ≡ Diameter of drop (m)
- $v$  ≡ Velocity (m/s)
- $\sigma$  ≡ Surface tension (N/m )

The Weber number indicates two different declarations. Firstly it indicates that the droplet will actually leave the nozzle. Secondly it describes when the droplet hits the

printing substrate whether it would splash. A higher Weber number indicates the kinetic energy is more dominant over the surface tension, which will result in better droplet formation although splashing occurs. The reverse is also true as a lower Weber number will indicate the surface tension to be more dominant over the kinetic energy, which will result in weak or even impossible drop formation however the splashing effect would decrease (Lindemann, 2006: 19). The splashing effect with different Weber numbers are demonstrated in Figure 24.

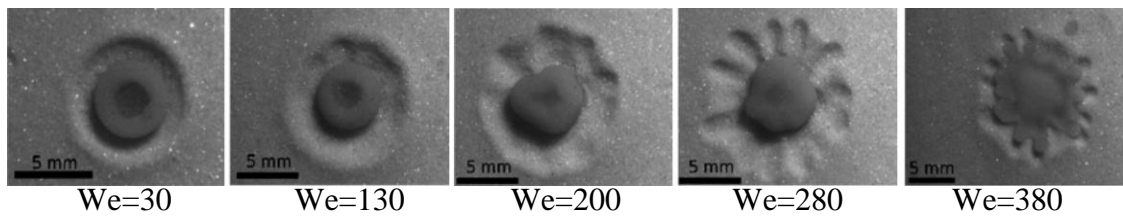
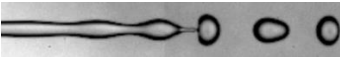


Figure 24. Weber number vs. splashing (Nefzaoui and Skurtys, 2012)

According to Lin and Reitz (1998) the Weber number can be divided into three regime types namely: The Rayleigh breakup regime, Wind-induced or drop on demand regime and the Atomization regime. Although the findings of Lin and Reitz (1998) referred to the jet breakup with fluid viscosities lower than 10 mPa.s, it can still be used as a guideline for this research.

Table 3. Different Weber number regimes

Regimes	Weber number
<p>The Rayleigh breakup regime – CIJ technologies normally use the Rayleigh breakup regime. When fluid is pressurized through a nozzle it breaks up in several single drops due to the surface disturbances, as demonstrated in Figure 25. These disturbances can be induced by a vibrating piezo transducer or environmental disturbances (Lin and Reitz, 1998).</p>  <p>Figure 25. Rayleigh breakup</p>	$8 < We \leq 12$

<p>Drop on demand regime – The drop on demand regime is used in DOD inkjet technologies. A drop is formed by ejecting a small amount of fluid through a small orifice diameter, by means of a pressure pulse. The DOD inkjet drop on demand regime is shown in Figure 26 (Lin and Reitz, 1998).</p>	$12 < We \leq 40$
<p>Atomization regime – The atomization regime is typically used for spray cans as demonstrated in Figure 27. The aerodynamic interaction causes irregularities in the original jet smooth jet surface, which leads to unstable wave growth on the jet surface producing unstable ligaments. The average drop size is relatively small compared to the orifice diameter size (Lin and Reitz, 1998).</p>	$We > 40$



**Figure 26. Drop on demand drop formation**

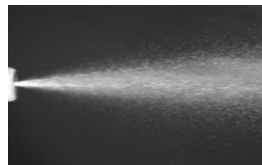


**Figure 27. Atomization regime**

### 2.5.3. Ohnesorge number

Although the Weber number is used to determine whether a specific fluid will produce an adequate droplet its shortcoming is its independence of the fluid's viscosity. To account for the shortcomings the Ohnesorge, also called stability, Laplace or Z number, is used. The Ohnesorge number includes the effects which the surface tension and viscosity of a fluid have on the drop formation process. The Ohnesorge number can be described as the ratio of the fluid viscosity to the fluid surface tension and can be calculated using the Eq.6. However the Ohnesorge number only reflects on the properties and size of the droplets and not the driving

conditions, which influences the drop velocity. Thus it must always be used in conjunction with the Reynolds number. The driving conditions will also influence the velocity of the drops. A high Ohnesorge number will imply that the viscous forces are more dominant over the surface tension forces. Thus most of the energy is converted into internal viscous dissipation, which means the drop formation is weak or even impossible.

$$\begin{aligned}
 Oh &= \frac{\sqrt{We}}{Re} \\
 &= \frac{\eta}{\sqrt{\rho \cdot d \cdot \sigma}}
 \end{aligned}
 \tag{Eq. 6}$$

Where:

- $Oh$  ≡ Ohnesorge number
- $We$  ≡ Weber number
- $Re$  ≡ Reynolds number
- $\eta$  ≡ Dynamic viscosity (Pa.s)
- $\rho$  ≡ Density (g / l)
- $d$  ≡ Nozzle orifice diameter (m)
- $\sigma$  ≡ Surface tension (N/m)

For a low Ohnesorge number the surface tension forces will be dominant over the viscous forces. When this happens most of the energy is converted into surface tension, which means a shear-shaped droplet will be formed (Hutchings and Martin, 2012: 7). The effect of the Ohnesorge number on the drop formation process is demonstrated in Figure 28.

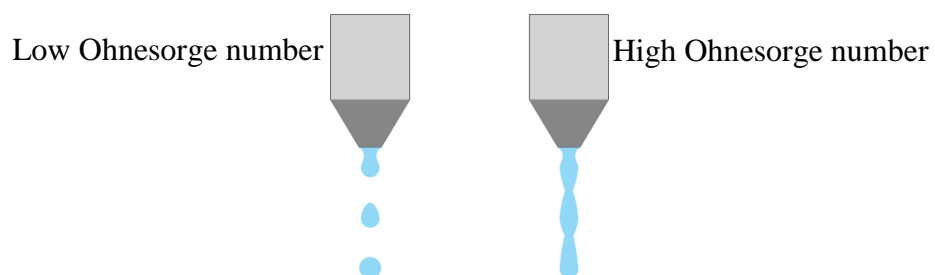


**Figure 28. Effect which the Ohnesorge number has on the drop formation**

The following table shows the experimental results of Reis, Ainsely and Derby (2005), the drop formation was recorded using DOD technologies with different Ohnesorge numbers.

**Table 4. Experimental results of Reis, Ainsely and Derby (2005)**

<b>Ohnesorge number</b>	<b>Results</b>
Oh < 0.1	The surface tension is too low and satellite drops occur. However it is possible to print with a Oh number lower than 0.1 as long as the satellite drops merge with the main droplet
0.1 ≤ Oh ≤ 1	It was found that adequate drop formation occurred.
Oh > 1	The viscous dissipation will prevent drop formation.

#### **2.5.4. Critical Weber number**

The Weber number is the most important dimensionless number with regards to the drop formation process. The critical Weber number is used to calculate a sufficient condition for drop breakup. The critical Weber number is calculated using the Weber number and the Ohnesorge number. Although the critical Weber number is not necessary, but when surpassed the drop breakup will occur. Drop formation is possible at lower Weber numbers as long as the supplied energy to the system is sufficient to overcome friction losses and the surface energy of a droplet. The equation below can be used to calculate the critical Weber number for a specific fluid viscosity (Lindemann, 2006: 37-40).

$$We_{critical} = 12 \cdot (1 + 1.077 Oh^{1.6}) \quad \text{Eq. 7}$$

Where:

- $We_{critical}$  ≡ Critical Weber number
- $We$  ≡ Weber number
- $Oh$  ≡ Ohnesorge number

## 2.6. Control parameters

According to the research of Lindemann (2006), the sufficient control parameters for the RPH could be calculated using the Weber, Reynolds, Ohnesorge and critical Weber dimensionless numbers. The critical pressure and time control parameters will be discussed below:

### 2.6.1. Critical pressure

The necessary pressure to eject a single droplet, from a nozzle orifice, can be calculated using an energetic estimation of the conditions in a simplified inkjet nozzle model. The energetic estimation model, shown in Figure 29, consists of a circular inlet channel and nozzle with a certain length using a fluid with a specific density, viscosity and surface tension (Lindemann, 2006:41). In order to eject a droplet from a nozzle orifice, the mechanical work ( $W_{\text{pressure}}$ ) generated by the fluid pressure must be equal to the total energy required for the drop formation process.

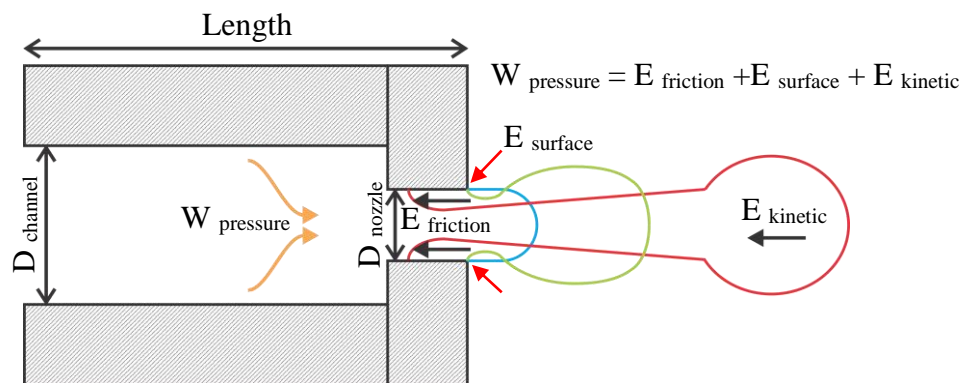


Figure 29. Energetic estimation model

The energy requirements for the drop formation process consist of three single expressions namely: energy loss due to friction in the channel which represents all viscous and geometrical pressure losses ( $E_{\text{friction}}$ ), the kinetic energy required for the free flying droplet ( $E_{\text{kinetic}}$ ) and the energy required to form a spherical droplet ( $E_{\text{surface}}$ ) (Lindemann, 2006:41). Thus the mechanical work required to eject a droplet from a nozzle orifice can be expressed using Eq. 8.

$$W_{pressure} = E_{friction} + E_{kinetic} + E_{surface} \quad \text{Eq. 8}$$

The different energy requirements used in Eq. 8 are addressed below:

- **Energy required to overcome friction ( $E_{friction}$ )**

The formula used to determine the required energy to overcome the friction inside the nozzle can be seen in Eq. 9. The nozzle length, resistance owing to the outflow of the nozzle orifice and resistance due to the cross section are considered to be infinitely small and are not taken into consideration (Lindemann, 2006:41-42).

$$E_{friction} = V_{drop} \cdot v_{channel} \cdot \frac{32 \cdot \eta \cdot l}{(D_{channel})^2} \quad \text{Eq. 9}$$

Where:

- $E_{friction}$  ≡ Energy loss due to the fluid nozzle outflow (J)
- $v_{channel}$  ≡ Fluid velocity through channel ( $\text{m}\cdot\text{s}^{-1}$ )
- $D_{channel}$  ≡ Diameter of channel (m)
- $V_{drop}$  ≡ Drop volume (l)
- $\eta$  ≡ Viscosity (Pa.s)
- $l$  ≡ Length of channel (m)

- **Energy required for the free flying drop ( $E_{kinetic}$ )**

The kinetic energy of a droplet is the energy which the droplet possesses owing to its velocity. The required energy necessary to accelerate a droplet to its intended velocity can be calculated using the following formula: (Lindemann, 2006:42):

$$E_{kinetic} = \frac{1}{2} \cdot \rho \cdot V_{drop} \cdot (v_{drop})^2 \quad \text{Eq. 10}$$

Where:

- $E_{kinetic}$  ≡ Required kinetic energy (J)
- $V_{drop}$  ≡ Drop volume (l)
- $v_{drop}$  ≡ Drop velocity ( $\text{m}\cdot\text{s}^{-1}$ )
- $\rho$  ≡ Density (g/l)

- **Energy required to form a spherical droplet ( $E_{surface}$ )**

The energy necessary for the fluid stream to detach from the nozzle and form a spherical shape due to the surface tension are shown in Eq. 11. However for this equation the drop diameter is considered to be equal to the nozzle orifice diameter (Lindemann, 2006:42).

$$E_{surface} = V_{drop} \cdot \frac{6 \cdot \sigma}{D_{nozzle}} \quad \text{Eq. 11}$$

Where:

- $E_{surface}$   $\equiv$  Surface energy required (J)
- $D_{nozzle}$   $\equiv$  Diameter of nozzle (m)
- $V_{drop}$   $\equiv$  Volume of drop (l)
- $\sigma$   $\equiv$  Surface tension (N/m)

By using the formulas provided in Eq. 9, Eq. 10 and Eq. 11 an extended equation can be formulated for the mechanical work required to eject a droplet. However it must be kept in mind that it would be very difficult to determine the fluid velocity inside the nozzle channel ( $v_{channel}$ ), thus by using the continuity equation the  $v_{channel}$  could be linked to the droplet velocity ( $v_{drop}$ ). Using the continuity equation, the  $v_{channel}$  could be expressed in the form of the  $v_{drop}$ , channel diameter ( $D_{channel}$ ) and nozzle diameter ( $D_{nozzle}$ ), shown in Eq. 12 (Lindemann, 2006:42):

$$v_{channel} = v_{drop} \cdot \frac{(D_{nozzle})^2}{(D_{channel})^2} \quad \text{Eq. 12}$$

The mechanical work required formula was simplified to:

$$\begin{aligned} W_{pressure} &= V_{drop} \left[ v_{channel} \cdot \frac{32 \cdot \eta \cdot l}{(D_{channel})^2} + \frac{6 \cdot \sigma}{D_{nozzle}} + \frac{1}{2} \cdot \rho \cdot (v_{drop})^2 \right] \\ &= V_{drop} \left[ \frac{32 \cdot \eta \cdot l \cdot (D_{nozzle})^2}{(D_{channel})^4} \cdot v_{drop} + \frac{6 \cdot \sigma}{D_{nozzle}} + \frac{1}{2} \cdot \rho \cdot (v_{drop})^2 \right] \quad \text{Eq. 13} \end{aligned}$$

However using an incompressible fluid the mechanical work required to eject a droplet from an orifice can be normalized to the pressure in a fixed volume. The fixed volume is considered to be a specific drop volume. The equation below demonstrates how the mechanical work required can be expressed by using the required pressure and drop volume (Lindemann, 2006:41).

$$W_{pressure} = p \cdot V_{drop} \quad \text{Eq. 14}$$

However by taking into consideration that the required mechanical work is equal to the product of the required pressure and drop volume (as stated in Eq. 14), the required pressure can be calculated by using Eq. 15 (Lindemann, 2006:42):

$$p \cdot V_{drop} = V_{drop} \left[ \frac{32 \cdot \eta \cdot l \cdot (D_{nozzle})^2}{(D_{channel})^4} \cdot v_{drop} + \frac{6 \cdot \sigma}{D_{nozzle}} + \frac{1}{2} \cdot \rho \cdot (v_{drop})^2 \right]$$

$$p = \frac{32 \cdot \eta \cdot l \cdot (D_{nozzle})^2}{(D_{channel})^4} \cdot v_{drop} + \frac{6 \cdot \sigma}{D_{nozzle}} + \frac{1}{2} \cdot \rho \cdot (v_{drop})^2 \quad \text{Eq. 15}$$

Where:

- $p$  ≡ Required pressure (Pa)
- $\eta$  ≡ Viscosity (Pa.s)
- $l$  ≡ Length of channel (m)
- $D_{nozzle}$  ≡ Diameter of nozzle (m)
- $D_{channel}$  ≡ Diameter of channel (m)
- $\sigma$  ≡ Surface tension (N/m)
- $\rho$  ≡ Density (g/l)
- $v_{drop}$  ≡ Drop velocity (m.s<sup>-1</sup>)

By taking advantage of the required pressure equation, shown in Eq. 15, the sufficient pressure for a droplet ejection with a known droplet velocity could be determined. However it must be kept in mind that this formula is only valid if a droplet is issued at all. The drop will be issued only when the critical drop velocity is met or exceeded. When the drop velocity is below the critical drop velocity, drop formation will not occur. Thus by using the critical Weber number formula in Eq. 8 a

critical pressure can be calculated which only depends on the media parameters, geometry parameters and the critical Weber number. The critical pressure can be calculated by replacing the velocity variables, in the required pressure formula, with critical velocities. The critical velocities can be calculated using (Lindemann, 2006:43):

$$v_{drop\,critical} = \sqrt{\frac{We_{critical} \cdot \sigma}{D_{nozzle} \cdot \rho}} \quad \text{Eq. 16}$$

The critical pressure can then be defined as the minimum pressure required obtaining an adequate drop formation process using an inkjet system with a specific fluid. The formula which can be used to calculate the critical pressure can be seen below:

$$\begin{aligned} P_{critical} &= \frac{32 \cdot \eta \cdot l \cdot (D_{nozzle})^2}{(D_{channel})^4} \cdot v_{drop\,critical} + \frac{6 \cdot \sigma}{D_{nozzle}} + \frac{1}{2} \cdot \rho \cdot (v_{drop\,critical})^2 \\ &= \frac{32 \cdot \eta \cdot l \cdot (D_{nozzle})^2}{(D_{channel})^4} \cdot \sqrt{\frac{We_{critical} \cdot \sigma}{D_{nozzle} \cdot \rho}} + \frac{6 \cdot \sigma}{D_{nozzle}} + \frac{1}{2} \cdot \frac{We_{critical} \cdot \sigma}{D_{nozzle}} \quad \text{Eq. 17} \end{aligned}$$

Where:

- $P_{critical}$   $\equiv$  Critical pressure (Pa)
- $We_{critical}$   $\equiv$  Critical Weber number
- $D_{channel}$   $\equiv$  Diameter of channel (m)
- $D_{nozzle}$   $\equiv$  Diameter of nozzle (m)
- $\eta$   $\equiv$  Viscosity (Pa)
- $l$   $\equiv$  Length of channel (m)
- $\sigma$   $\equiv$  Surface tension (N/m)
- $\rho$   $\equiv$  Density (g/l)

### 2.6.2. Critical time

The critical time can be defined as the maximum time which the fluid must flow out of the nozzle orifice to obtain a droplet. However for this formula the drop diameter is considered to be equal to the nozzle's diameter (Lindemann, 2006:44).

$$\begin{aligned}
t_{critical} &= \frac{V_{drop}}{Q_{critical}} \\
&= \frac{2}{3} \cdot \sqrt{\frac{(D_{nozzle})^3 \rho}{We_{critical} \cdot \sigma}}
\end{aligned}
\tag{Eq. 18}$$

Where:

- $t_{critical}$   $\equiv$  Critical time (s)
- $V_{drop}$   $\equiv$  Volume of drop (l)
- $Q_{critical}$   $\equiv$  Critical volume flow
- $We_{critical}$   $\equiv$  Critical Weber number
- $D_{nozzle}$   $\equiv$  Diameter of nozzle (m)
- $\sigma$   $\equiv$  Surface tension (N/m)
- $\rho$   $\equiv$  Density (g/l)

## 2.7. Summary

This chapter addressed the different available inkjet technologies that will serve as a guideline to develop the RPH. The fluid properties, which have to be kept in mind when designing an inkjet system, were also addressed. These fluid properties included the fluid viscosity, surface tension and density. The fluid mechanics which can be used to analyse a fluid's behavior inside a print head were also noted. The fluid mechanics addressed were the Reynolds, Weber, Ohnesorge and Critical Weber numbers. Inkjet control parameters, determined by previous research in the inkjet field, were also studied. The control parameters addressed included the critical pressure and time.

In Chapter 3, the physical design of the RPH will be shown with regard to the theoretical study addressed in Chapter 2.

## Chapter 3            The more ‘rugged’ printing head

### 3.1. Introduction

The previous chapter considered the theory and operation of the different inkjet technologies. It also showed how to mathematically determine two important inkjet control parameters namely the critical pressure and the critical time. This chapter will focus on the practical design and construction of the RPH.

### 3.2. Inkjet technologies

Before a decision could be made about which of the inkjet technologies (discussed in Chapter 2) would be used as a guideline to develop the RPH, the different inkjet technologies were compared with each other. A comparison between the various inkjet technologies can be seen in Table 5.

**Table 5. Comparison between the different inkjet technologies**

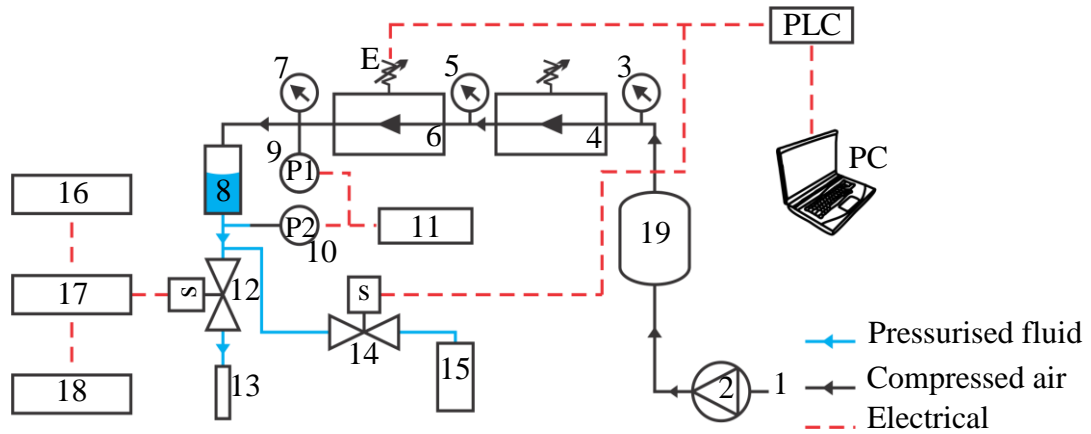
<b>Print technology</b>	<b>Advantage / disadvantage of inkjet technology.</b>
Continuous inkjet	This inkjet technology has a very low fluid viscosity range of between 2.8 and 6 mPa.s. It also requires very complicated control techniques.
Thermal drop on demand	Limited to fluid viscosities below 30 mPa.s. Unwanted chemical reactions may occur due to its working. If a viscosity over 30 mPa.s is used nozzle blockage may occur.
Electrostatic inkjet	Only a specialised print fluid can be used. The fluid consists of electrically charged conventional pigments in non-conductive fluid.
Piezo electric drop on demand	Limited to fluid viscosities below 30 mPa.s., however specialised piezoelectric drop on demand units capable of operating at higher viscosities are available.

Solenoid based inkjet	<p>A major advantage of this type of inkjet technology is the nozzle can easily be changed. Thus it will be easy to experiment with different nozzle orifice diameter sizes. Due to the lack of documented research done on this technology no printable fluid property ranges could be found. Thus the solenoid based inkjet technology could <b>possibly</b> be used with a wider range of fluid properties.</p>
-----------------------	--

As shown in Table 5, the solenoid-based inkjet technology can possibly be used with a wider range of fluid properties, compared to that of the other mentioned inkjet technologies, owing to its flexible design. Owing to this fact it was decided to use the solenoid based inkjet technology as a guideline to develop the RPH.

### 3.3. The RPH setup

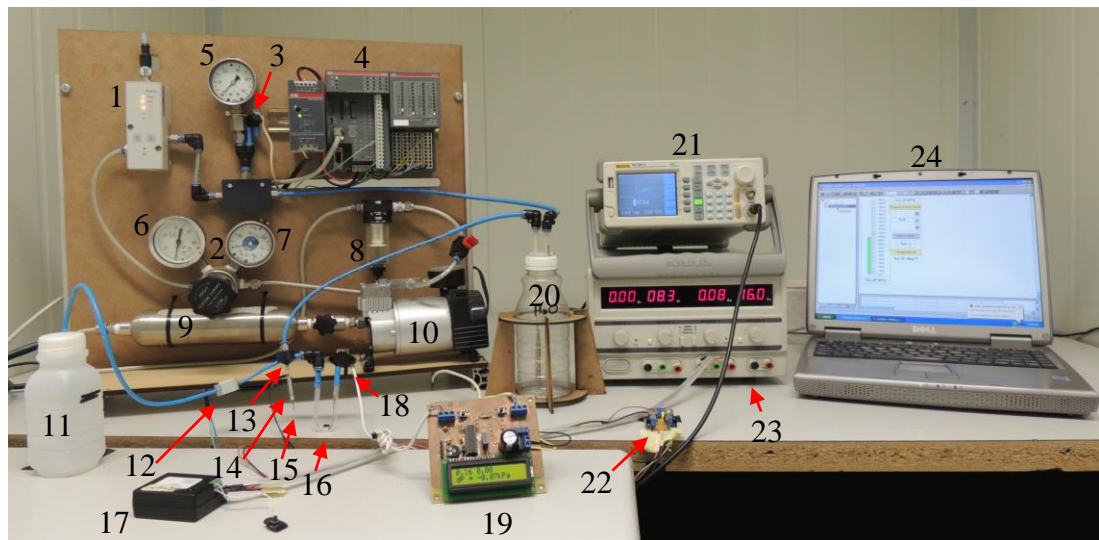
The RPH will operate on the same principle as solenoid-based inkjet systems described in Chapter 2. A block diagram and a photo of the RPH are shown in Figure 30 and Figure 31. In order for the fluid to flow through the nozzle's orifice, the fluid pressure must be equal or higher than the critical pressure. The fluid pressure was obtained using compressed air. The compressor supplied air to the pressurized buffer tank. The buffer tank was used to eliminate any pressure spikes during the operation of the compressor. A pressure limit regulator was then used to ensure the input pressure, supplied to the electronic pressure regulator, does not exceed 400 kPa, as this is its maximum input pressure. The output pressure set point of the electronic pressure regulator was controlled using a PLC (Programmable Logic Controller). The PLC was connected to a PC (Personal Computer) which enabled the output pressure set point to be adjusted using a graphical PC interface. The output pressure signal of the electronic pressure regulator was also measured using the PLC and displayed graphically on the PC interface. The electronic pressure regulator's output pressure would be equal to the air pressure inside the sample fluid reservoir, which would pressurize the fluid solution. Owing to the plastic fluid reservoir used the pressure could not exceed 150 kPa.



1. Air inlet	2. Compressor
3. Analog pressure gauge (Buffer tank)	4. Pressure limit regulator
5. Analog pressure gauge (Electronic pressure regulator inlet)	6. Electronic pressure regulator
7. Analog pressure gauge (Electronic pressure regulator outlet)	8. Sample fluid reservoir
9. MPX5700DP pressure sensor 1	10. MPX5700DP pressure sensor 2
11. Pressure display unit	12. VHS valve
13. Nozzle	14. Purge solenoid valve
15. Purge tank	16. Power supply
17. Spike and hold unit	18. Signal generator
19. Buffer tank	

**Figure 30. Block diagram of the RPH**

Pressures higher than 150 kPa would cause the fluid reservoir to burst or explode. A purge solenoid valve, connected to the inlet of the VHS valve, is used to purge the RPH's fluid system. A fluid purge is done in order to ensure the fluid system is free of any air bubbles, as air bubbles can influence the results. If the purge solenoid valve is switched it will enable the fluid to flow through the valve and into a purge waste tank. Two MPX5700DP pressure sensors were used to measure the pressure difference between the electronic pressure regulator's outlet and the fluid pressure at the VHS valve's inlet. This was done to compensate for any pressure losses or gains owing to the different fluid heights between the sample fluid reservoir and the VHS valve's inlet height. The two pressures and the pressure difference were displayed on the pressure display unit using a 2x16 Liquid Crystal Display (LCD) unit. In order for the fluid to flow through the VHS valve and nozzle to exit the orifice, the valve has to be switched for a specific time. A spike and hold unit was used to ensure the correct switching parameters for the VHS valve were met.



1. Electric pressure regulator	2. Pressure limit regulator unit
3. MPX5700DP pressure sensor 1	4. PLC
5. Analog pressure gauge (Electronic pressure regulator outlet pressure)	6. Analog pressure gauge ( Electronic pressure regulator inlet pressure)
7. Analog pressure gauge (Buffer tank)	8. Water trap
9. Buffer tank	10. Compressor
11. Purge tank	12. Purge solenoid valve
13. VHS valve connector	14. VHS valve
15. Nozzle	16. U connector for MPX5700DP
17. Spike and hold unit	18. MPX5700DP pressure sensor 2
19. Pressure display unit	20. Sample fluid reservoir
21. Signal generator	22. Spike and hold unit power supply
23. Power supply	24. PC

**Figure 31. The RPH experimental setup**

The control unit was powered using a dual power supply unit, whereby the necessary control signals for the switching of the VHS valve was supplied using a signal generator. Thus the control signal's frequency and pulse width can easily be changed. All the main components, seen in Figure 31, will be addressed below:

### 3.3.1. VHS valve

The valve is one of the most important components for such a printing head and must meet the following requirements:

- High chemical resistance
- Fast response and switching times
- A flexible design
- Able to withstand high pressures
- Long lifespan

The INKX0511400A Very High Speed (VHS) solenoid valve, which is shown in Figure 32, meets all of the requirements mentioned above.

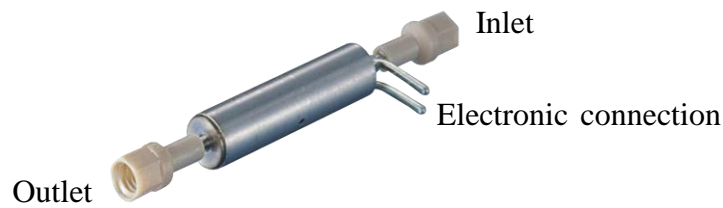


**Figure 32. The Lee Corporation's VHS valve**

In this document the VHS solenoid valve will be referred to as the VHS valve. The VHS valve is manufactured by The Lee Corporation and its specifications are given below:

- The VHS valve's wetted material (material that comes in contact with the fluid) includes Ethylene Propylene Diene Monomer (EPDM), PolyPhenylene Sulfide (PPS), Polyether ether ketone (PEEK), Stainless steel and polyepoxides (Epoxy). All of the materials mentioned above offer excellent abrasion resistance, they also have a wide chemical resistant range.
- By using a spike and hold or fast response unit the VHS valve will be able to operate with frequencies up to 1200 Hz with a response time of 0.25 ms. Thus the VHS valve would be able to operate with a pulse width of 416.66 us using a 50% duty cycle. (The Lee Corporation, 2008).
- The VHS valve offers a compact and flexible design. Both inlet and outlet consist of a screw-in connector (The Lee Corporation, 2008).
- The VHS valve has a pressure operating range of between 0 and 850 kPa (The Lee Corporation, 2008).
- The VHS valve will operate for a minimum of 250 million actuations (The Lee Corporation, 2008).

### **3.3.2. Nozzles**

The micro-dispense nozzles manufactured by The Lee Corporation, seen in Figure 33, offer a convenient method of dispensing small fluid amounts, in the micro- to

nanolitre range, when used with the VHS valve. Micro-dispense nozzles comprise of a threaded end which enables it to screw into the VHS valve's outlet. The threaded design makes the changing of nozzle easy and provides a reliable and leak-proof connection between the VHS valve and nozzle (The Lee Corporation, 2008). It was decided to use three different nozzle orifice diameter sizes for this research, in order to determine what the effect of the nozzle orifice diameter size on the control parameters. The nozzle orifice diameter sizes of 0.127, 0.191 and 0.254 mm were selected, as they covered the available small, medium and large orifice diameter size range.



**Figure 33. The Lee Corporation's micro-dispense nozzle design**

### **3.3.3. Spike and hold unit**

The spike and hold unit, manufactured by the Lee Corporation, is used to optimize the valve signal supplied to the VHS valve. The VHS valve requires a high voltage spike in order to decrease its actuate time, however owing to the high voltage much more heat will be generated. After the valve has opened the supplied voltage must be reduced to its operating voltage, to prevent permanent valve damage owing to the heat generated by the solenoid. A negative spike will occur when the VHS valve's supply voltage drops to 0 V. The negative spike is generated by the collapse of the magnetic field around the solenoid. The spike and hold unit suppresses the negative spike otherwise it could damage or destroy any electronic components connected to the VHS supply line. The control and valve signals are demonstrated in Figure 34. The spike duration can be adjusted, between 0.3 and 5 ms, by adjusting the potentiometer VR shown in Figure 35. However at long spike durations permanent VHS valve damage could occur, owing to the increased valve temperature. The connections to and from the spike and hold unit can be seen in Figure 35.

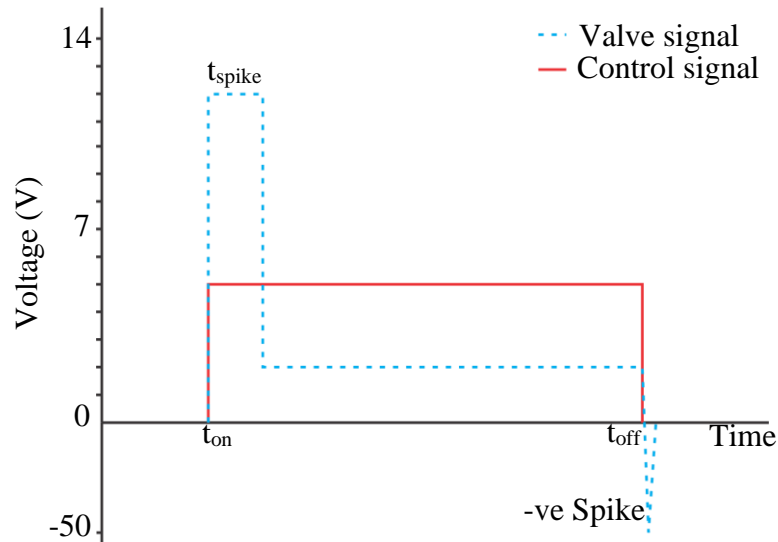


**Figure 34. Spike and hold unit wave forms**



**Figure 35. The Lee Corporation's spike and hold unit**

### 3.3.4. Dual voltage power supply

As demonstrated in Figure 36 the spike and hold unit requires two voltages namely the hold voltage and a spike voltage. The dual power supply, shown in Figure 36, converts the input voltage to two voltages namely the hold voltage (1.5 V) and the spike voltage (12V). These voltages are the optimal working VHS valve voltages according to manufacturers. The dual power supply comprises two LM317 variable voltage circuits connected in parallel. The PCB and circuit diagram of the dual power supply can be seen in Figure 36 and Figure 37.

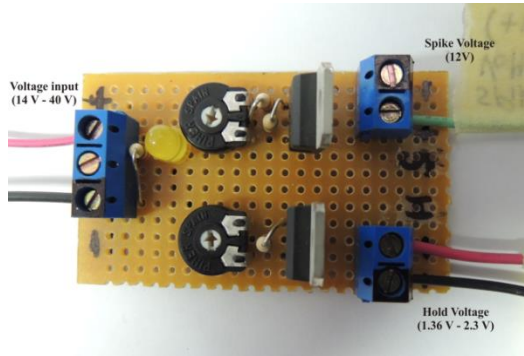


Figure 36. Dual power supply

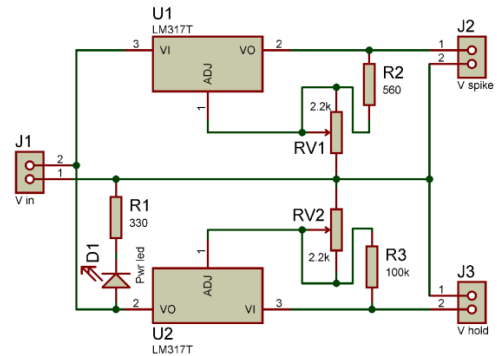


Figure 37. Dual power supply circuit

### 3.3.5. Differential pressure sensor and display

Two Motorola MPX5700DP pressure sensors, shown in Figure 38, were used to measure the pressure difference between the electronic pressure regulator's outlet and the fluid pressure at the VHS valve's inlet. Fluid pressure in a closed system varies with a change in elevation, thus it must always be measured relative to a reference point. In this case the glycerol-water mixture fluid level served as the reference point. Elevation refers to the vertical distance, in meters, between the reference point and the measuring point. Upward elevation is always represented as positive and downwards negative, thus a higher measuring point will have a larger elevation point compared to a lower measuring point. The change in pressure in a homogeneous liquid can be determined using the following equation:

$$\Delta p = \rho \cdot g \cdot h \quad \text{Eq. 19}$$

Where:

- $\Delta p$   $\equiv$  Difference in pressure (kPa)
- $h$   $\equiv$  Vertical elevation (m)
- $\rho$   $\equiv$  Density (kg/m<sup>3</sup>)
- $g$   $\equiv$  Acceleration of gravity (m/s<sup>2</sup>)

The MPX5700DP pressure sensor is manufactured from piezoresistive material and has a pressure operating range of between 0 and 700 kPa (Motorola, 2001). The MPX5700DP differential sensor consists of two pressure inlets namely: the pressure inlet and the vacuum inlet. The pressure which had to be measured was connected to

the pressure inlet, while the vacuum inlet was left open. The differential pressure sensor's output voltage would be directly proportional to the pressure difference between the measured pressure and the ambient pressure.



**Figure 38. MPX5700DP pressure sensor**

Both of the MPX5700DP pressure sensor outputs were connected to the A/D inputs of a PIC16F690 microcontroller, which would convert the analog signal to a digital value. The digital value could then be used to determine the output voltage using the following:

$$P = \left( \frac{\left( \frac{V_{out}}{V_s} \right) \pm Error}{0.0012858} \right) - 0.04 \quad \text{Eq. 20}$$

Where:

$P$   $\equiv$  Pressure (kPa)

$V_{out}$   $\equiv$  Output voltage of sensor (V)

$V_s$   $\equiv$  Supply voltage to sensor (V)

$ERROR$   $\equiv$  Compensating for the sensor error

The two inlet pressures as well as the pressure difference between the two inlets were displayed by means of a 2x16 LCD screen. The pressure measuring circuit diagram can be seen in Figure 39. The firmware and circuit board, seen in Figure 40, was designed in such a manner to make provision for automatically determining the MPX5700DP ERROR component, shown in Eq. 20, by pressing a zero button for each of the two sensors. The firmware code for the PIC microcontroller can be seen in Annexure A.

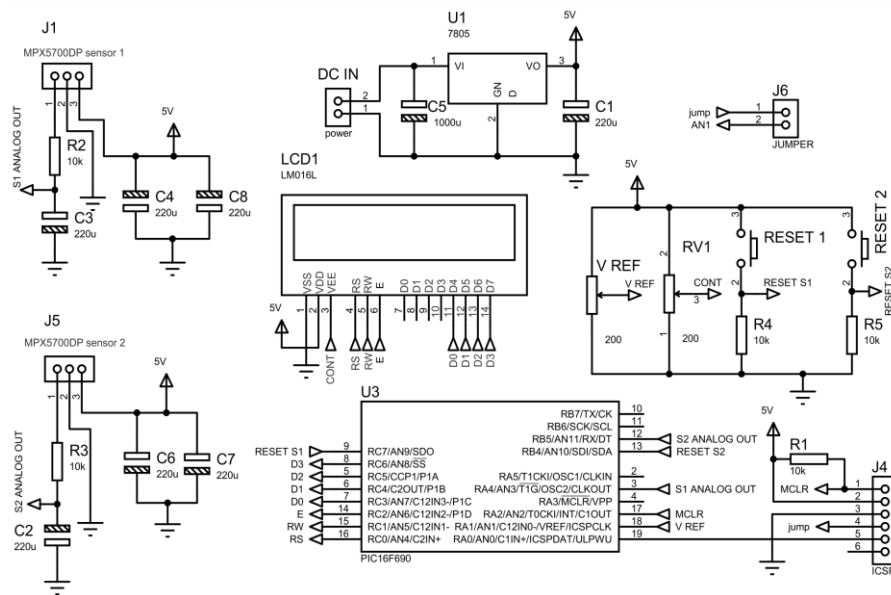


Figure 39. MPX5700DP pressure measuring circuit diagram

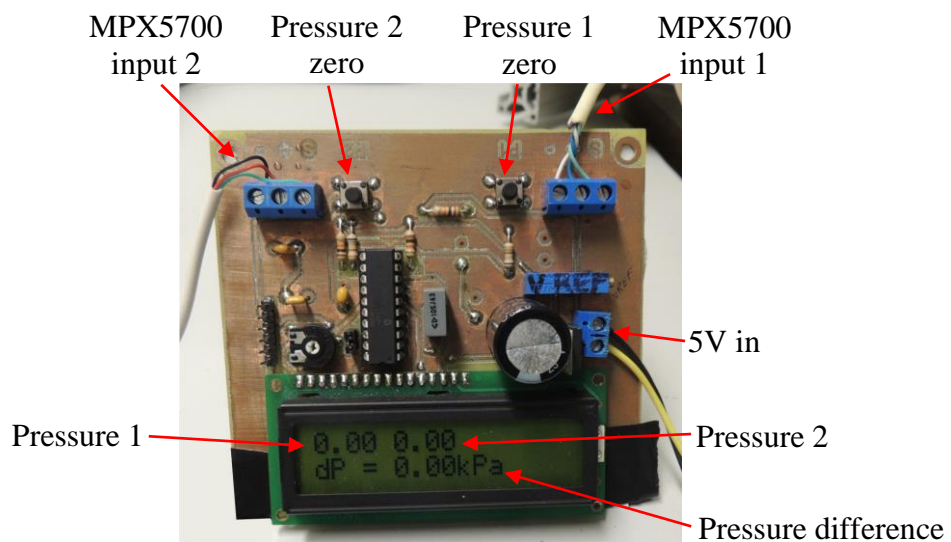
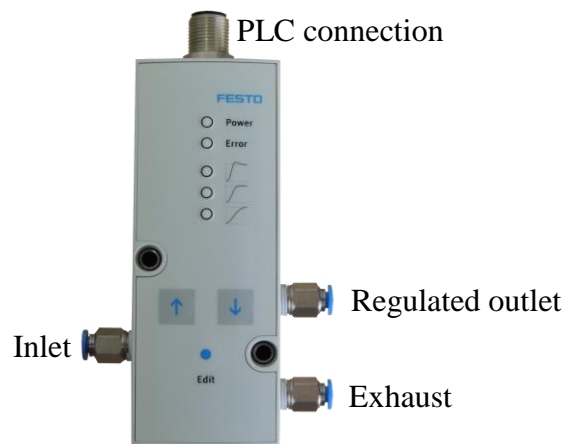


Figure 40. The MPX5700DP pressure display unit

### 3.3.6. Electronic pressure regulator

The VPPM electronic pressure regulator, shown in Figure 41, is manufactured by Festo and is used to regulate the outlet pressure proportional to its specified set point. If the actual valve (outlet pressure) differs from the set point value the valve would actuate until it reaches the specified set point valve. The internal set point of the VPPM electronic pressure regulator is proportional to the 4-20 mA input signal,

which was supplied by the PLC unit. The VPPM electronic pressure regulator also generates a 4-20 mA signal proportional to the regulated outlet pressure, which was also connected to the PLC's analog input. The measured output was then graphically displayed on the PC. The operating pressure range of the electronic pressure regulator is between 2 and 200 kPa with a maximum hysteresis of 2 kPa.



**Figure 41. Festo's electronic pressure regulator**

### **3.3.7. Programmable logic controller**

ABB's programmable logic controller (PLC) was used to control and measure the output air pressure using the electronic pressure regulator. It was decided to use the PLC because of the following two reasons: Firstly the programming of the module is much faster than with other controllers (e.g. PIC microcontroller). The other reason is the PLC has a function that data can be displayed visually on the PC. The pressure at the outlet of the electronic pressure regulator will be displayed by means of a pressure graph, which can be seen in Figure 42.

The set point pressure can also be adjusted by clicking on the pressure set block where a numeric input window will appear. The numeric input is limited between 1 and 150 kPa as this is the operating range of the electronic pressure regulator. The PLC was programmed using the Continuous Function Chart (CFC) programming language and can be seen in Annexure B. The PLC used was a midrange controller (PM554). The controller has seven digital inputs and five digital outputs. An

expansion module (AX521) was then connected to the controller to add four analog inputs and outputs.

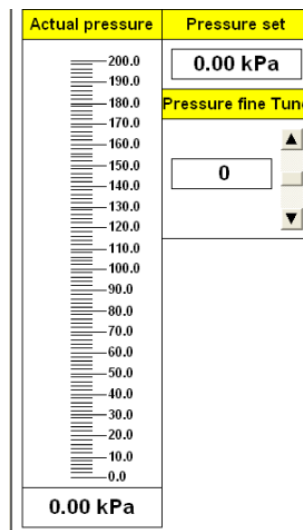


Figure 42. PC visual interface

### 3.4. Summary

In this chapter the different inkjet technologies were compared against each other in order to determine which technology would be the best to serve as a guideline to develop the RPH. The physical design of the RPH was also given. The main components of the print head were discussed. The main components included the VHS valve, nozzle, spike and hold unit, dual voltage regulator, differential pressure sensor, electronic pressure regulator and PLC controller. When all the components were assembled the RPH was constructed.

In Chapter 4, an analytic analysis was done on the RPH, using different fluid solutions, to determine the print head's critical pressure and time.

## **Chapter 4            Analytical analysis**

### **4.1.    Introduction**

In this chapter, different fluid solutions were prepared in order to determine the effect which the fluid properties have on the drop formation process. The fluid properties include the fluid's viscosity, surface tension and density. The critical pressure and time were then theoretically calculated for each of the solutions, using the different nozzle orifice diameter sizes. The nozzle sizes mentioned in the previous chapter will be used in the calculations.

### **4.2.    Fluid solutions**

In order to determine the effects that the fluid properties have on the drop formation process, different fluid solutions were prepared. These fluid solutions had different viscosities, densities and surface tensions. As the research of Cheng (2008) showed the Weber and Reynolds number will change according to the fluid's properties. When a solute substance dissolves in a solvent substance it is known as a solution. Solvents can be divided into the following classes:

- Polar solvents – Solvents which consist of strong dipolar molecules having hydrogen bonding.
- Semi-polar solvents – Solvents which consist of strong dipolar molecules without hydrogen bonding.
- Non-polar – Molecules which consist of small or no dipolar characters.

In order to obtain a solution the solute and solvent must be of the same class, in other words 'like dissolves like'. Solvents can fit into more than one of the classes, mentioned above. For example glycerol is considered to be polar and semi-polar solvent, thus glycerol is an excellent solvent (Troy, 2006: 221-222). Glycerol solutions are widely used in experiments to determine the effect which the change in viscosity has on the fluid flow behaviour. If glycerol is used as the solvent the solute

must also be polar in order to obtain a solution. There are a number of polar solutes, for example distilled water, ethanol, methanol, benzene, acetone, etc. (Troy, 2006: 221-222). Polar solvents and solutes use hydrogen bonds to form a solution. Hydrogen bonds consist of OH (Hydroxyl) groups to form bonds between a solute and a solvent. A hydroxyl group consists of an oxygen and a hydrogen atom. As demonstrated in Figure 43, both oxygen and hydrogen atoms are considered to be neutral of charge.

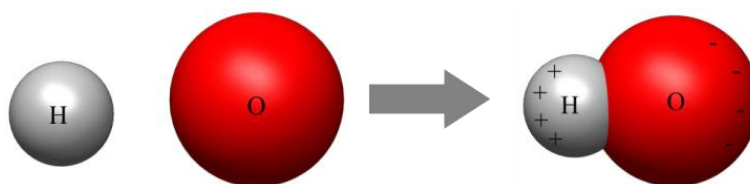


**Figure 43. Hydroxyl group**

An atom that is neutral of charge consists of an equal number of protons and electrons, thus balancing each other out. However, when the oxygen and hydrogen atoms form a bond, a hydroxyl group is formed. Even though the group is still considered to be neutral of charge, the uneven distribution of the charges results in a partial positive and a partial negative. The hydrogen in the hydroxyl group is partially positive whereas the oxygen is partially negative. Owing to the partial charges formed, the hydroxyl group is considered to be polar. Hydroxyl groups will form weak bonds with each other because of the partial charges. The partial positive charged hydrogen will form a weak bond with a partial negative charged oxygen from a different hydroxyl group. However the bonds are constantly ripped apart, owing to the fact that the molecules always move around (Masterjohn, 2005).

### **4.3. Test solutions**

Different glycerol-water mixtures were chosen as the test solutions. Glycerol was chosen as the solvent and distilled water was chosen as the solute, owing to their structure. Distilled water will be referred to as water in the following text. Water mixed with glycerol will form a solution owing to the fact that they are all polar

elements with hydroxyl groups. Figure 44 and Figure 45 show the structures of glycerol and water, the hydroxyl groups are indicated in the red dashed blocks. The viscosity, density and surface tension for the different glycerol-water solutions were not calculated theoretically, owing to the high error margin but were rather determined practically using a viscometer and tensiometer (Cheng, 2008).

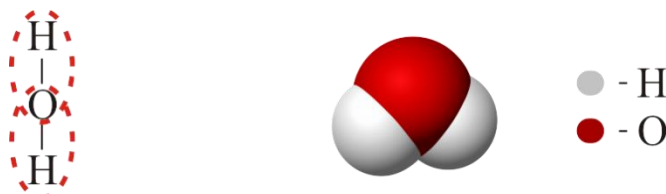


Figure 44. Water 2D and 3D structural formula

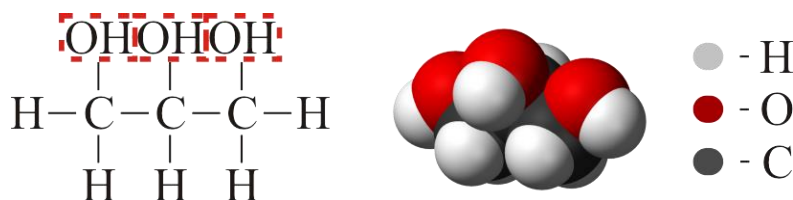


Figure 45. Glycerol 2D and 3D structural formula

The following methods were used to determine the viscosity, density and surface tension of the different glycerol-water solutions:

#### 4.3.1. Viscosity and density measurement

The device used to determine the viscosity of a fluid is known as a viscometer. Many studies have been done to find methods to accurately determine the viscosity of fluids. The main measurement methods are the Rotational, Capillary, Vibratory and Ultrasonic methods (Kazys and Rekuviene, 2011). The viscosity and density of the different glycerol mixtures were determined using an Anton Paar SVM 3000 rotational viscometer due to its high accuracy. The SVM 3000, shown in Figure 46, uses the Stabinger and oscillating U tube method to determine a fluid's density as well as its kinematic and dynamic viscosity. The Stabinger measuring principle is shown in Figure 47. The Stabinger measuring method consists of a copper housing,

an outer tube and a lightweight rotor. Within the copper housing the outer tube, filled with the sample fluid, rotates at a constant speed.



**Figure 46. Anton Paar SVM 3000 viscometer**

A lightweight rotor containing magnets floats in the sample fluid. The rotor will start to turn due to the shear force of the sample fluid; it will also be centred in the outer tube owing to its low density and centrifugal forces. By using the speed difference between the rotating rotor and outer tube the dynamic viscosity can be calculated. The speed of the rotor is determined by means of a hall-effect sensor, thus there is no physical connection to the rotor (Paar, 2013).

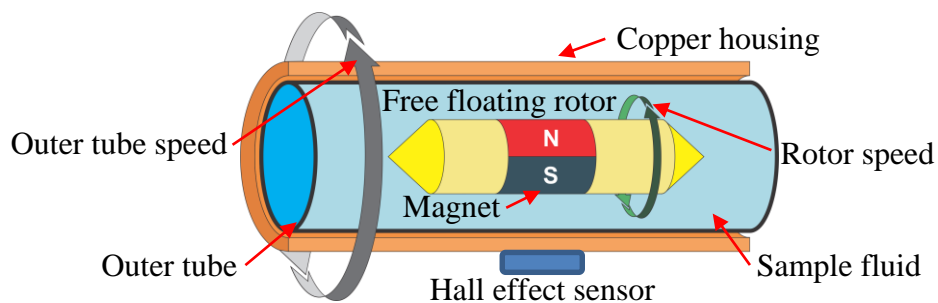


**Figure 47. Stabinger measuring principle**

The density of a fluid, or gas, can be determined by its resonance frequency, which can be obtained using the oscillating U tube method. The oscillating U tube method, as demonstrated in Figure 48, consists of a cantilever mounted U tube, mounting base, permanent magnets and inductor coils. The U tube is usually made out of glass

or stainless steel, which is mounted onto a base. A Pair of permanent magnets are bracketed onto the U tube, which extends through two inductor coils. Alternating current (AC) is fed to one of the coils, which will cause a magnetic field around the coil. The permanent magnet, which extends through the inductive coil, will start to swing due to the generated magnetic field. This will cause the U tube to vibrate at a certain frequency, however the frequency can be adjusted by changing the supply AC frequency.

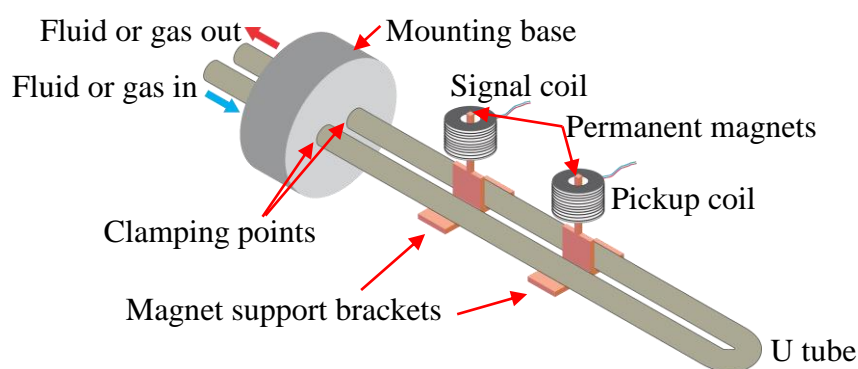


**Figure 48. Oscillating U tube method**

An AC signal will be introduced in the second coil due to the swing of the permanent magnet through the second inductive coil. The AC signal introduced in the second inductor coil can be used to determine if the U tube is at its resonance oscillating frequency. The resonance frequency is inversely proportional to the square root of the summed up mass of the tube and its contents from the clamping points onwards. Thus the density of a fluid or gas can be determined from a one-time fill sample or a circulating sample (Hebra, 2010: 237-238). As mentioned in Chapter 2, the temperature will have an effect on the viscosity and density of a fluid, thus the temperature of the solutions must be kept constant through all of the experiments. The solution's temperature can be controlled by the viscometer. The temperature of the solutions was set to lab temperature which in this case was 20°C.

Using a syringe a 5 ml fluid sample was taken from a solution. However it must be ensured that there are no air bubbles present in the sample, as this would cause an incorrect viscosity and density reading. The syringe was connected to the filling

support connector, which is connected to the viscometer's density and viscosity measuring cells. By gently pushing the syringe plunger rod down, the fluid sample enters the measuring cells. The measuring cell's fluid outputs are connected to a waste tank, thus when the fluid sample enters the waste tank the measuring cells will be filled with the fluid sample. When the measuring cells were filled with the fluid sample the measuring cycle was started. It took 5 minutes to complete a measuring cycle, which determined the kinetic viscosity, dynamic viscosity and density of a fluid sample and the results would be displayed on the LCD screen. In order to prepare for the next fluid sample the measuring cells must be rinsed and dried to ensure the previous fluid sample would not affect the readings of the current sample. The necessary steps used to rinse and dry the measuring cells were:

1. Firstly an air source was connected to the filling support connector to push the solution out of the measuring cells and into the waste tank.
2. Acetone was then supplied to the measuring cells to dissolve all of the remaining solution.
3. The air source was then used to push the acetone-solution mixture into the waste tank and was also used to speed up the evaporation process of the remaining acetone-solution mixture. It took 1 min for the acetone-solution to evaporate. Once the density returned to 0 all of the acetone-solution had evaporated.

#### **4.3.2. Surface tension measurement**

The surface tensions of the different fluid samples were determined by using an Optical Contact Angle (OCA) measuring device, manufactured by Dataphysics. The OCA 20 can be used to determine the following: fluid static contact angle, fluid dynamic contact angle, fluid surface tension, material surface energy and dispersion of polar contributions of surface free energy (Maier, 2002: 7). The main components of the OCA, demonstrated in Figure 49, are a video camera, light source, syringe (filled with the sample fluid), dosage needle and an electronic dispensing unit. In order to obtain the surface tension, of a fluid, the pendant drop-method was used. Using the pendant drop-method the syringe is filled with the sample fluid, however it

must be ensured that there are no air bubbles present in the fluid as this can cause an incorrect surface tension reading.

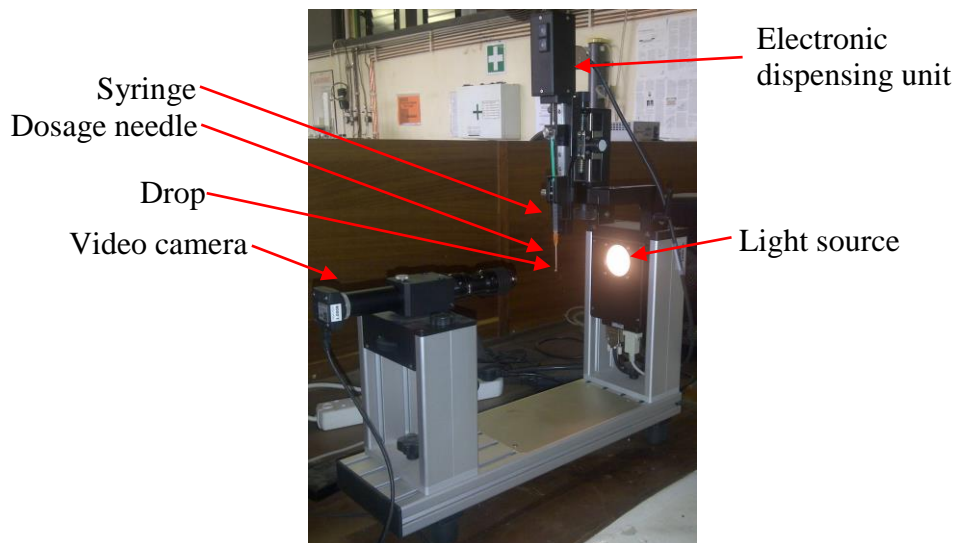


**Figure 49. Optical contact angle instrument**

A dosage needle with a specific size is then connected to the syringe's tip. The electronic dispensing unit will press down on the syringe's plunger rod, which will cause a drop to form out of the lower end of the dosing needle. The drop is monitored with the video camera, which is connected to the OCA Personal Computer (PC) software. The image of a drop, on the OCA software, can be seen in Figure 50.

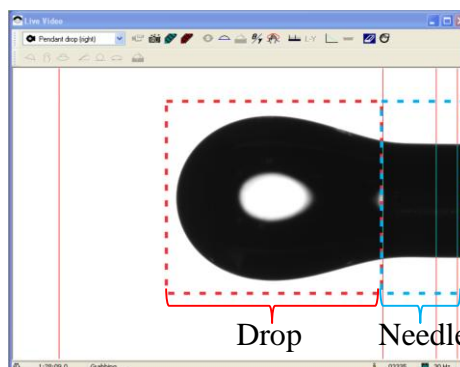


**Figure 50. Live view of drop**

The shape of the drop will depend on two forces namely: the gravitation force and the surface tension of the fluid. Thus the surface tension of a fluid can be

mathematically determined by using the Young-Laplace equation on the drop shape. Two parameters must be defined in the OCA PC software to calculate the surface tension of a fluid namely: the fluid's density and the outer diameter size of the dosage needle. The dosage needle's outer diameter is used as a reference to determine the actual size of the droplets (Maier, 2002: 71-72). The following steps were followed to analyse the fluid samples:

1. Using the syringe 5 ml was taken from the fluid sample. A 0.165 mm dosage needle was then attached to the syringe's tip. The syringe and dosage needle were then placed into the electronic dispensing unit.
2. The electronic dispensing unit was triggered via the OCA software to dispense a drop. The surface tension was calculated at the maximum drop size. If the drop size exceeds the maximum drop size it would detach from the dosage needle.
3. After the sample was analysed the syringe and dosage needle were disposed of to prevent contamination of the fluid samples, which would affect the surface tension readings.

#### **4.4. Glycerol solution properties**

Different viscosity, density and surface tension combinations were obtained using different ratios of glycerol-water mixtures. The initial glycerol-water solution was mixed 15% glycerol and 85% water, after which the % glycerol increased by 5% increments to a maximum of 80%. As the % glycerol increased the % water decreased by 5% decrements to a minimum of 20%. The change in the surface tension, density and viscosity of the different glycerol-water solutions can be seen in Table 6.

Using the data in Table 6 a graph of the % v/v glycerol against the viscosity and density was plotted and can be seen in Figure 51. As seen in the graph, the plot of the % v/v glycerol against the density can be classified as a linear plot whereby the plot of the % v/v glycerol against the viscosity can be classified as a non-linear plot.

**Table 6. Fluid properties of glycerol-water solutions**

% v/v Glycerol	Solution volume (ml)	Viscosity (mPa.s)	Density (g/cm <sup>3</sup> )	Surface tension (mN/m)
15	500	1.63	1.03	70.84
20	500	1.88	1.05	70.52
25	500	2.32	1.06	70.15
30	500	2.47	1.07	69.34
35	500	3.76	1.09	68.67
40	500	4.17	1.10	68.4
45	500	6.20	1.12	68.3
50	500	7.90	1.13	67.85
55	500	11.46	1.15	67.4
60	500	15.26	1.16	66.8
65	500	20.35	1.17	66.5
70	500	26.27	1.18	66.08
75	500	57.78	1.20	65.44
80	500	76.94	1.21	65.12

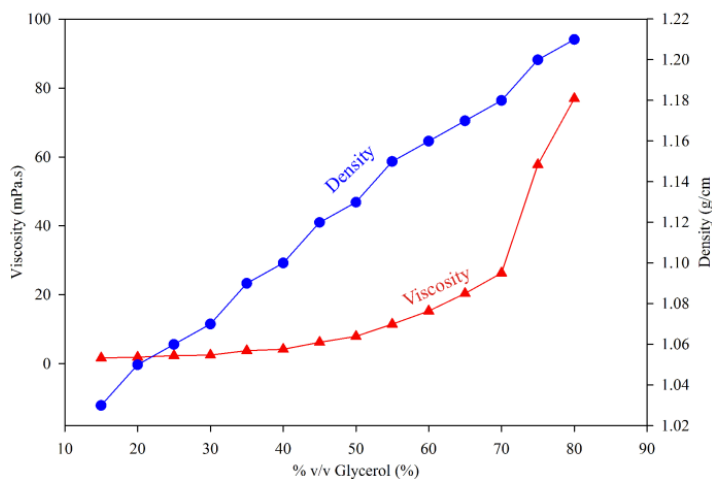


**Figure 51. % v/v glycerol vs. viscosity and density**

A statistical analysis, using CurveExpert, was done on the density and viscosity plot, seen in Figure 51, to determine the mathematical relationship between the % glycerol

and the solution's density and viscosity. The mathematical relationship for the two plots is given in Eq. 21 and Eq. 22.

$$y(x) = 0.0028 \cdot x + 0.99$$

$$\therefore \text{Density} = 0.0028 \cdot (\% \text{ v/v glycerol}) + 0.99 \quad \text{Eq. 21}$$

$$y(x) = 0.53 \left( 1 + \frac{0.15 \cdot x}{-22.98} \right)^{-6.67}$$

$$\therefore \text{Viscosity} = 0.53 \left( 1 + \frac{0.15 \cdot (\% \text{ v/v glycerol})}{-22.98} \right)^{-6.67} \quad \text{Eq. 22}$$

Using the data in Table 6 the graph % v/v glycerol against the surface tension was plotted as can be seen in Figure 52. As seen in the graph the plot can be classified as a linear plot. A statistical analysis was also done on the % v/v glycerol vs. surface tension plot to determine the mathematical relationship between the surface tension and the % glycerol mixture (in the glycerol-water solution) and can be seen in equation Eq. 23.

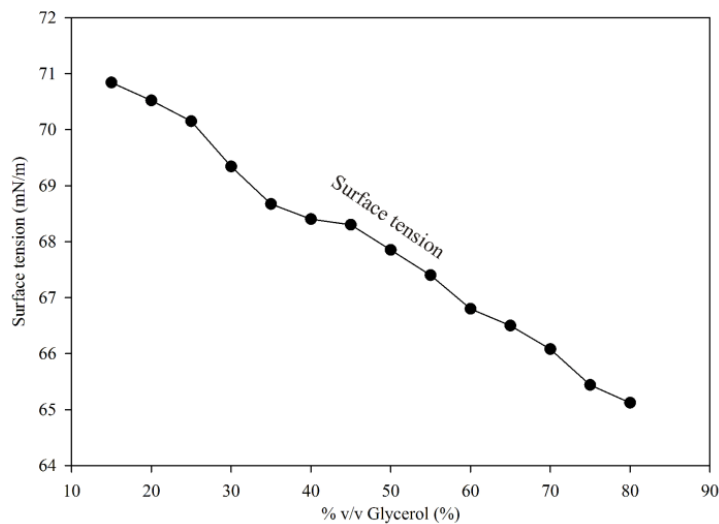


**Figure 52. % v/v glycerol vs. surface tension**

$$y(x) = -0.088 \cdot x + 72.12$$

$$\therefore \text{Surface tension} = -0.088 \cdot (\% \text{ v/v glycerol}) + 72.12 \quad \text{Eq. 23}$$

#### 4.5. Theoretical analysis

Using the different glycerol-water solutions the various Ohnesorge number, critical Weber number, critical pressure and critical time values were calculated for each of the three nozzles orifice diameter sizes, using the formulas given in Chapter 2. Except for the different nozzle orifice diameter sizes the nozzle geometry parameters remained constant throughout all of the calculations. The nozzle geometry includes the channel length, nozzle length and chamber diameter or shape. The different nozzle orifice diameter sizes were 0.127 mm, 0.191 mm and 0.254 mm, while the channel length and diameter were 16.5 mm and 0.75 mm respectively. The theoretically calculated Ohnesorge number, critical Weber number, critical pressure and critical time values for the 15% v/v glycerol solution, using a nozzle orifice diameter size of 0.127 mm, are demonstrated below:

$$\begin{array}{lll} \eta = 0.00163 & D_c = 0.00075 & Cl = 0.0165 \\ \rho = 1030 & \sigma = 0.07084 & D_n = 0.000127 \end{array}$$

$$\begin{aligned} Oh &= \frac{\eta}{\sqrt{\rho \cdot D_n \cdot \sigma}} \\ &= \frac{0.00163}{\sqrt{1030 \cdot 0.000127 \cdot 0.07084}} \\ &= 0.017 \end{aligned} \quad \text{Eq. 24}$$

$$\begin{aligned} We_{critical} &= 12 \cdot (1 + 1.077 Oh^{1.6}) \\ &= 12 \cdot (1 + 1.077 \frac{\eta^{1.6}}{\sqrt{\rho \cdot d \cdot \sigma}}) \\ &= 12.019 \end{aligned} \quad \text{Eq. 25}$$

$$\begin{aligned} P_{critical} &= \frac{32 \cdot \eta \cdot l \cdot (D_{nozzle})^2}{(D_{channel})^4} \cdot \sqrt{\frac{We_{critical} \cdot \sigma}{D_{nozzle} \cdot \rho}} + \frac{6 \cdot \sigma}{D_{nozzle}} + \frac{1}{2} \cdot \frac{We_{critical} \cdot \sigma}{D_{nozzle}} \\ &= 6.811 \text{ kPa} \end{aligned} \quad \text{Eq. 26}$$

$$t_{critical} = \frac{2}{3} \cdot \sqrt{\frac{(D_{nozzle})^3 \rho}{We_{critical} \cdot \sigma}}$$

Eq. 27

$$= 33.19 \text{ } \mu s$$

The theoretically calculated Ohnesorge number, critical Weber number, critical pressure and critical time values for each of the different glycerol-water solutions, using the three nozzle orifice diameters, are shown in Table 7.

**Table 7. Theoretical control parameters**

% v/v Glycerol (%)	Nozzle orifice size (mm)	Ohnesorge number	Weber number	p critical (kPa)	t critical ( $\mu s$ )
15	0.127	0.017	12.01	6.81	33.19
	0.191	0.014	12.014	4.66	61.22
	0.254	0.012	12.01	3.66	93.9
20	0.127	0.019	12.02	6.79	33.58
	0.191	0.016	12.01	4.66	61.94
	0.254	0.014	12.01	3.69	95.01
25	0.127	0.024	12.03	6.79	33.81
	0.191	0.019	12.02	4.7	62.38
	0.254	0.017	12.01	3.75	95.69
30	0.127	0.025	12.03	6.72	34.16
	0.191	0.021	12.02	4.66	63.04
	0.254	0.018	12.02	3.74	96.69
35	0.127	0.039	12.07	6.75	34.6
	0.191	0.031	12.05	4.78	63.87
	0.254	0.027	12.04	3.94	97.99
40	0.127	0.043	12.08	6.75	34.81
	0.191	0.035	12.06	4.81	64.26
	0.254	0.03	12.04	4	98.6

% v/v Glycerol (%)	Nozzle orifice size (mm)	Ohnesorge number	Weber number	p critical (kPa)	t critical ( $\mu$ s)
45	0.127	0.063	12.15	6.89	35.05
	0.191	0.051	12.11	5.05	64.75
	0.254	0.044	12.08	4.37	99.4
50	0.127	0.08	12.22	6.98	35.21
	0.191	0.065	12.16	5.23	65.12
	0.254	0.057	12.13	4.66	100
55	0.127	0.116	12.40	7.21	35.38
	0.191	0.094	12.29	5.64	65.56
	0.254	0.082	12.23	5.28	100.8
60	0.127	0.154	12.67	7.46	35.36
	0.191	0.125	12.46	6.07	65.68
	0.254	0.109	12.37	5.95	101.1
65	0.127	0.205	13.02	7.87	35.07
	0.191	0.167	12.73	6.71	65.4
	0.254	0.145	12.58	6.89	100.9
70	0.127	0.264	13.53	8.37	34.66
	0.191	0.215	13.10	7.47	64.76
	0.254	0.187	12.88	8	100.5
75	0.127	0.579	17.38	11.82	30.99
	0.191	0.472	15.88	12.27	59.79
	0.254	0.409	15.09	14.69	94.07
80	0.127	0.769	20.49	14.43	28.73
	0.191	0.627	18.12	15.72	56.34
	0.254	0.544	16.87	19.37	89.55

As discussed in Chapter 2, the critical Weber number is used to calculate the correct condition for drop breakup. Thus theoretically if the Weber number surpasses the critical Weber number, droplet breakup will occur. However one of the shortcomings

of the Weber number is its independence of the fluid's viscosity, thus the Ohnesorge number is used. As can be seen in section 2.4.3, the Ohnesorge number only reflects on the properties and size of the droplets formed and does not take the driving conditions into consideration. According to the findings of Reis, Ainsley and Derby (2005), an adequate drop formation process will occur at Ohnesorge numbers between 0.1 and 1, as can be seen in Table 4. Thus theoretically if the Ohnesorge number falls between 0.1 and 1 an adequate drop formation process will occur, these limits can serve as the minimum and maximum limits.

From the data in Table 7 it was noticed that an increase in the Ohnesorge number caused an increase in the critical pressure. It was also observed that the increase in the Ohnesorge number caused an increase in the critical time up to a certain point, where if that point was exceeded the critical time decreased. Two graphs were plotted to determine the relationship between the Ohnesorge number and the critical pressure and critical time. A statistical analysis, using CurveExpert, was done for both these graphs to determine their mathematical relationship. The plot of the Ohnesorge number against the critical pressure for all three nozzles orifice sizes can be seen in Figure 53.

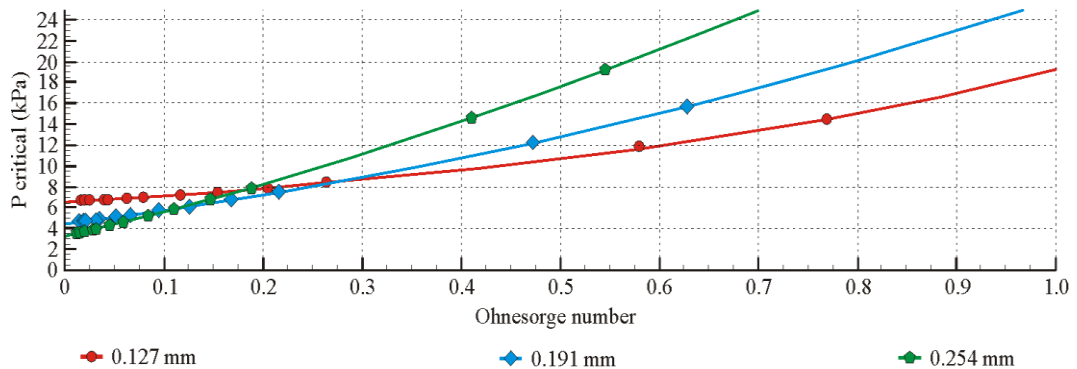


**Figure 53. Ohnesorge number vs p critical**

The hyperbolic decline model mostly fitted on the Ohnesorge number vs. critical pressure plots for all three nozzle orifice diameter sizes. The mathematical relationship for nozzle orifice diameters 0.127, 0.191 and 0.254 mm can be seen in

Eq. 28, Eq. 29 and Eq. 30. The hyperbolic decline model for all three nozzles is shown in Figure 54, using the red, blue and green lines.

$$y(x) = 6.54 \cdot \left(1 + \frac{(0.33 \cdot x)}{-1.10}\right)^{\left(\frac{-1}{0.33}\right)}$$

$$\therefore P_{critical(0.127)} = 6.54 \cdot \left(1 + \frac{(0.33 \cdot Oh)}{-1.10}\right)^{\left(\frac{-1}{0.33}\right)} \quad \text{Eq. 28}$$

$$y(x) = 4.42 \cdot \left(1 + \frac{(-0.46 \cdot x)}{-0.36}\right)^{\left(\frac{-1}{-0.46}\right)}$$

$$\therefore P_{critical(0.191)} = 4.42 \cdot \left(1 + \frac{(-0.46 \cdot Oh)}{-0.36}\right)^{\left(\frac{-1}{-0.46}\right)} \quad \text{Eq. 29}$$

$$y(x) = 3.37 \cdot \left(1 + \frac{(-0.71 \cdot x)}{-0.16}\right)^{\left(\frac{-1}{-0.71}\right)}$$

$$\therefore P_{critical(0.254)} = 3.37 \cdot \left(1 + \frac{(-0.71 \cdot Oh)}{-0.16}\right)^{\left(\frac{-1}{-0.71}\right)} \quad \text{Eq. 30}$$

Using the data in Table 7 the plot of the Ohnesorge number against the critical time, for all three nozzle diameter sizes can be seen in Figure 54. The mathematical model that mostly fitted all three of the plots was the Hoerl model. The Hoerl model for all three nozzles is demonstrated, using red, blue and green lines.

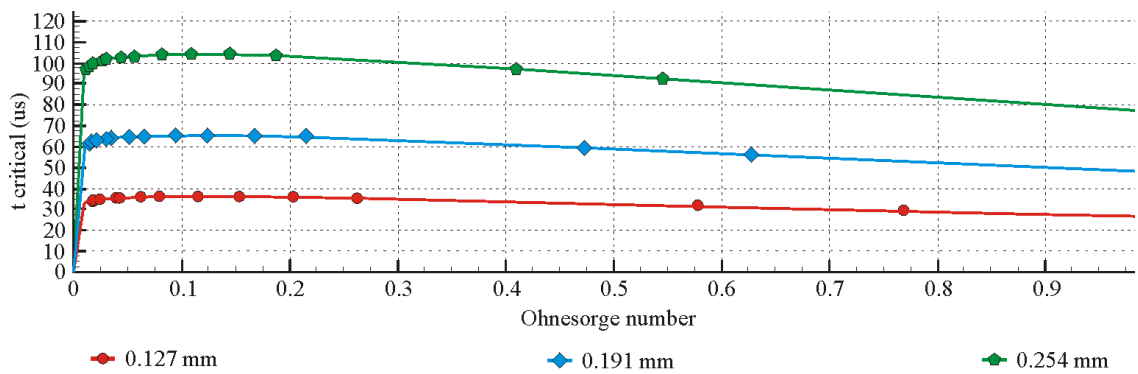


**Figure 54. Ohnesorge number vs. t critical**

The mathematical relationship of the Ohnesorge number vs. critical time for nozzle orifice diameters 0.127, 0.191 and 0.254 mm can be seen below:

$$y(x) = (42.38 \cdot 0.62^x) \cdot x^{0.057}$$

$$\therefore t_{critical(0.127)} = (42.38 \cdot 0.62^{oh}) \cdot oh^{0.057} \quad \text{Eq. 31}$$

$$y(x) = (77.98 \cdot 0.62^x) \cdot x^{0.054}$$

$$\therefore t_{critical(0.191)} = (77.98 \cdot 0.62^{oh}) \cdot oh^{0.054} \quad \text{Eq. 32}$$

$$y(x) = (119.68 \cdot 0.62^x) \cdot x^{0.052}$$

$$\therefore t_{critical(0.254)} = (119.68 \cdot 0.62^{oh}) \cdot oh^{0.052} \quad \text{Eq. 33}$$

#### 4.6. Summary

In Chapter 4, fourteen test solutions were prepared in order to determine the effect which the fluid properties have on the drop formation process. The test solutions consisted of different glycerol-water mixtures. The initial glycerol-water solution was mixed 15% glycerol and 85% water, where after the % glycerol increased by 5% increments to a maximum of 80%. As the % glycerol increased the % water decreased by 5% decrements to a minimum of 20%. The different solutions' fluid properties were not determined theoretically owing to the large error margin. The fluid properties were rather determined practically using a viscometer and tensiometer. The results showed that an increase in the glycerol mixture caused an increase in the solution's viscosity and density and a decrease in the surface tension. The Ohnesorge number was determined for each solution in order to determine the effect which the fluid properties have on the drop formation process. The Ohnesorge number was plotted against the theoretically calculated pressure and time.

In Chapter 5, it is determined whether the theoretically calculated critical time and pressure could be used practically with the more RPH to obtain an adequate drop formation process.

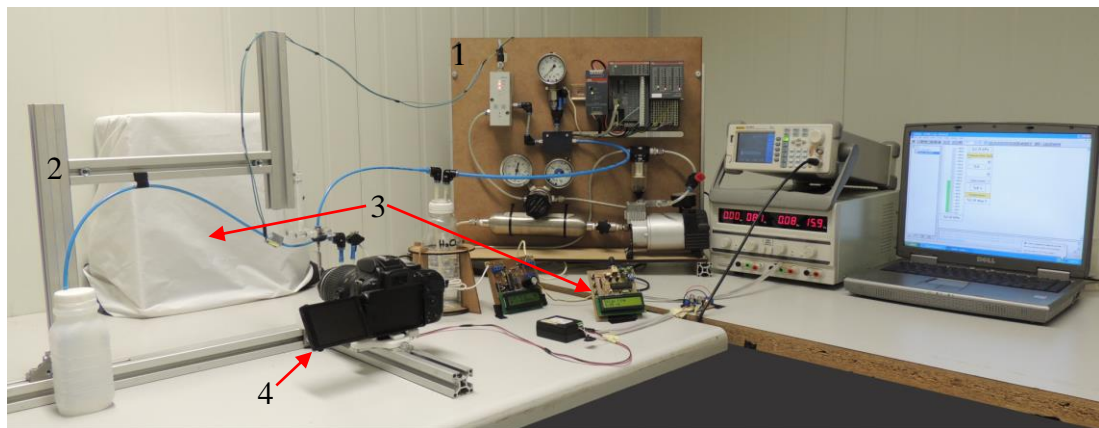
## Chapter 5 Experimentation and results

### 5.1. Introduction

In this chapter, it is determined whether the theoretically determined control parameters could be used practically with the RPH. The RPH control parameters would also be determined using a practical approach. The theoretically determined control parameters would be compared against the practical determined control parameters.

### 5.2. Experimental setup

The experimental setup used to test and determine practically the control parameters for the RPH is shown in Figure 55.



1. RPH experimental setup	3. Flash and delayed trigger unit
2. Camera and nozzle rig	4. Macrophotography rig

Figure 55. Experimental setup

Using the experimental setup shown in Figure 55, a photo of a dispensed droplet could be taken. This was done to determine the effects which the fluid properties, nozzle orifice diameter sizes and control parameters have on the drop formation process. The experimental setup consisted of:

- The RPH (addressed in section 3.3),

- the macrophotography rig,
- the flash & flash delayed trigger unit and
- the camera and nozzle rig.

Each of these components, except the RPH setup, will be discussed below:

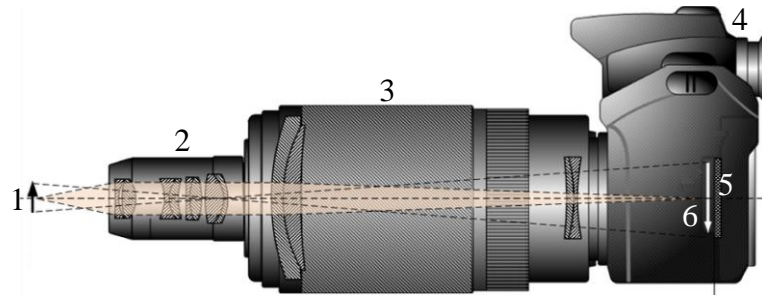
### **5.2.1. Macrophotography rig**

Macrophotography can be defined as the art of taking a photo of a subject at a very short focal distance. Macrophotography can be used to take a photo of a phenomena, item or event, which cannot be seen with the naked eye, to be analysed at a later stage. The ratio of a subject on the film/sensor plate of the camera is known as the reproduction ratio. In macrophotography the reproduction ratio is known to be greater or equal to a ratio of 1:1. The reproduction ratio is also directly proportional to the magnification. There are a number of techniques which can be used to configure a Digital Single-Lens Reflex (DSLR) camera to be used in macro photography (Kamps, 2007:4). The most common macrophotography techniques include:

- Reversed-lens,
- Fixed macro lens,
- Extension tubes,
- Object-telephoto lens combinations.

Using the object-telephoto lens combination technique the reproduction ratio can easily be altered, by changing the objective lens which is represented by nr 2 in Figure 56. Thus it was decided to use the object-telephoto lens combination technique in this research. It was determined experimentally that using a Nikon D5100 DSLR camera, Nikkor 18-55 mm lens and an Olympus 4X microscope objective lens, which was connected in an Object-telephoto lens combination technique provided a sufficient reproduction ratio to be used in this research. The Nikkor 18-55 mm lens was adjusted to a focal length of 55 mm whereby an Olympus

4X microscope objective lens was connected to the front of the Nikkor lens by means of a lens adapter ring. The reproduction ratio, could be calculated using the Eq. 34.



1. Object size	4. Nikon DSLR camera
2. 4X microscope objective lens	5. CMOS sensor
3. 18-55 mm Nikon lens	6. Object size on CMOS sensor

**Figure 56. The object-telephoto lens combination technique**

The reproduction ratio of the macrophotography rig used, was calculated to be 1:1.09. The photo of the nozzle and droplet used for the calculation is demonstrated in Figure 57.

$$1: \frac{S_s}{O_s} \quad \text{Eq. 34}$$

Where:

$S_s \equiv$  Size of the object on the sensor (mm)

$O_s \equiv$  Actual size of the object

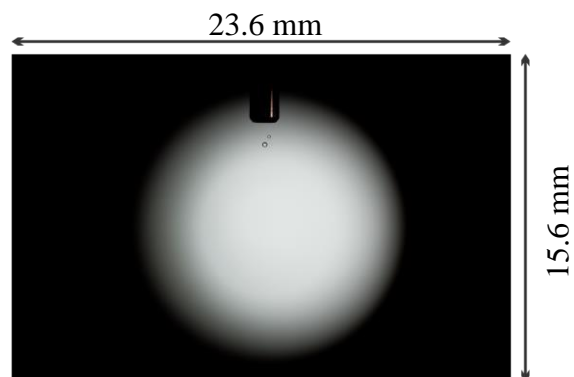


**Figure 57. Reproduction ratio**

The CMOS sensor size of the Nikon D5100 is 23.6 mm x 15.6 mm. Thus the original photo size will be 23.6 mm x 15.6 mm. The nozzle's diameter size was measured at 1.3 mm, whereas the nozzle diameter size in the photo was measured at 1.423 mm. A photo of the macrophotography rig used in this research can be seen in Figure 58.

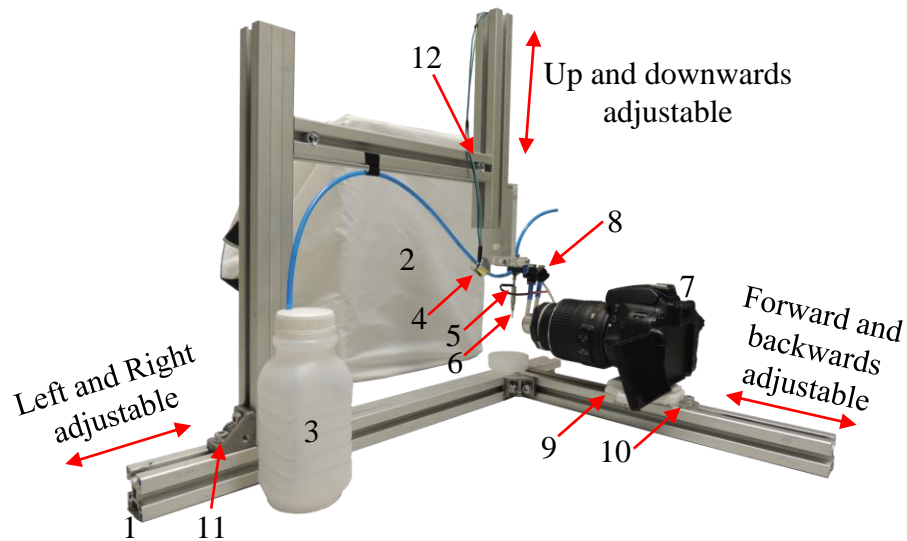


**Figure 58. Macrophotography rig**

### **5.2.2 Camera and nozzle rig**

In order to ensure that each of the droplet photos was taken at exactly the same angle, a camera and nozzle rig was constructed. The camera and nozzle rig was constructed using 25 mm extruded aluminum bars, which made it easy to assemble and adjust. The complete camera and nozzle rig can be seen in Figure 59. A camera saddle plate was custom-designed, using CAD, and was then 3D printed, using entry level FDM printers at the VUT I2P lab. The camera saddle was mounted onto the extruded aluminum, which ensured the camera stays at exactly the same orientation during the experiments. However the saddle could be adjusted forward and backwards by loosening the FB lock screw. The camera was adjusted forward/backwards to ensure the nozzle and droplets is in focus. The VHS valve connector was connected onto a Perspex plate which was connected to the extruded aluminum bar. The VHS valve was then connected to the VHS valve connector. The height of the VHS valve could be adjusted by loosening screw UD. Loosening screw UD enabled the extruded aluminum bar together with the Perspex holder, VHS valve connector and the VHS valve to move up or downwards. The height of the VHS valve was adjusted so that

only the nozzle tip could be seen in the top part of the photo. The VHS valve could also be adjusted sideways by loosening lock screw LR. This was done to ensure the VHS valve's nozzle is in the middle of the photo.



1.	25 mm extruded aluminum bar	7.	SLR Nikon camera
2.	Soft box	8.	MPX5700DP pressure sensor
3.	Purge tank	9.	Camera saddle plate
4.	Purge solenoid valve	10.	F/B lock screw
5.	VHS valve	11.	L/R lock screw
6.	Nozzle	12.	U/D lock screw

**Figure 59. Camera and nozzle rig**

In order for the droplets to be crisp and not blurry in the photo, the light source and the shutter speed of the DSLR camera had to be perfectly synchronized with each other. In order to avoid a synchronization problem between the shutter speed and light source, all of the photos were taken using the darkroom method. Using the dark room method, the shutter of the camera is left open. Owing to the lack of light no exposure would take place. The exposure time set on the camera just has to be long enough for the action to happen while the shutter is still open. A flash was then fired in order for the droplet to be exposed onto the DSLR camera's sensor. The flashlight duration will now become the actual exposure time. By using a soft box it was ensured that a diffused soft light was obtained. The flash was placed behind the soft box, which is seen in Figure 59.

### 5.2.3. Flash delay unit

By using a flash delay unit it was ensured that the flash fired at exactly the correct time in order to ‘freeze’ the droplet in the photo at the correct spot. The flash delay unit creates a time delay between the VHS valve’s supply signal and the flash firing signal. The delay time can also be adjusted using the flash delay unit seen in Figure 60. The flash delay unit will start the delay as soon as a rising edge is detected at the VHS valves supply signal. After the delay time has passed, a positive pulse will be generated which is supplied to the flash trigger input. A positive pulse on the flash trigger input would cause the flash to fire.

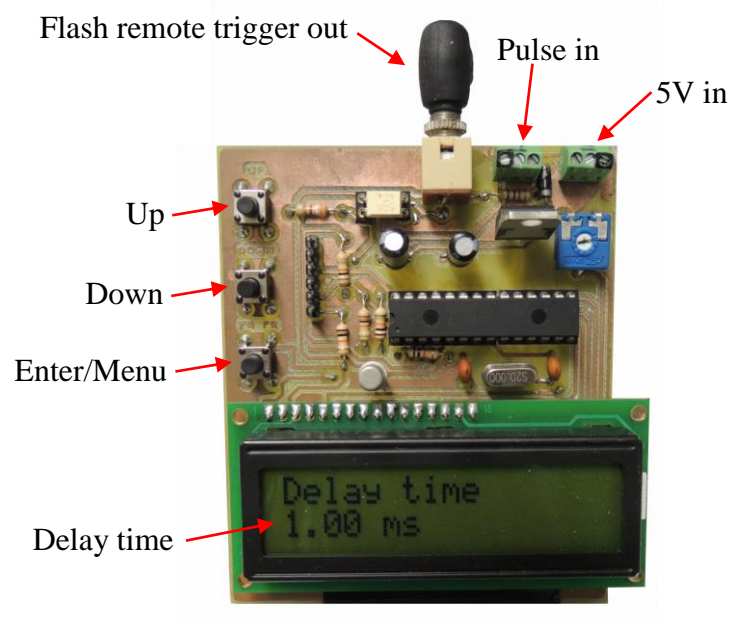


Figure 60. Delay unit PCB

The flash delay unit was controlled using a PIC18F2220 microcontroller. The circuit diagram of the flash delay unit can also be seen in Figure 61. Pressing the Enter/Menu button once, the time delay unit will go to the ms adjustment option. Pressing the Enter/Menu button again the unit will save the ms delay value and continue to the  $\mu$ s adjustment option. The  $\mu$ s delay value could then be saved by pressing the Enter/Menu buttons once more. At this stage the unit would be ready to provide the new desired time delay. When the time delay unit is in the  $\mu$ s or ms adjustment option the value could be adjusted either the up or down button. The total

delay time would be displayed on a 2x16 LCD display. The written firmware code for the PIC microcontroller can be seen in Annexure C.

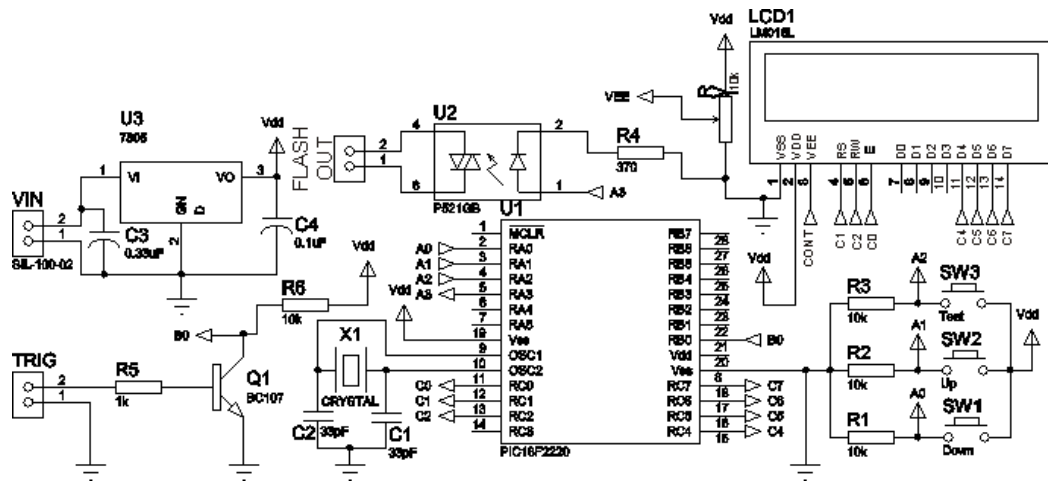


Figure 61. Flash trigger circuit

### 5.3 Practical critical pressures

As can be seen in section 4.5 all of the critical pressures and times were theoretically calculated to determine the required fluid pressure and maximum valve actuation time necessary to obtain drop formation for the RPH. As can be seen in Table 7 (on page 62), the actuation times varied from 28.73 to 101.1  $\mu$ s. According to the recommended VHS valve operating parameters, addressed in section 3.3.1, the recommended minimum valve pulse width is 416  $\mu$ s. This means that the VHS valve will not be able to work at the theoretically calculated critical times as the pulse width will be lower than the recommended minimum valve pulse width.

In the following experiment the critical pressures will be determined practically using the recommended minimum VHS valve pulse width. As the recommended minimum VHS valve pulse width is much higher than any of the calculated theoretically critical times, the pulse width supplied to the VHS valve remained constant while the fluid pressure was increased. This was done in order to determine the minimum fluid pressure required to obtain drop formation for each of the glycerol-water solutions and nozzle orifice diameter sizes. Although the practical

critical pressures values cannot be directly compared to the theoretically critical pressure values owing to the constant VHS valve pulse width used. However the practical critical pressure values for each of the glycerol-water solutions will be plotted onto a graph using the different nozzle orifice diameter sizes to determine if there are any similarities between the practical mathematical model and the theoretical mathematical model. The initial fluid pressure for each glycerol-water solution and nozzle orifice diameter sizes was 2 kPa and was increased by 2 kPa increments up to the point where multiple droplets were dispensed. According to the research of Tsai & Hwang (2008) an increase in the fluid pressure would cause an increase in the drop ligament. When the droplet ligament exceeds a certain length it will break away from the main droplet and satellite drops will form due to the Rayleigh breakup regime. However it must also be kept in mind that the droplet ligament length will depend on the fluid's properties. Although the research of Tsai and Hwang (2008) was on piezoelectric printing heads and not solenoid based printing heads, as used in this research, the behaviour of the dispensed fluid would still remain the same.

Pressure increments of 2 kPa were chosen owing to the pressure hysteresis of the VPPM electronic pressure regulator. Pressure increments smaller than 2 kPa would not readjust the VPPM electronic regulator's set point and would not adjust the output pressure. A 19.83 Hz square wave signal with an edge time of 5 ns, pulse amplitude of 5 V and a duty cycle of 0.83 % was supplied to the spike and hold unit by means of a signal generator. A 19.83 Hz square wave with a 0.83 % duty cycle results in a wave period of 50.416 ms and a pulse width of 416.6  $\mu$ s. The flash delay unit was triggered on the rising edge of the square wave supplied to the spike and hold unit. The delay duration of the flash delay unit differed between the different solutions. An increase in the drop velocity caused a decrease in the delay duration. A photo of a droplet was taken after 50 VHS valve supply pulses passed. This was done for the RPH to stabilize. The temperature of all the glycerol-water solutions was kept constant at 20°C throughout all of the experiments. An example of a complete pressure sweep using the 70% v/v glycerol solution with a nozzle orifice diameter size of 0.254 mm is shown in Figure 62. The flash delay unit was set to a 3 ms delay

for the entire sweep. As can be seen in Figure 62, drop formation only occurred at pressures of 68 kPa and above. The fluid pressures below 68 kPa were not sufficient to produce a droplet owing to the fluid properties. Although it can also be seen, that the main droplet splits up into a main and satellite droplet at pressures higher than 90 kPa.

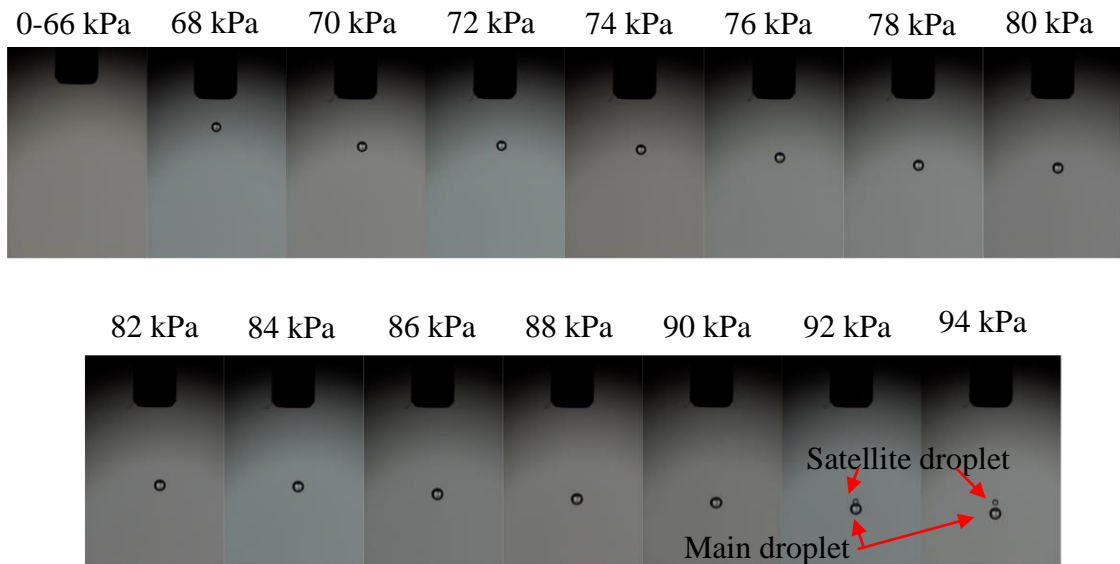


**Figure 62. 70% v/v glycerol pressure sweep with the 0.254 mm nozzle**

It was also noticed that an increase in the fluid pressure resulted in an increase in the main droplet's velocity and size. The size of the main droplet increased up to a point where it split into a main and satellite droplet. In order to compare the increase in the size of the droplets the volume for each of the droplets were calculated. The droplet volume could be calculated by using the following equation:

$$V = \frac{4}{3}\pi\left(\frac{D}{2}\right)^3 \quad \text{Eq. 35}$$

Where:

$V$   $\equiv$  Volume (l)

$D$   $\equiv$  Diameter of Droplet (m)

The physical diameter of each of the droplets could be determined by using the nozzle diameter as reference. The physical diameter of the nozzle was measured at a size of 1.3 mm, whereby the nozzle diameter measured in the photos was 1.319 mm using Corel Draw (**note:** the photos in Figure 62 are not the same size as the original photos due to the space limitation of the page size in this document, the original size of the photos are 23.6 mm x 15.6 mm). By taking the difference between the physical nozzle size and photo measured nozzle size into consideration a ratio of 0.986 was calculated. By using the calculated ratio the physical size of the droplets could be calculated by multiplying the ratio with the measured droplet diameter size in the photo. The following table shows the difference in droplet diameter and volume for each of the different pressures:

**Table 8. 70% v/v glycerol dispensed volumes**

Droplet	Measured droplet size (mm)	Ratio	Physical size (mm)	Dispensed volume (pl)
0-66	---	---	---	---
68	0.322	0.986	0,317	16.74
70	0.336	0.986	0,331	19.08
72	0.341	0.986	0,336	19.83
74	0.343	0.986	0,338	20.16
76	0.351	0.986	0,346	21.64
78	0.357	0.986	0,352	22.82
80	0.361	0.986	0,356	23.67
82	0.374	0.986	0,369	26.48
84	0.377	0.986	0,372	26.89
86	0.381	0.986	0,376	27.83
88	0.387	0.986	0,382	29.08
90	0.4	0.986	0,394	32
92	Main droplet (0.382) Satellite droplet (0.192)	0.986	0,377 0,189	31.48
94	Main droplet (0.380) Satellite droplet (0.197)	0.986	0,375 0,194	31.53

As can be seen in Table 8, an increase in the pressure of the glycerol-water solution caused an increase in the total volume dispensed from the nozzle using a constant pulse width.

A complete pressure sweep was done for each of the glycerol-water solutions and nozzle orifice diameter sizes. However the entire pressure sweep for each of the glycerol-water solutions and nozzle orifice diameter sizes will not be shown in the document due to the space constraint. Only the pressures at which the drop formations process started, which is also known as the practical critical pressure, will be shown. The practical critical pressure for all the glycerol-water solutions using nozzle orifice diameter sizes, 0.254, 0.191 and 0.127 mm, are shown in Figure 63 to Figure 65.

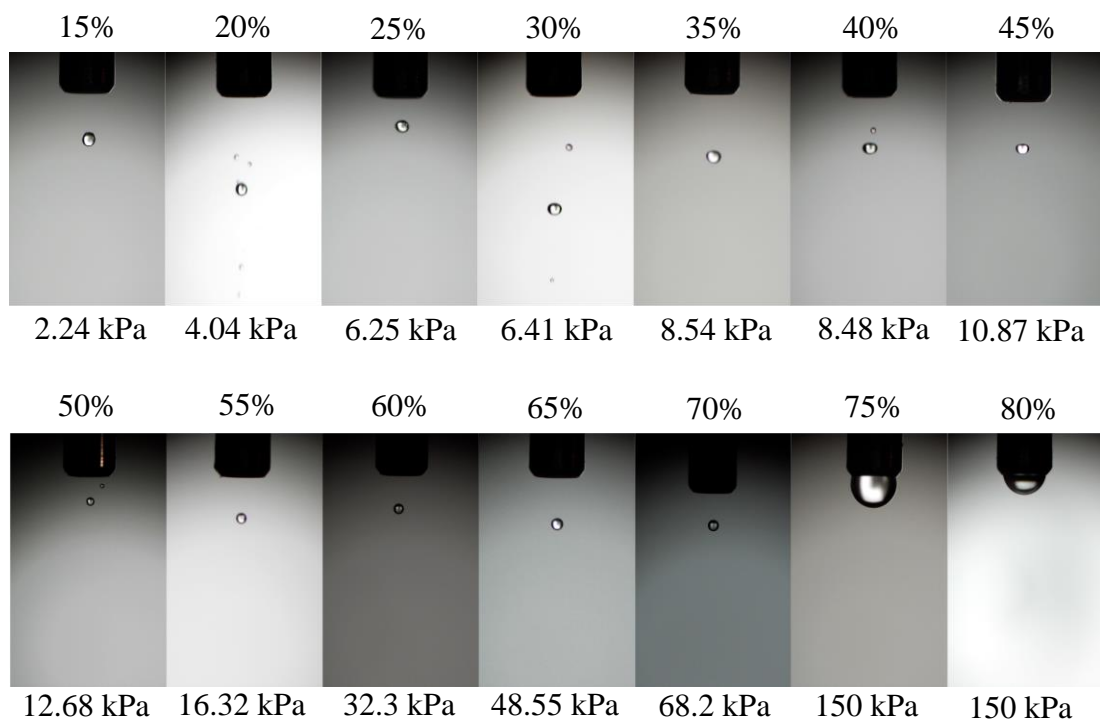


**Figure 63. Practical fluid pressures for 0.254 mm nozzle**

As can be seen in Figure 63, an increase in the % glycerol caused an increase in the practical critical pressure using a nozzle orifice diameter size of 0.254 mm. However no drop formation occurred at solutions 80 and 75 % v/v glycerol. The maximum

fluid pressure achievable in the experimental setup was used for these solutions. After 50 pulses, at which the photo was taken, only nozzle wetting occurred. For these solutions the mechanical work generated by the applied fluid pressure was not equal or larger to the total energy required for the drop formation process, which is explained in Section 2.6. The fluid pressures were measured on the inlet of the VHS valve, thus it may vary to the air regulator's output. All the parameters for the practical critical pressures, seen in Figure 63 are summarized in Table 9.

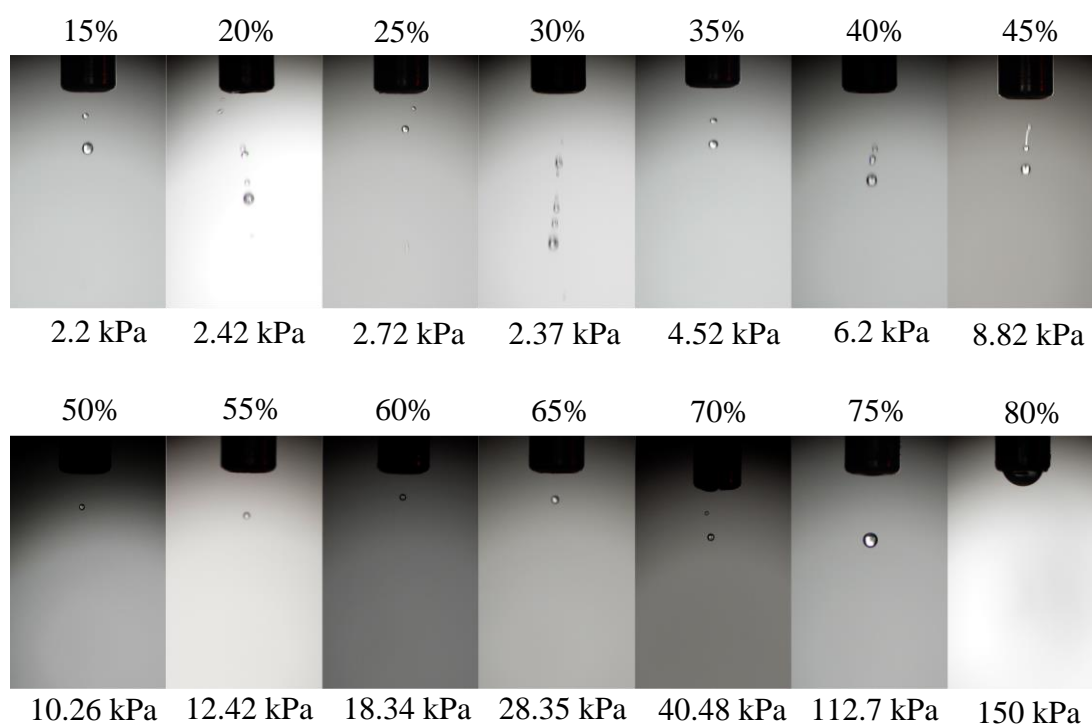


**Figure 64. Practical fluid pressures for 0.191 mm nozzle**

The results in Figure 64 showed that an increase in the % glycerol also caused an increase in the practical critical pressure, using a nozzle orifice diameter size of 0.191 mm. Only nozzle wetting occurred for the 80 % v/v glycerol solution at the maximum pressure achievable. The photo of the nozzle was also taken after 50 pulses. An explanation for not obtaining drop formation for the 80 % v/v glycerol solution would also be due to the insufficient mechanical work generated by the applied fluid pressure. All the parameters for the practical critical pressures, seen in Figure 64 are summarized in Table 9.

It was also determined using the results shown in Figure 65, that an increase in the % glycerol caused an increase in the practical critical pressure, using a nozzle orifice diameter size of 0.127 mm. It is also seen that only nozzle wetting occurred at solutions 75 and 80% v/v glycerol at a maximum pressure. The photos of the nozzle wetting for these solutions were also taken after 50 pulses. The possible explanation for this phenomenon would also be due to insufficient mechanical work generated by the applied fluid pressure. All of the parameters for the practical critical pressures, seen in Figure 65, can also be seen in Table 9.

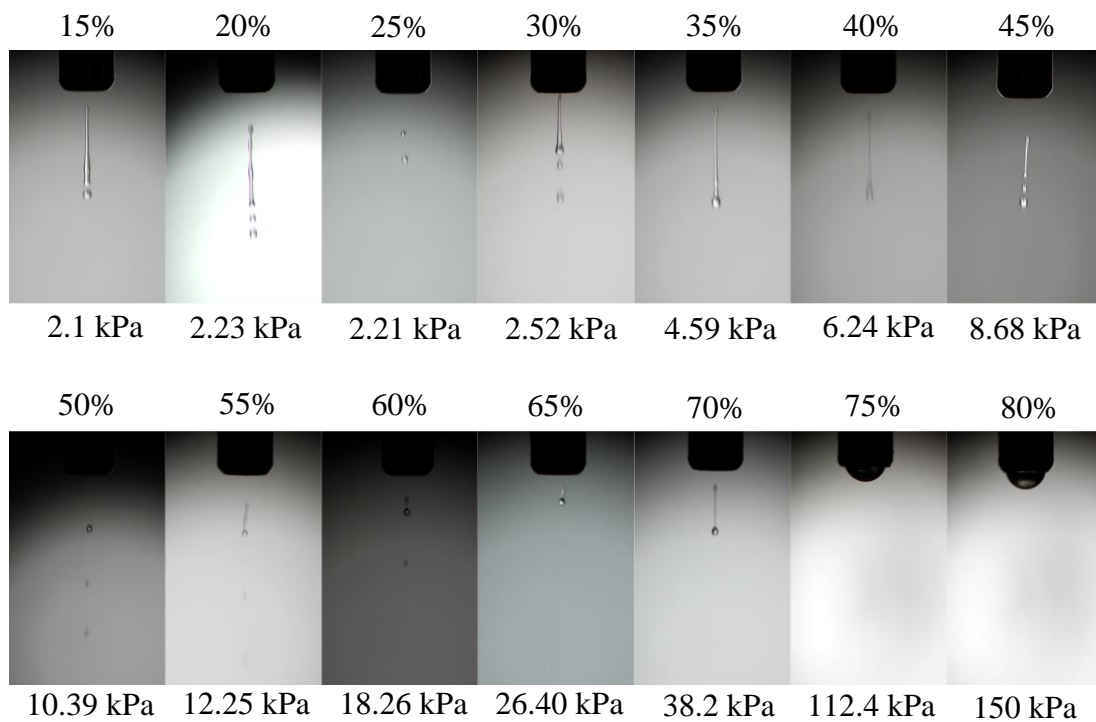


**Figure 65. Practical fluid pressures for the 0.127 mm nozzle**

As seen in Table 9 the VHS valve inlet fluid pressure of the different glycerol-water solutions were not the same as the desired pressure. This was due to the regulation pressure error of the electronic pressure regulator. The average pressure error rate of the electronic pressure regulator, using the data in Table 9 was calculated to be 0.31 kPa. All of the ‘VHS valve inlet fluid pressures’, given in Table 9, are also considered to be the practical critical pressure.

**Table 9. Practical critical fluid pressure**

% v/v Glycerol (%)	Nozzle orifice diameter size (mm)	Oh number	Valve pulse duration ( $\mu$ s)	Desired pressure (kPa)	Regulator's output pressure (kPa)	VHS valve inlet fluid pressure (kPa)
15	0.127	0.017	416.66	2	2.32	2.1
	0.191	0.014		2	2.7	2.2
	0.254	0.012		2	2.49	2.24
20	0.127	0.019	416.66	2	2.1	2.23
	0.191	0.016		2	2.25	2.42
	0.254	0.014		4	4	4.04
25	0.127	0.024	416.66	2	2.1	2.21
	0.191	0.019		2	2.6	2.72
	0.254	0.017		6	6.05	6.25
30	0.127	0.025	416.66	2	2.27	2.52
	0.191	0.021		2	2	2.37
	0.254	0.018		6	6.20	6.41
35	0.127	0.039	416.66	4	4.2	4.59
	0.191	0.031		4	4	4.52
	0.254	0.027		8	8.2	8.54
40	0.127	0.043	416.66	6	6.13	6.24
	0.191	0.035		6	6.1	6.2
	0.254	0.03		8	8.27	8.48
45	0.127	0.063	416.66	8	8.41	8.68
	0.191	0.051		8	8.6	8.82
	0.254	0.044		10	10.6	10.87
50	0.127	0.08	416.66	10	10.16	10.39
	0.191	0.065		10	10.09	10.26
	0.254	0.057		12	12.41	12.68

% v/v Glycerol (%)	Nozzle orifice diameter size (mm)	Oh number	Valve pulse duration ( $\mu$ s)	Desired pressure (kPa)	Regulator's output pressure (kPa)	VHS valve inlet fluid pressure
55	0.127	0.116	416.66	12	12.37	12.25
	0.191	0.094		12	12.5	12.42
	0.254	0.082		16	16.4	16.32
60	0.127	0.154	416.66	18	18.20	18.26
	0.191	0.125		18	18.27	18.34
	0.254	0.109		32	32	32.3
65	0.127	0.205	416.66	26	26.6	26.40
	0.191	0.167		28	28.5	28.35
	0.254	0.145		48	48.6	48.55
70	0.127	0.264	416.66	38	38.4	38.2
	0.191	0.215		40	40.67	40.48
	0.254	0.187		68	68.54	68.2
75	0.127	0.579	416.66	---	---	---
	0.191	0.472		112	112.3	112.7
	0.254	0.409		---	---	---
80	0.127	0.769	416.66	---	---	---
	0.191	0.627		---	---	---
	0.254	0.544		---	---	---

All of the practical critical pressures and the Ohnesorge numbers in Table 9 were analyzed using CurveExpert. This was done to determine whether the mathematical model of the practical critical pressures would correlate to that of the theoretical determined critical pressures. The hyperbolic decline mathematical model, which mostly fitted the Ohnesorge number vs critical pressure plot for all three nozzle orifice diameters in Section 4.5, were also used for the practical mathematical analysis. The plot, using the hyperbolic decline mathematical model, of the Ohnesorge number vs practical critical number for all three nozzle orifice diameter

sizes can be seen in Figure 66. As can be seen in Figure 66, the hyperbolic decline mathematical model fitted the curves for all three nozzle orifice diameter sizes. The mathematical relationship for nozzle orifice diameters 0.127, 0.191 and 0.254 mm can be seen below:

$$y(x) = 1.487 \cdot \left(1 + \frac{(-0.658 \cdot x)}{-0.024}\right)^{\left(\frac{-1}{-0.658}\right)}$$

$$\therefore P_{critical(0.127)} = 1.487 \cdot \left(1 + \frac{(-0.658 \cdot Oh)}{-0.024}\right)^{(1.52)} \quad \text{Eq. 36}$$

$$y(x) = 1.169 \cdot \left(1 + \frac{(-0.703 \cdot x)}{-0.014}\right)^{\left(\frac{-1}{-0.703}\right)}$$

$$\therefore P_{critical(0.191)} = 1.169 \cdot \left(1 + \frac{(-0.703 \cdot Oh)}{-0.014}\right)^{(1.422)} \quad \text{Eq. 37}$$

$$y(x) = 2.774 \cdot \left(1 + \frac{(-0.494 \cdot x)}{-0.024}\right)^{\left(\frac{-1}{-0.494}\right)}$$

$$\therefore P_{critical(0.254)} = 2.774 \cdot \left(1 + \frac{(-0.494 \cdot Oh)}{-0.024}\right)^{(2.024)} \quad \text{Eq. 38}$$

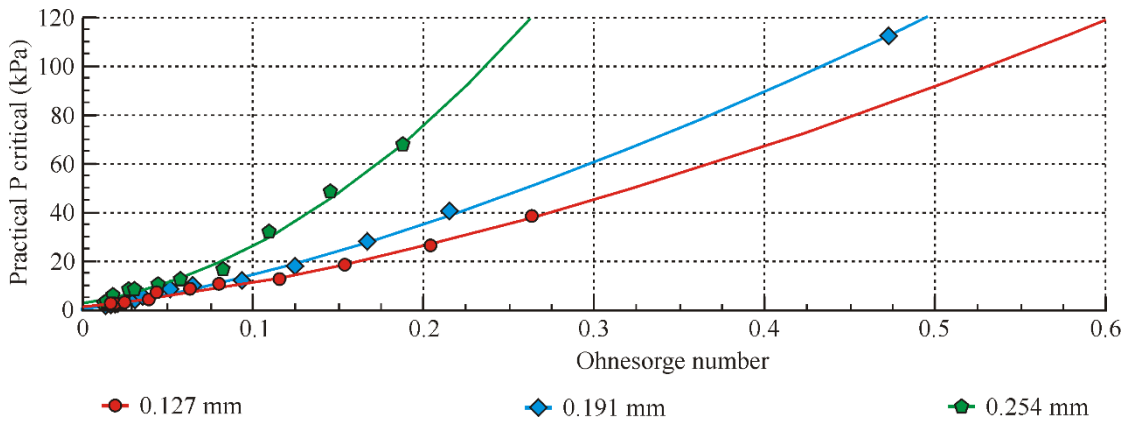


**Figure 66. Ohnesorge number vs. practical critical pressure**

Although the mathematical model of the theoretical critical pressures could be used for the practical critical pressures using a constant pulse width, the slopes between the practically determined graphs differed to that of the theoretically determined graphs.

## **5.4 Valve pulse width**

As mentioned previously the VHS valve manufacturer suggested minimum valve pulse width of 416.66  $\mu\text{s}$ , however it was discovered during the practical critical pressures experiments that the VHS valve is able to actuate at pulse widths lower than 416.66  $\mu\text{s}$ . However the minimum pulse width at which the VHS valve can operate will depend on the fluid's properties and pressure, owing to its mechanical actuation process. Thus the suppliers recommended 416.66  $\mu\text{s}$  as the minimum pulse width, to ensure that the VHS valve would be able to operate across a wide range of fluid properties. Assuming the VHS valve can operate at valve pulse widths lower than 416.66  $\mu\text{s}$ , the droplet size can then be changed, at a constant pressure, by changing the pulse width supplied to the VHS valve.

In the following experiment it would be determined whether the droplet size at the practical critical pressures, addressed in section 5.2.3, can be reduced to the same size as the nozzle orifice diameter size. The droplet diameter size must be equal to the orifice diameter size, in order to compare the practical results to that of the theoretical results given in Table 7. In the theoretical equation which was used to calculate the maximum time required for an adequate drop formation process, seen in Eq. 18, the droplet diameter was considered being equal to the nozzle orifice diameter. The following section will address two aspects namely:

- Whether the VHS valve can operate at pulse widths lower than the recommended 416  $\mu\text{s}$ .
- In case the VHS valve can operate at pulse times lower than 416  $\mu\text{s}$ , determining the practical critical times for each of the practical critical pressures to reduce the droplet's diameter to the same size as the nozzle orifice diameter size.

### **5.4.1 Minimum valve pulse width**

The following experiment was done to determine whether the VHS valve can operate at pulse widths lower than 416.66  $\mu\text{s}$ . In order to accomplish this water was pressurized at 100 kPa and a fixed nozzle orifice diameter size of 0.254 mm was selected. The pressure, for the water, and nozzle orifice diameter size were randomly

selected because the aim of this experiment is to determine if the VHS valve can operate at pulse widths lower than 416  $\mu\text{s}$  and not to determine whether fluid pressure or nozzle orifice size has an effect on the drop formation process. Water had a viscosity of 1.04 mPa.s, density of 0.998  $\text{g}/\text{cm}^3$  and a surface tension of 72 mN/m. The results obtained in this experiment are shown in Figure 67. The results showed, at pulse widths lower than 140  $\mu\text{s}$  no valve actuation occurred. However it was determined at pulse widths between 141 and 170  $\mu\text{s}$  valve actuation occurred, but not enough for drop formation to occur. The mechanical work at these pulse widths were not enough for drop formation thus only nozzle wetting occurred. It was also found at pulse widths higher than 170  $\mu\text{s}$  drop formation occurred due to sufficient valve actuation. This proved the VHS valve would be able to actuate at pulse widths lower than the specified 416.66  $\mu\text{s}$ . Although the VHS valve was able to operate at lower pulse widths, the minimum pulse widths were still much higher than the theoretically determined critical times.

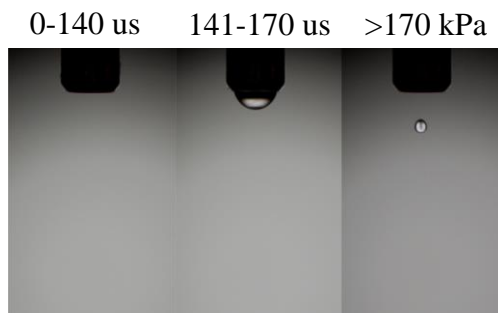


**Figure 67. VHS minimum pulse width**

#### **5.4.2 Practical critical time**

In the following experiment the practical critical times for each of the practical critical pressures and nozzle orifice diameter sizes will be determined. The practical critical time can be described as the pulse width, supplied to the VHS valve, where the droplet's diameter is the same as the nozzle orifice diameter, at the constant practical critical pressures. The temperature of all the glycerol-water solutions was kept constant at 20°C throughout all of the experiments, as an increase in the solution's temperature will result in a change in the fluid's properties. A square wave with a period of 50 ms, an edge time of 5 ns and pulse amplitude of 5 V was supplied

to the spike and hold unit by means of a signal generator. The initial pulse width of the square wave was 2  $\mu$ s and was increased by 2  $\mu$ s increments up to the point where satellite droplets occurred. However the period of the square wave remain constant while the duty cycle changed. After each pulse width increment, a photo was taken to determine the droplet diameter size. The flash delay unit was triggered on the rising edge of the square wave supplied to the spike and hold unit. The delay duration of the flash delay unit differed between the different glycerol-water solutions and nozzle orifice diameter sizes. An increase in the drop velocity caused a decrease in the delay duration. However the flash delay time was not specified, as drop velocity is not important in the following experiment. The practical critical pressure for each of the nozzle orifice diameter sizes and glycerol-water solutions are shown in Table 9. The practical critical pressure was entered into the PLC graphical user interface and was then considered as the desired pressure. The electronic pressure regulator will then regulate the output pressure according to the entered desired pressure. However owing to the electronic pressure regulator's regulation error, the regulated output pressure was not exactly the same as the entered desired pressure. All of the droplet diameter sizes were determined using the same method addressed in Section 5.3. A ratio was determined using the difference between the actual nozzle diameter size and the nozzle diameter size measured in the photo. The actual droplet diameter size was then determined by multiplying the ratio with the droplet diameter size measured in the photo. Corel Draw software was used to measure all of the nozzle and droplet diameters. The physical diameter of all three nozzles was measured at 1.3 mm. The actual droplet diameters for all of the different nozzle orifice diameter sizes and glycerol-water solutions were determined in this experiment. This was done to compare the actual droplet diameter size against the nozzle orifice diameter size. An example of a complete pulse width sweep done on a 35% v/v glycerol solution with a nozzle orifice diameter size of 0.191 mm are shown in Figure 68. The results seen in Figure 68 and the measured droplet diameters and the ratios are summarized in Table 10. The flash delay time was kept constant at 2 ms. However it must be kept in mind that the droplets were not measured using the photos in Figure 68. The dimensions of the photos, seen in this document were modified owing to the size constraint of the page.

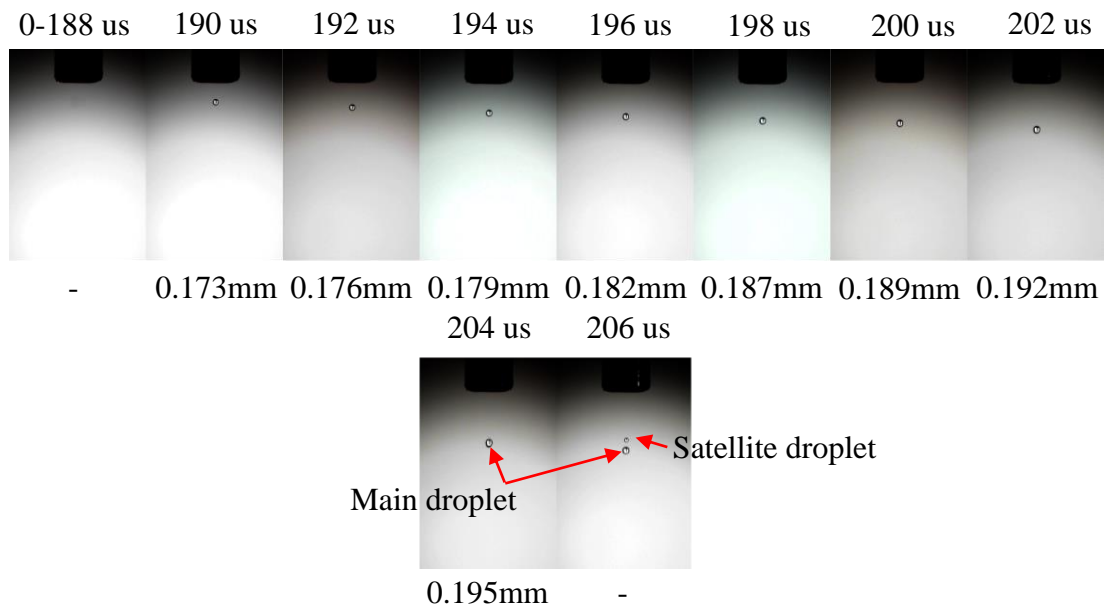


**Figure 68. 35% v/v glycerol time sweep using a 0.191 mm nozzle**

**Table 10. Droplet diameters**

Fluid pressure (kPa)	Pulse width ( $\mu$ s)	Photo measured droplet diameter (mm)	Ratio	Actual droplet diameter (mm)
4.50	0-188	(no droplet)	0.986	---
4.50	190	0.176	0.986	0.173
4.50	192	0.178	0.986	0.176
4.50	194	0.183	0.986	0.179
4.50	196	0.185	0.986	0.182
4.50	198	0.190	0.986	0.187
4.50	200	0.192	0.986	0.189
4.50	202	0.195	0.986	0.192
4.50	204	0.198	0.986	0.195
4.50	206	(multiple droplets)	0.986	---

As can be seen in Table 10, drop formation only occurred at pulse widths above 188 us. Although when the pulse width exceeded 204 us, satellite droplets occurred. This was due to the increase of the droplet ligament, which was addressed in Section 5.3.

The results also showed that an increase in the pulse width caused an increase in the actual drop diameter.

A complete pulse width sweep was done for each of the glycerol-water solutions and nozzle orifice diameter sizes. However the entire pulse width sweep, for each of the glycerol-water solutions and nozzle orifice diameter sizes, could not be shown in the document due to the space constraint. Only the pulse widths at which droplet diameter sizes were the same or closest to the used nozzle orifice diameter sizes, which is also known as the practical critical time, are shown. The practical critical times for all the glycerol-water solutions using nozzle orifices diameter sizes of 0.254, 0.191 and 0.127 mm are shown in Figure 69 to Figure 71. It must be kept in mind that the % v/v glycerol will have an effect on the Ohnesorge number, as previously discussed.

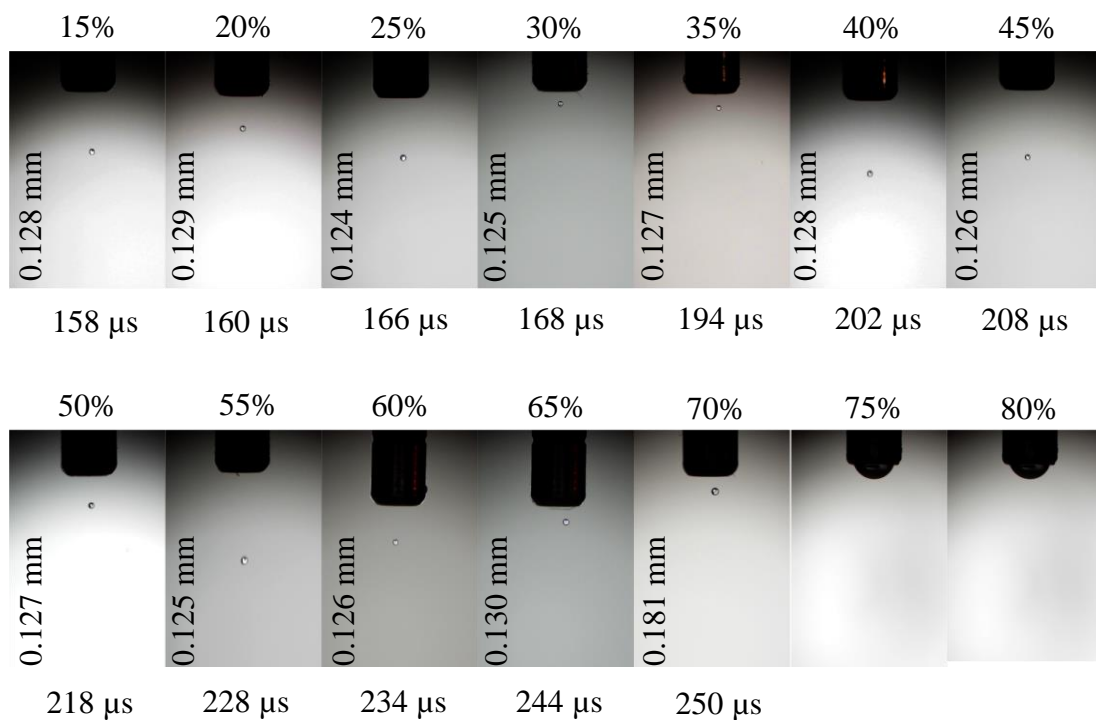


**Figure 69. Practical critical pulse widths for the 0.127 mm nozzle**

As can be seen in Figure 69, the increase in % glycerol caused an increase in the practical critical time using a nozzle orifice diameter size of 0.127 mm. It was also

determined that the droplet diameter sizes remained close to the nozzle orifice diameter size, except for solutions 70% to 80 v/v glycerol. The smallest droplet diameter size which could be obtainable for the 70% v/v glycerol solution was 0.181 mm using a pulse width of 250  $\mu$ s. At pulse widths lower than 250  $\mu$ s, either nozzle wetting occurred or no drop formation took place. For solutions 75% and 80% v/v glycerol, nozzle wetting or no drop formation occurred at lower pulse widths. However at higher pulse widths fluid exited the nozzle but the form of a fluid stream.

According to the results shown in Figure 70, the increase in % glycerol also caused an increase in the practical critical time using a nozzle orifice diameter size of 0.191 mm. All of the glycerol-water solution's droplet diameters remained close to that of the nozzle orifice diameters, except for solutions 70 to 80% v/v glycerol.

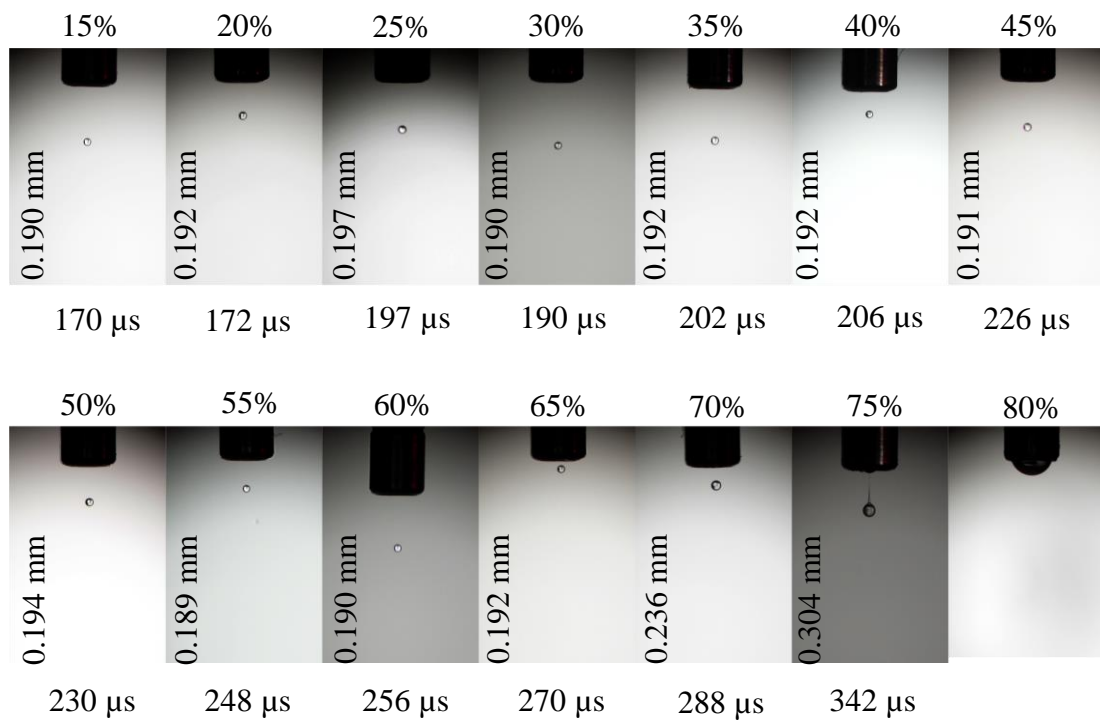


**Figure 70. Practical critical pulse widths for the 0.191 mm nozzle**

The minimum droplet diameter size which could be obtained using the 70 and 75% v/v glycerol solutions were 0.236 mm and 0.304 mm using pulse widths of 288  $\mu$ s and 342  $\mu$ s. At pulse widths lower than 288  $\mu$ s and 342  $\mu$ s, either nozzle wetting occurred or no drop formation took place. For the 80% v/v glycerol solution only

nozzle wetting or no drop formation occurred using lower pulse widths. However at higher pulse widths fluid exited the nozzle but the form of a fluid stream.

The results in Figure 71 also showed that an increase in the % glycerol caused an increase in the practical critical time using a nozzle orifice diameter size 0.254 mm. The droplet diameter size of all the glycerol-water mixtures remained close to that of the nozzle orifice diameter size, except for solutions 65 to 80% v/v glycerol. For solutions 65 and 70% v/v glycerol the minimum droplet diameters which could be obtained were 0.283 mm and 0.323 mm using a pulse width of 278  $\mu$ s and 280  $\mu$ s.

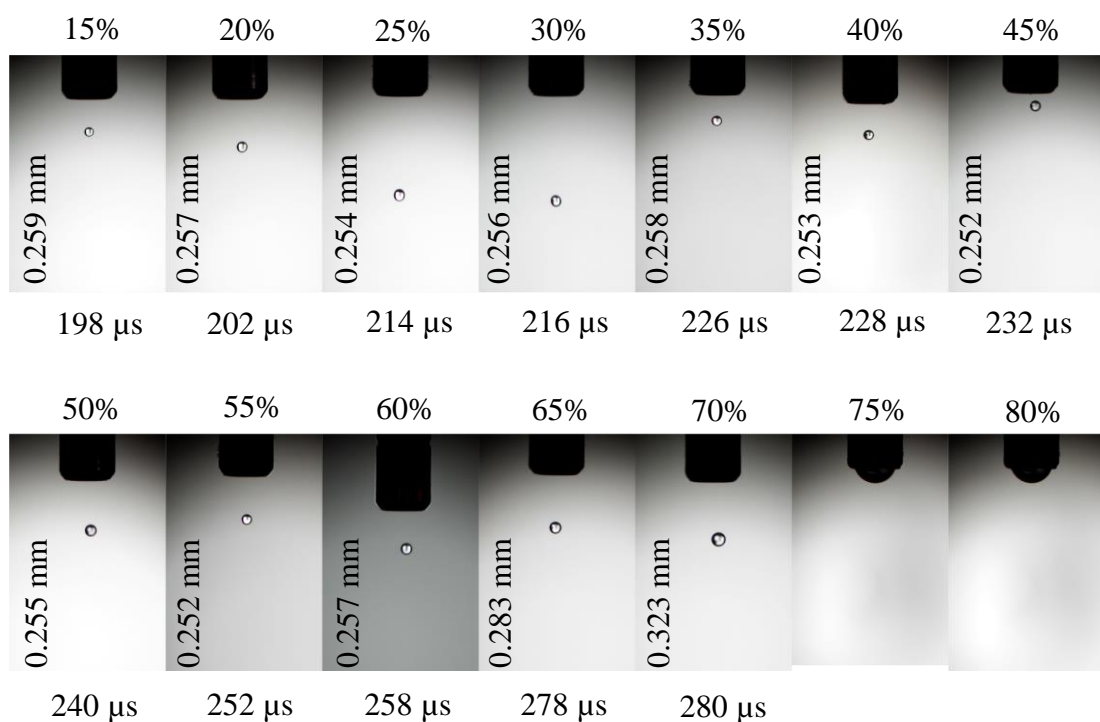


**Figure 71. Practical critical pulse widths for the 0.254 mm nozzle**

At pulse widths lower than 278  $\mu$ s and 280  $\mu$ s, either nozzle wetting occurred or no drop formation took place. For solutions 75 and 80% v/v glycerol only nozzle wetting or no drop formation occurred using lower pulse widths. However at higher pulse widths fluid exited the nozzle but the form of a fluid stream.

The results for all of the practical critical pulse widths, shown in Figure 69 to Figure 71, are summarized in Table 11. It can be seen that the valve inlet pressure is not exactly the same as the desired valve inlet pressure, due to the pressure regulator's pressure regulating error. The droplet size error for each of the glycerol-water solutions and nozzle orifice diameter sizes are shown in Table 11. The droplet size error demonstrated the difference, in percentage, between the droplet diameter size and the nozzle diameter size.

**Table 11. Pulse widths**

% v/v Glycerol (%)	Nozzle orifice size (mm)	Oh number	Desired valve inlet pressure (kPa)	Valve inlet pressure (kPa)	Pulse time ( $\mu$ s)	Droplet diameter (mm)	Droplet size error (%)
15	0.127	0.017	2.1	1.98	158	0.128	0.79
	0.191	0.014	2.2	2.2	170	0.190	0.52
	0.254	0.012	2.24	2.16	198	0.259	1.97
20	0.127	0.019	2.23	2.12	160	0.129	1.57
	0.191	0.016	2.42	2.40	172	0.192	0.52
	0.254	0.014	4.04	4.16	202	0.257	1.18
25	0.127	0.024	2.21	2.19	166	0.124	2.36
	0.191	0.019	2.72	2.75	178	0.197	3.14
	0.254	0.017	6.25	6.13	214	0.254	0
30	0.127	0.025	2.52	2.49	168	0.125	1.57
	0.191	0.021	2.37	2.46	190	0.190	0.52
	0.254	0.018	6.41	6.30	216	0.256	0.79
35	0.127	0.039	4.59	4.48	194	0.127	0
	0.191	0.031	4.52	4.50	202	0.192	0.52
	0.254	0.027	8.54	8.54	226	0.258	1.57
40	0.127	0.043	6.24	6.10	202	0.128	0.79
	0.191	0.035	6.2	6.26	206	0.192	0.52
	0.254	0.03	8.48	8.3	228	0.253	0.39

% v/v Glycerol (%)	Nozzle orifice size (mm)	Oh number	Desired valve inlet pressure (kPa)	Valve inlet pressure (kPa)	Pulse time ( $\mu$ s)	Droplet diameter (mm)	Droplet size error (%)
45	0.127	0.063	8.68	8.83	208	0.126	0.79
	0.191	0.051	8.82	8.80	226	0.191	0
	0.254	0.044	10.87	10.92	232	0.252	0.79
50	0.127	0.08	10.39	10.4	218	0.127	0
	0.191	0.065	10.26	10.18	230	0.194	1.57
	0.254	0.057	12.68	12.75	240	0.255	0.39
55	0.127	0.116	12.25	12.4	228	0.125	1.57
	0.191	0.094	12.42	12.44	248	0.189	1.05
	0.254	0.082	16.32	16.2	252	0.252	0.79
60	0.127	0.154	18.26	18.35	234	0.126	0.79
	0.191	0.125	18.34	18.26	256	0.190	0.52
	0.254	0.109	32.3	32.24	258	0.257	1.18
65	0.127	0.205	26.40	26.29	244	0.13	2.36
	0.191	0.167	28.35	28.28	270	0.192	0.52
	0.254	0.145	48.55	48.59	278	0.283	11.42
70	0.127	0.264	38.2	38.32	250	0.181	42.52
	0.191	0.215	40.48	40.60	288	0.236	23.56
	0.254	0.187	68.2	68.35	280	0.323	27.17
75	0.127	0.579	---	---	---	---	---
	0.191	0.472	112.7	112.12	342	0.304	59.16
	0.254	0.409	---	---	---	---	---
80	0.127	0.769	---	---	---	---	---
	0.191	0.627	---	---	---	---	---
	0.254	0.544	---	---	---	---	---

All of the practical critical times and the Ohnesorge numbers, seen in Table 11, were analysed using CurveExpert. All the droplet diameters with a droplet size error

bigger than 3.14% were not considered in this analysis, as the droplet's diameter was too big compare to the nozzle orifice diameter size. This was done to determine whether the mathematical model of the practical critical times will correlate to that of the theoretical determined critical pressures. The Hoerl model, which mostly fitted the Ohnesorge number vs t critical for all three nozzle orifice diameters in Section 4.5, could not be used for the practical mathematical analysis. This was due to the fact that Hoerl mathematical model did not fit the Ohnesorge number vs practical t critical plot for either of the nozzle orifice diameters. The mathematical model that mostly fitted the plot of the Ohnesorge number vs practical t critical for all three nozzle orifice diameters were the Logistic power model. The Logistic power model curves for each nozzle diameter size are shown in Figure 72, using red, blue and green lines. The mathematical relationship for nozzle orifice diameters 0.127, 0.191 and 0.254 mm can be seen below:

$$y(x) = \frac{273.802}{\left(1 + \left(\frac{x}{0.012}\right)^{-0.714}\right)}$$

$$\therefore t_{critical(0.127)} = \frac{273.802}{\left(1 + \left(\frac{Oh}{0.012}\right)^{-0.714}\right)} \quad \text{Eq. 39}$$

$$y(x) = \frac{385.114}{\left(1 + \left(\frac{x}{0.025}\right)^{-0.438}\right)}$$

$$\therefore t_{critical(0.191)} = \frac{385.114}{\left(1 + \left(\frac{Oh}{0.025}\right)^{-0.438}\right)} \quad \text{Eq. 40}$$

$$y(x) = \frac{308.139}{\left(1 + \left(\frac{x}{0.003}\right)^{-0.446}\right)}$$

$$\therefore t_{critical(0.254)} = \frac{308.139}{\left(1 + \left(\frac{Oh}{0.003}\right)^{-0.446}\right)} \quad \text{Eq. 41}$$

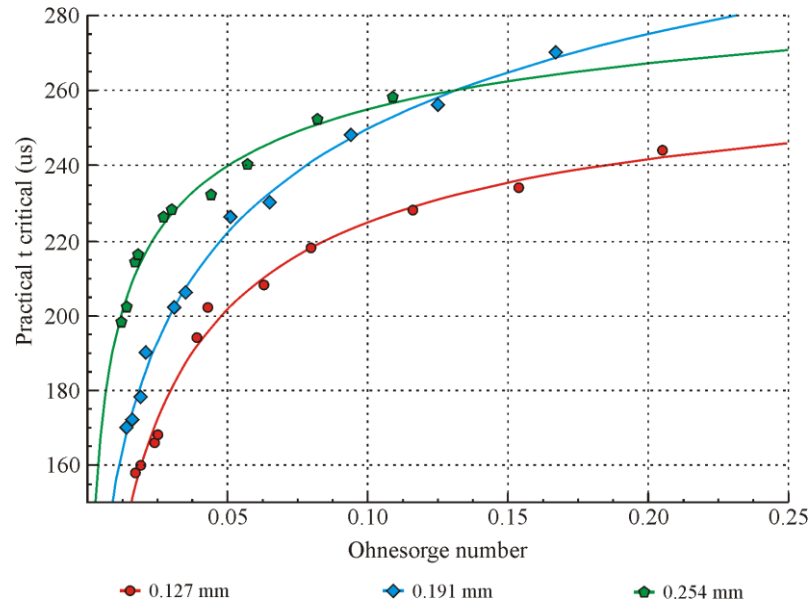


**Figure 72. Ohnesorge number vs. valve pulse time**

## 5.5 Summary

In Chapter 5, it was determined that the theoretical calculated parameters could not be used practically with the RPH. The critical time and pressure, for all of the fluid solutions, were then determined practically using the RPH experimental setup. The practically determined critical pressure and time were plotted and were mathematically analysed in order to determine the mathematical models. The results of the practically determined control parameters were compared against the theoretically determined parameters.

In Chapter 6, the practically determined critical time and pressure equations would be validated using non-glycerol-water mixtures.

## Chapter 6 Validation of results

### 6.1. Introduction

In the previous chapter, mathematical equations were formulated to determine the critical pressure and time for various glycerol-water solutions using nozzle orifice diameter sizes 0.127, 0.191 and 0.254 mm. In this chapter the results of the formulated mathematical equations will be validated in order to determine whether the equations could be used with non-glycerol-water solutions.

### 6.2. Validation of the critical pressure and time formula

In order to determine whether the practical formulated critical pressure and time equations, discussed in Section 5.3 and 5.4.2, could be used for non-glycerol-water solutions, different fluid solutions, shown in Table 12, were used. The 65% glycerol-water solution was used as a reference in order to ensure that the experimental setup and calculated critical pressure and time are the same as the practical results obtained in Chapter 5. The fluid properties for each of the solutions, in Table 12, were determined using the same manner used for the glycerol-water solutions in Table 6.

**Table 12. Different validation fluid solutions with their fluid properties**

Solution	Viscosity (mPa.s)	Density (g/cm <sup>3</sup> )	Surface tension (mN/m)
65% glycerol - water solution (control)	20.35	1.17	66.5
Z Corp binder	1.22	1	33.67
Voxeljet VX 500 binder	2.84	1.12	35.85
Voxeljet VX 1000 binder	12.92	1.13	39.61
40% v/v glycerol - ethanol solution	19.1	1.01	25.59
50% v/v glycerol - ethanol solution	30.02	1.04	26.75
60% v/v glycerol - ethanol solution	76.62	1.1	30.16

### 6.2.1. Practical critical pressure and time calculations

The critical pressure and time for each of the solutions, shown in Table 12, were determined for nozzle diameters 0.127, 0.191 and 0.254 mm, using Equations 36 – 41. The calculations showed that the critical pressure for the 60% v/v glycerol - ethanol solution, using a 0.127 mm nozzle orifice, exceeded the maximum pressure of the RPH. The critical pressure for this solution is shown in Table 13 and is indicated in red. Due to this reason the 60% v/v glycerol - ethanol solution will not be used in the 0.127 mm nozzle orifice diameter validation experiments.

**Table 13. Critical pressure and time for each of the validation fluid solutions using a 0.127 mm nozzle**

Solution	0.127 mm		
	Oh	P <sub>critical</sub> (kPa)	t <sub>critical</sub> (μs)
65% glycerol - water mixture	0.205	26.26	241.888
Z Corp binder	0.019	2.786	158.292
Voxeljet VX 500 binder	0.04	4.561	192.134
Voxeljet VX 1000 binder	0.171	20.943	238.13
40% v/v glycerol - ethanol solution	0.333	50.291	250.472
50% v/v glycerol - ethanol solution	0.505	89.781	256.072
60% v/v glycerol - ethanol solution	1.18	307.373	263.838

It was also determined that the critical pressure for the 60% v/v glycerol - ethanol solution, using a 0.191 mm nozzle orifice, exceeds the maximum pressure of the RPH setup. The critical pressures for this solution is shown in Table 14 and is indicated in red. Due to this reason the 60% v/v glycerol - ethanol solution will also not be used in the 0.191 mm nozzle orifice diameter validation experiments.

The critical pressure calculation also showed that critical pressures for the 50 and 60 % glycerol – ethanol solutions, using nozzle orifice size of 0.254 mm, exceeded the maximum pressure of the RPH setup. The critical pressures for these two solutions are shown in Table 15 and are indicated in red. Owing to this reason the 50 and 60%

v/v glycerol - ethanol solution will not be used in the 0.254 mm nozzle orifice diameter validation experiments.

**Table 14. Critical pressure and time for each of the validation fluid solutions using a 0.191 mm nozzle**

Solution	0.191 mm		
	Oh	P <sub>critical</sub> (kPa)	t <sub>critical</sub> (μs)
65% glycerol - water mixture	0.167	28.213	268.31
Z Corp binder	0.015	2.62	171.693
Voxeljet VX 500 binder	0.032	4.62	203.518
Voxeljet VX 1000 binder	0.14	22.558	261.875
40% v/v glycerol - ethanol solution	0.272	53.169	284.929
50% v/v glycerol - ethanol solution	0.412	92.828	297.817
60% v/v glycerol - ethanol solution	0.963	298.849	320.368

**Table 15. Critical pressure and time for each of the validation fluid solutions using a 0.254 mm nozzle**

Solution	0.254 mm		
	Oh	P <sub>critical</sub> (kPa)	t <sub>critical</sub> (μs)
65% glycerol - water mixture	0.145	45.413	261.694
Z Corp binder	0.013	4.511	203.181
Voxeljet VX 500 binder	0.028	6.991	225.154
Voxeljet VX 1000 binder	0.121	34.9	258.477
40% v/v glycerol - ethanol solution	0.236	99.119	269.638
50% v/v glycerol - ethanol solution	0.357	203.553	275.458
60% v/v glycerol - ethanol solution	0.835	982.959	284.985

### 6.2.2. Validation experimental results

Using the experimental setup as explained in Section 5.2, the practical critical pressures and times of the different solutions were verified. The temperature of all the solutions were kept constant at 20°C throughout all of the experiments. This was done to ensure the solution's properties do not change owing to the change in

temperature. A square wave with a period of 50 ms, an edge time of 5 ns and pulse amplitude of 5 V was supplied to the spike and hold unit by means of a signal generator. The pulse width of the supplied signal and fluid pressure will be equal to that of the practical critical times and pressure given in Table 13 to Table 15. As previously mentioned the 65% glycerol-water solution was used as the reference to compare whether the results that will be obtained in the following experiments correlate to the results in Table 11.

As can be seen in Figure 73, a single droplet was dispensed from all three nozzle orifice sizes using the 65% glycerol-water solution. Using Corel Draw software the different droplet diameters were determined, as explained in Section 5.4.2. The droplet diameter sizes for each of the three droplets are indicated in the figure below. The droplet diameter sizes of these droplets differed from the results obtained in Section 5.4.2. However the difference between the droplet sizes shown in Figure 73 compared to the results shown in Table 11 are still in spec and is considered to be comparable.



**Figure 73. 65% glycerol-water solution**

However as can be seen in Figure 74 to Figure 78, multiple drops were dispensed from each of the three nozzle orifice diameter sizes. Thus the control parameters proved to be wrong for the non-glycerol-water solutions. Satellite drops formed due to long droplet ligaments, the long ligament will break up into a main droplet and satellite drops due to the Rayleigh breakup regime (Tsai and Hwang, 2008).



**Figure 74. Z corp solution**



**Figure 75. VX 500 solution**

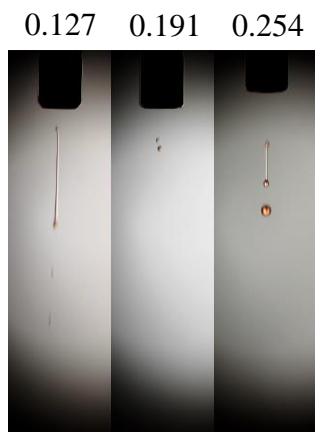


**Figure 76. VX1000 solution**

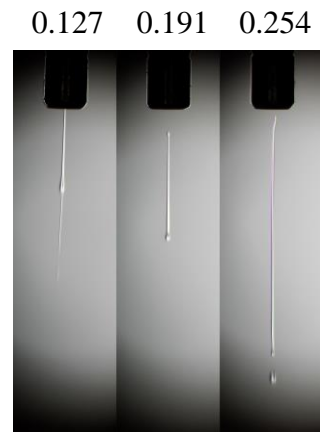


**Figure 77. 40% glycerol - ethanol solution**



**Figure 78. 50% glycerol - ethanol solution**

### 6.3. Plotting of the solutions

In order to further validate the results obtained in Section 6.2.2, a 2D matrix was printed/plotted using the same solutions and control parameters. This was done in order to determine the effect which satellite droplets have on the printing/plotting of the solution. A matrix plotter was used to plot/print all of the solutions. This special plotter was designed by the author; and for clarity the construction is discussed in Annexure D.

#### 6.3.1. XY matrix plotter setup

As mentioned previously, the solutions verified will be plotted to determine the effect which satellite droplets have on the printing/plotting of the solutions. Using the XY matrix plotter the solutions were plotted in a 2D matrix format. The critical time and pressure were adjusted according to the calculated data shown in Table 13 to Table 15. The critical pressure for the different solution – nozzle combinations was adjusted using the PLC which controlled the electronic pressure regulator. Therefore the distance between the droplets, size of the matrix and the critical time for the different solution – nozzle combinations were adjusted using the Cerebot MX4cK™ Board controller. A total of 16 droplets were printed/plotted onto a thin plastic sheet in a 4 x 4 matrix, where the droplets were spaced 2 mm from another. The plot for the reference solution, 65% glycerol-ethanol solution, using all three nozzle orifice sizes can be seen in Figure 79. As seen in the Figure, there were no visible satellite drops and the droplets are nice and neat in circular form.

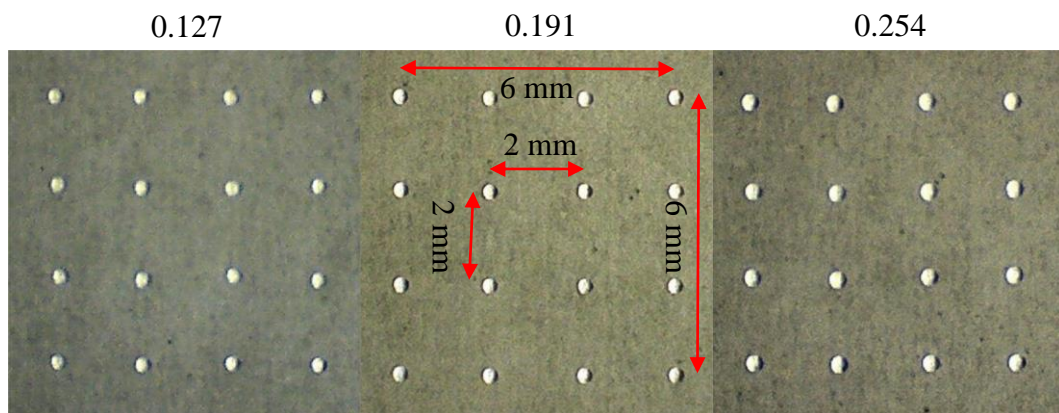
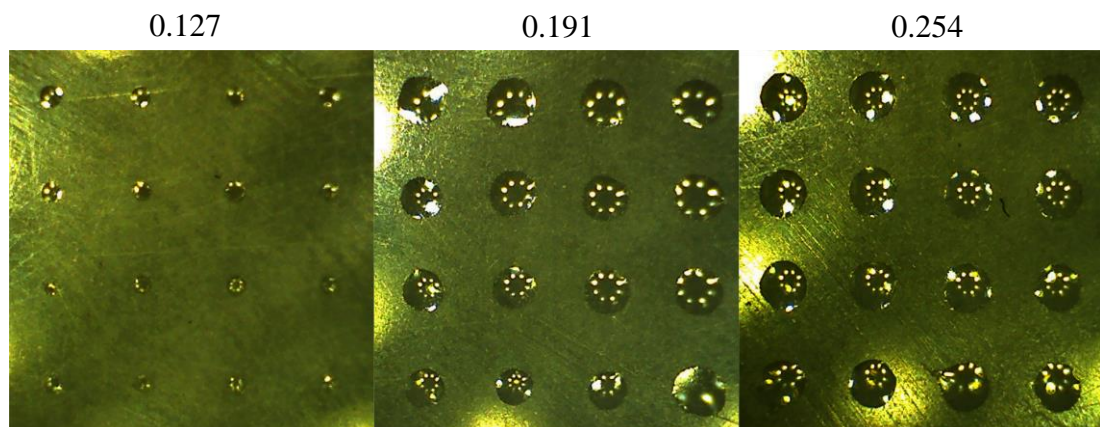


Figure 79. 65% glycerol-ethanol solution 2D plotting results

It was observed that the non-glycerol-water solution droplets proved to be much bigger and that there were signs of satellite drops. However it must also be kept in mind that the wetting angles would differ between the different solutions. It was noticed that the wetting angles for all of the non-glycerol-water solutions were less compared to that of the glycerol-water solution. Owing to this reason the physical drop size on the plastic substrate could not be directly compared to that of the glycerol-ethanol solution's droplets, as the droplets would be more thinly spread across the printing substrate. As can be seen in Figure 80 to Figure 84 most of the satellite drops have the same trajectory as the main droplet. This makes it impossible to detect the satellite droplets as they will merge with the main droplet forming a bigger droplet onto the plastic printing substrate. However when the satellite drops do not have the same trajectory as the main droplet, the satellite drops would be visible around the main droplet. The plotting of the Z corp solution is demonstrated in Figure 80.



**Figure 80. Z corp 2D plotting results**

The plotting of the VX 500 solution are shown in Figure 81. The satellite drops can clearly be seen around the main droplets with the 0.254 mm nozzle.

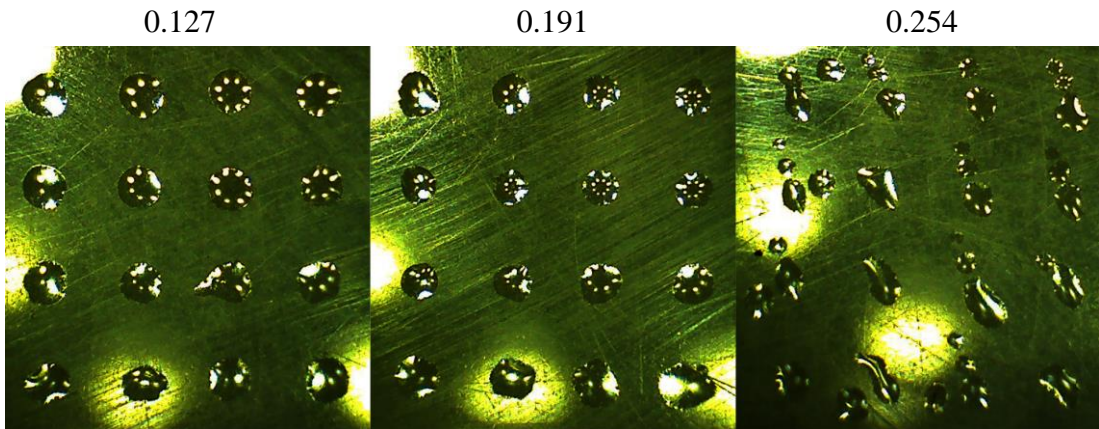


**Figure 81. VX 500 2D plotting results**

The plotting for the VX 1000, 40% glycerol-ethanol and 50% glycerol-ethanol solutions are shown in Figure 82 to Figure 84.

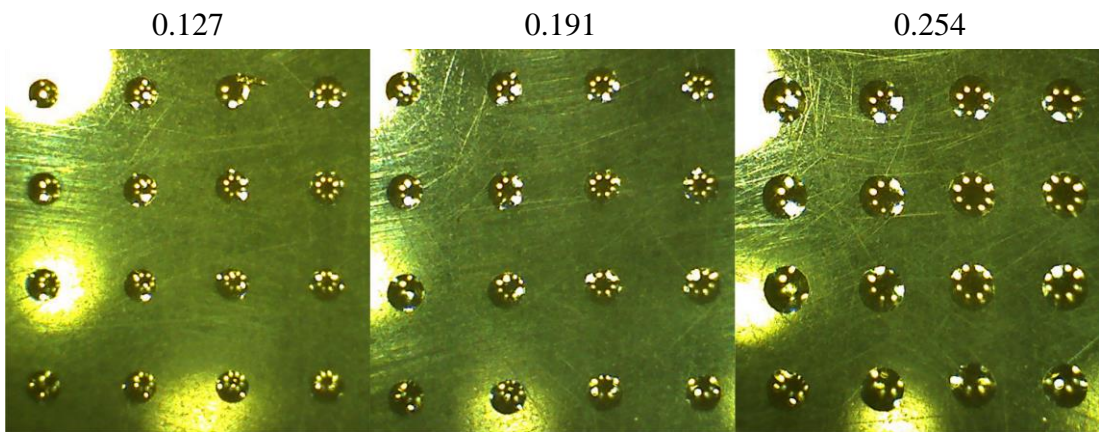


**Figure 82. VX 1000 2D plotting results**

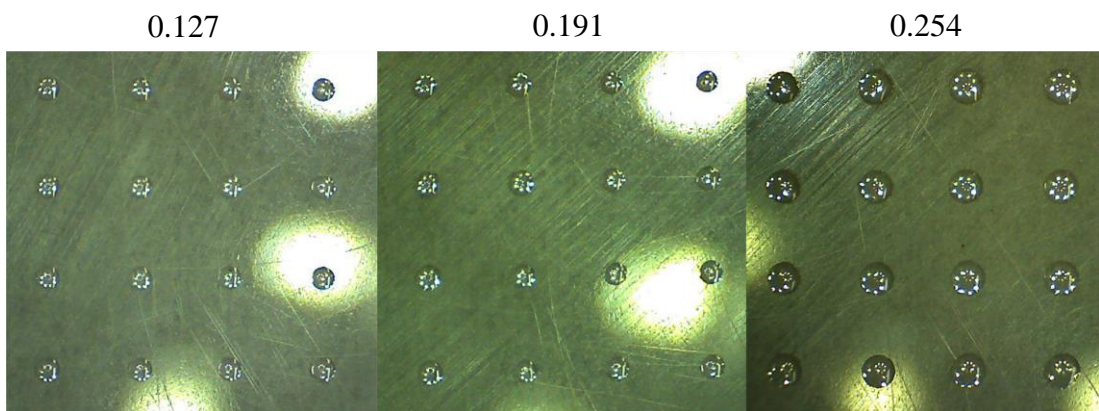


**Figure 83. 40% glycerol-ethanol solution 2D plotting results**

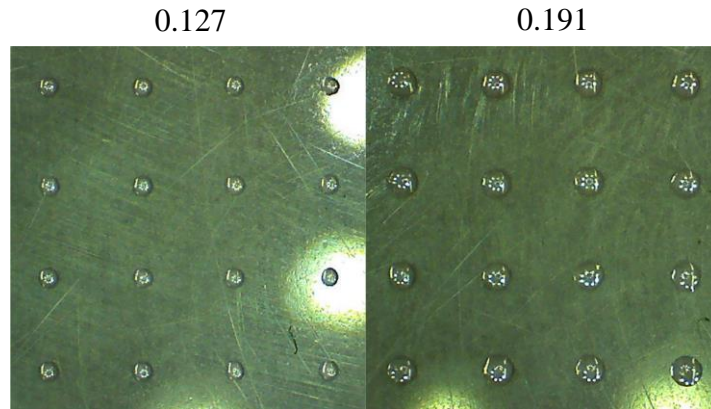


**Figure 84. 50% glycerol-ethanol solution 2D plotting results**

The droplets of the glycerol-water solutions plot showed the droplets to be of the same size and no satellite droplets were visible using the practically formulated formulas to determine the critical pressure and time. It was determined that it would be possible to plot/print with the non-glycerol-water solutions using the practically formulated formulas. However the quality of the print would not be acceptable due to the satellite drops. It would also be very difficult to determine the drop size as the satellite drops will influence the size of the main droplet on the printing substrate. However the effects which the drop size and satellite drops have on the printing quality would not be discussed in this research thesis, as it will form part of a different research topic. Although the practical critical pressure and time formulas obtained in the previous chapter did not work for non-glycerol-water solutions, the methods used to determine the equations could still be used to determine the practical critical pressure and time for non-glycerol-water solutions.

#### **6.4. Summary**

In Chapter 6, the practically determined mathematical models, for the critical time and pressure, were validated using non-glycerol-water solutions. The results showed that the drop formation process was not optimized for the non-glycerol-water solutions, using the practically determined critical time and pressure mathematical models. Multiple droplets were dispensed when using the non-glycerol-water solutions. The different solutions were also plotted in a 2D matrix in order to

determine the effects which the satellite droplets have on the printing/plotting of the non-glycerol-water solutions. It was determined that the practically determined mathematical models could only be used for glycerol-water solutions. However the RPH experimental setup, developed in this research, could be used to determine any solution's control parameters.

Chapter 7 is the final section in this thesis. It will deal with the conclusions and recommendations that evolved from the study of the development of a RPH.

## **Chapter 7                    Conclusions**

### **7.1.    Introduction**

The research to develop a RPH system was carried out and conclusions have been made from the results obtained. The intended objectives were achieved and the recommendations for future research, in the 3D printing field, will also be discussed.

### **7.2.    Conclusions**

#### **7.2.1.    Construction of the RPH experimental setup**

The RPH was designed and constructed, using the solenoid inkjet technology as reference. Three different nozzle orifice sizes were used namely a 0.127, 0.191 and 0.254 mm nozzle orifice diameter. Using the experimental setup, droplets ejected from the VHS valve's nozzle could be photographed in order to be analysed. Fourteen different glycerol-water test solutions were prepared in order to obtain results from solutions with different fluid properties. The fluid properties included the viscosity, density and surface tension of the solution. The % glycerol mixture for each of the glycerol-water solutions were varied in order to obtain different fluid properties for each of the different fluid solutions. The different solutions' fluid properties were determined practically, due to the high error margin when determining theoretically. All of the solutions' fluid temperature was kept constant at 20 °C, as the fluid temperature has an effect of the fluid's properties. The results for the different solutions showed that an increase in the percentage of glycerol in the glycerol mixture caused an increase in the solution's viscosity and density, however a decrease in the surface tension.

#### **7.2.2.    Control parameters**

##### **7.2.2.1.            Theoretically calculated control parameters**

The control parameters of the RPH were theoretically calculated for each of the glycerol-water solutions and nozzle orifice diameter sizes. The control parameter

formulas used were obtained by previous research done. However the research focused more on the piezoelectric printing technology. The control parameters consisted of the critical pressure and time. Both of the critical numbers were calculated using the Weber, Reynolds, Ohnesorge and critical Weber dimensionless numbers. The Ohnesorge number only reflected on the fluid's properties and size of the droplets formed and did not take the driving conditions into consideration. Thus it was decided to compare the Ohnesorge number against the critical time and pressure. The theoretically determined critical pressures showed that an increase in the Ohnesorge number caused an increase in the critical pressure. However it was also determined that the increase in the Ohnesorge number caused an increase in the critical time up to a certain point, where if that point were exceeded the critical time decreased. The Ohnesorge number was plotted against the critical time and pressure for each of the different glycerol-water solutions and nozzle diameter sizes. A statistical analysis was then done on both these graphs for each of the glycerol-water solutions and nozzle orifice diameter sizes to determine their mathematical relationship. It was determined that the model which mostly fitted onto the Ohnesorge number vs. critical pressure plots were the Hyperbolic decline model. Whereby the mathematical model that mostly fitted on the Ohnesorge number vs. critical time plots was the Hoerl model.

#### **7.2.2.2. Practically calculated control parameters**

All of the theoretically calculated critical times varied from 28.73 to 101.1  $\mu$ s. The VHS valve, used in the RPH, would not be able to work at the theoretically calculated critical times, as the pulse widths were much lower than the recommended minimum valve pulse width. The theoretical critical times calculated were mostly used for the piezoelectric inkjet technologies which were able to achieve much lower pulse widths. Thus the control parameters were determined practically for the RPH. The critical pressure and time were determined for each of the different glycerol-water solutions as well as for each nozzle orifice diameter size. The results showed that an increase in the Ohnesorge number caused an increase in the critical time and pressure. All of the practical critical pressures and times were plotted against the Ohnesorge numbers in order to determine whether the mathematical model of the

practical critical pressures would correlate with that of the theoretical determined critical pressures. Although the theoretical critical pressures mathematical model, as well as the hyperbolic decline mathematical model, could be used for the practical critical pressures the slopes between the practical plots differed to that of the theoretical plots. Whereby the Hoerl model, which mostly fitted the theoretically calculated critical time vs. Ohnesorge number plots, could not be used for the practical mathematical analysis. The mathematical model that mostly fitted the practically determined critical time vs. Ohnesorge number plots was the logistic power model.

### **7.2.3. Validation of the control parameters**

In order to determine whether the practical formulated critical pressure and time equations could be used for non-glycerol-water solutions, different non-glycerol-water solutions were used. The practically determined formulas were used to determine the critical pressure and time for these non-glycerol-water solutions. However the results showed that the practically determined critical pressure and time formulas could not be used with non-glycerol-water solutions. When using the practically determined critical pressure and time formulas, the drop formation process, of the non-glycerol-water solutions, was not optimized and satellite droplets occurred. The satellite droplets formed due to the long droplet ligaments. Although the practically determined critical pressure and time did not work for non-glycerol-water solutions, the methods used to determine the control parameters could still be used to determine the practical critical pressure and time for Newtonian non-glycerol-water solutions.

### **7.3. Recommendations**

Investigations into implementation of fluid heaters on the RPH to enable the system to print with higher viscosity fluids should be undertaken as the increase in a fluid's temperature causes the viscosity to decrease.

The method used to determine the practical critical pressure and time should be tested with new binder powder combinations that have not been optimized to work with a certain inkjet technology.

Further research must be done on the VHS valve used in the RPH to determine the VHS's lifetime. As the VHS uses mechanical parts and would fail after a certain number of valve actuations.

The Z axis should be added to the XY plotter construction to test the RPH with different binder powder combinations. However the implementation of the RPH into the complete powder 3D printer can be divided into more than one research study.

Further research must be done using non-Newtonian fluid with the RPH as non-Newtonian fluid's properties are dependent on the shear rate.

#### **7.4. Patent registration**

As mentioned in the contribution of this work, owing to the innovative nature of the project, as well as the multi-, inter- and transdisciplinary approach, it is envisaged that the project will yield more than one patent. No patents have been registered on the RPH, however it is envisaged that future patents will be registered on this work. Especially, when this research would serve as a platform to develop new binder-powder combinations.

## References

AGRAWAL, S.K. (2001) *Fluid mechanics and machinery*. India: Tata McGraw-Hill Publishing.

ARANJO, B., SOORI, P.K. and TALUKDER, P. (2012) Stepper Motor Drives for Robotic Applications. In: *Proceedings of Melaka: Power Engineering and Optimization Conference (PEDCO), Melaka, June 2012*, pp. 361-366.

BABIARZ, A.J. (2006) Jetting Small Dots of High Viscosity Fluids for Packaging Applications. In: *Proceedings of SMTA Pan Pacific conference, Pan Pacific, January 2006*.

BEURER, G. and KRETSCHMER, J. (1997) Function and performance of a shear mode piezo printhead. In: *Proceedings of International Conference on Digital Printing Technologies, Storrs, June 1997*, pp. 621-625.

BUTT, H. and KAPPL, B. (2010) *Surface and Interfacial forces*. Germany: Wiley-VCH verlag GmbH & Co. KGaA Weinheim.

BRUN AHL, J. (2003) *Physics of Piezoelectric Shear Mode Inkjet Actuators*. Stockholm: Kungl Tekniska Hogskolan.

CAGLAR, C. (2009) *Studies of inkjet printing technology with the focus on electric materials*. Finland: Tampere University of Technology.

CHAUDHARY, K.C., REDEKOPP, I.G. and MAXWORTHY, T. (1979) The Non-Linear Capillary Instability of a Liquid Jet. *Journal Fluid Mechanics*, 96(2), pp. 257-312.

CHENG, N.S. (2008) Formation for viscosity of Glycerol-water mixture. *Industrial and Engineering Chemistry Research*. 47, pp. 3285-3288.

CHUA, C.K., LEONG, K.F. and LIM, C.S. (2003) *Rapid prototyping: Principles and Applications 2<sup>nd</sup> ed.* USA: World Scientific Publishing Co. Pte. Ltd.

COTTELEER, M., HOLDOWSKY, J. & MOHTO, M. (2014) The 3D opportunity primer: The basic of additive manufacturing. [in press] *Deloitte University Press*. [Online] Available from: <http://dupress.com/articles/the-3d-opportunity-primer-the-basics-of-additive-manufacturing/> [Accessed: 16/03/2015].

DIEGEL, O. (2012) Verbal communication with Prof Olaf Diegel. Additive Manufacturing (3D Printing) expert. Massey University : New Zealand. February 2012.

GLYNNE-JONES, P., COLETTI, M., WHITE, N.M., GABRIEL, S.B. and BRAMANTI, C. (2010) A feasibility study on using inkjet technology, micropumps, and MEMs as fuel injectors for bipropellant rocket engines. *Acta Astronautic*, 67, pp. 194-203.

HALL, R.F., BERGER, P.D. and COLLINS, H.M. (1995) *Pesticide formations and application systems*. Philadelphia: American society for testing materials.

HEBRA, A.J. (2010) *The Physics of Metrology*. Germany: Springer.

HUTCHINGS, I.M. and MARTIN, G.D. (2012) *Inkjet technology*. United Kingdom: John Wiley & Sons Ltd.

KAMPS, H.J. (2007) *Macro photography photo workshop*. Indiana: Wiley Publishing Inc.

KAZYS, R. and REKUVIENE, R. (2011) Viscosity and density measurement methods for polymer melts. *Ultragarsas*, 66(4), pp. 20-25.

KUMAR, S. and PITYANA, S. [2010] Laser Based Additive Manufacturing of Metal. In: *Proceedings of 2<sup>nd</sup> International Conference of Laser and Plasma Applications, Algeria, February 2010.*

KRUTH, J.P. (1991) Material in-process manufacturing by rapid prototyping technologies. *CIRP Annals*, 40(2), pp. 603-614.

KYSER, E.L. and SEARS, S.B. (1976) Method and apparatus for recording with writing fluids and drop projection means thereof. United States. Available from <http://www.google.com/patents/US3946398> [Accessed 15 September 2014].

LIN, S.P. and REITZ, R.D. (1998) Drop and Spray formation from a Liquid jet. *Annual review of fluid mechanics*, 30, pp. 85-105.

LINDEMANN, T. (2006) *Droplet generation from the nanoliter to the femtoliter range*. Breisgau: Albert Ludwigs University.

LIOU, F.W. (2008) *Rapid prototyping and engineering applications: A toolbox for Prototype Development*. USA: CRC Press.

MAIER, G. (2002) *Operating manual OCA*. Germany: Dataphysics Instruments GmbH.

MASTERJOHN, C. (2005) *Cholesterol's Hydroxyl Group*. [Online] Available from: [http://www.cholesterol-and-health.com/Cholesterol\\_Hydroxyl.html](http://www.cholesterol-and-health.com/Cholesterol_Hydroxyl.html) [Accessed 15/05/2013].

MUNSON, B.R. and YOUNG, D.F. (1998) *Fundamentals of fluid mechanics 3<sup>rd</sup> ed.* Canada: John Wiley & Sons Inc.

NEFZAOU, E. and SKURTYS, O. (2012) Impact of a liquid drop on a granular medium: Inertia, viscosity and surface tension effects on the drop deformation. *Experimental Thermal and Fluid Science*, 41, pp. 43–50.

NEWCOMBE, G. (2009) *Meeting the needs of the Packaging Industry*. Tonejet Ltd.

NIGRO, S. and SMOUSE, E. (1999) *Hewlett-Packard inkjet printing technology: the state of the art*. Canada: Hewlett Packard.

NMB MINEBEA. (2010) *The Permanent Magnet in Motors- Construction and Operating Theory*. [Online] Available from: <http://www.nmbtc.com/step-motors/engineering/construction-and-operating-theory.html> [Accessed: 18/02/2013].

MASTERJOHN, C. (2005) *Cholesterol's Hydroxyl Group*. [Online] Available from: [http://www.cholesterol-and-health.com/Cholesterol\\_Hydroxyl.html](http://www.cholesterol-and-health.com/Cholesterol_Hydroxyl.html) [Accessed 15/05/2013].

OZAETA, J.R. (2008) *Development of a cell depositing system using inkjet technology*. California: California Polytechnic State University.

PAAR, A. (2013) *Measuring the Physical and Chemical Properties of Oil sample*. USA: Anton Paar.

PIMBLEY, W.T. (1984) Drop Formation from a Liquid Jet: A Linear One-Dimensional Analysis Considered as a Boundary Value Problem. *IBM Journal*, 29, pp.148-156.

PHAM, D.T. and GAULT, R.S. (1998) A comparison of rapid prototyping technologies. *International Journal of Machine Tools & Manufacturing*, 38(10-11), pp. 1257-1287.

RAMIN, E. (2010) *Automated design of trabecular structures*. England: Loughborough University.

RAPID MANUFACTURING ASSOCIATION. (2011) *AM Technologies*. [Online]. Available from: <http://www.ciri.org.nz/nzrma/technologies.html>. Accessed: 16/05/2012.

REIS, N., AINSELY, C. and DERBY, B. (2005) Inkjet delivery of particle suspensions by piezo-electric droplet ejectors. *Journal of Applied Physics*, 97.

RONCHI, C., BEUKERS, R., HEINZ, H., HIERAUT, J.P. and SELFSLANG, R. (1992) Graphite Melting Under Laser Heating. *International Journal of Thermophysics*, 13(1), pp. 116-129.

THE LEE CORPORATION. (2008) *VHS 25+ Nanoliter Dispensing Valves*. [Online] Available from: [http://www.theleeco.com/\\_\\_85256B740051C08B.nsf/0/495B9554AC723C4D85256783006A1F83?Open&Highlight=0,INKX0511400A](http://www.theleeco.com/__85256B740051C08B.nsf/0/495B9554AC723C4D85256783006A1F83?Open&Highlight=0,INKX0511400A). Accessed: 30/04/2013.

THE LEE CORPORATION. (2008) *Lee Micro-Dispense Nozzles*. [Online] Available from: [http://www.theleeco.com/\\_\\_85256B180052B667.nsf/0/7A969BFD7099CCBD85257322006EAE3E?Open&Highlight=0,nozzles](http://www.theleeco.com/__85256B180052B667.nsf/0/7A969BFD7099CCBD85257322006EAE3E?Open&Highlight=0,nozzles). Accessed: 30/04/2013.

TROY, D.B. (2006) *Remington: The science and Practice of Pharmacy*. USA: Lippincott William & Wilkins.

TSAI, M. and HWANG, W. (2008) Effects of Pulse Voltage on the roplet Formation of Alcohol and Ethylene Glycol in a Piezoelectric Inkjet Printing Process which Bipolar Pulse. *Material Transactions*, 49(2), pp. 331–338.

VISWANATH, D.S., GHOSH, T.K., PRASAD, D.H.L., DUTT, N.V.K and RANI, K.Y. (2007) *Viscosity of liquids: Theory, Estimation, Experiment, and data*. The Netherlands: Springer.

VOWELL, S. (2009) *Microfluidics: The Effects of Surface Tension*. USA: University of Washington.

WEI, J. (2007) *Product engineering Molecular structure and properties*. New York: Oxford University Press Inc.

WESTERHOF, N., STERGIOPULOS, N. and NOBLE, M.I.M. (2010) *Snapshots of Hemodynamics*. New York: Springer.

WHITE, F.M. (1999) *Fluid mechanics 4<sup>th</sup> ed.* USA: McGraw-Hill Science.

## **Bibliography**

AHN, D., KWEON, J., CHOI, J. and LEE, S. (2012) Quantification of surface roughness of parts processed by laminated object manufacturing. *Journal of Materials Processing Technology*, 212(2), pp. 339-346.

BARTOLO, P.J. (2011) *Stereolithography: Materials, Processes and applications*. London: Springer.

BERDAN, B. (2012) *Macrophotography: tools, tips and techniques for digital photography*. Canada: Canadiannaturephotographer.

CAGLAR, C. (2009) *Studies of inkjet printing technology with the focus on electric materials*. Finland: Tampere University of Technology.

DECKARD, C. (1986) *Method and apparatus for producing parts by selective sintering*. United States. Available from: <http://www.google.com/patents/US4863538> [Accessed: January 2015].

DOLENC, A. and MAKELA, I. (1994) Slicing procedures for layer manufacturing techniques. *Computer-Aided Design*, 26(11), pp. 119-126.

ENDO, I., SATO, Y., SAITO, S., NAGAIRI, T. and OHNO, S. (1979) *Liquid jet recording process and apparatus*. Great Britain. Available from: <http://www.google.tl/patents/CA1127227A1?cl=en> [Accessed 7 December 2013].

GIBSON, I., ROSEN, D.W. and STUCKER, B. (2010) *Additive Manufacturing Technologies: Rapid Prototyping to Direct Digital Manufacturing*. New York, USA: Springer.

HYDROMOTION. (2007) *Technology page*. [Online]. Available from: <http://www.hydrmotion.com/tech.html> [Accessed: 6/11/2012].

ION, J.C. (2005) *Laser Processing of engineering materials: Principles, procedure and industrial applications*. Oxford, UK: Elsevier Butterworth-Heinemann.

KIPPHAN, H. (2004) *Handbook of Print Media*. New York: Springer.

LE, H.P. (1998) Progress and trends in ink-jet printing technology. *Journal of Imaging Science and Technology*, 42, pp. 49-62.

MAKALESEN. (1988) *Apparatus and method employing phase charge ink*. United States. Available from: <http://www.google.tl/patents/US4742364> [Accessed: 18 October 2012].

PALM, W. (1998) *Rapid prototyping Primer*. [Online]. Available from: <http://www.me.psu.edu/lamancusa/rapidpro/primer/Chapter2.htm> [Accessed: 10/04/2012].

PAREDES, X., PENSADO, A., COMUNAS, M.J.P. and FERNANDEZ, J. (2010) How Pressure Affects the Dynamic Viscosities of Two Poly (propylene glycol) Dimethyl Ether Lubricants. *J. Chemistry Engineering Data*, 55(9), pp. 4088-4094.

WICKS, Z.W., JONES, F.N., PAPPAS, S.P and WICKS, D.A. (2007) *Organic coatings Science and technology third edition*. New Jersey: John Wiley & Sons Inc.

YAN, X. and GU, P. (1996) A review of rapid prototyping technologies and systems. *Computer-Aided Design*, 28(4), pp. 307-318.

YOUNG, D.F., MUSON, B.R., OKIISHI, T.H. and HUEBSCH, W.W. (2010) *A brief introduction to fluid mechanics 5<sup>th</sup> ed*. USA: John Wiley & Sons.

## Annexure A

```
#include "pressure_monitor.h"
#include <lcd-flex.c>

void main()
{

int i;
float pdiff;

float value1;
float Pressure1;
float a1;
float b1;
float c1;
float d1;
float error1 = 0;
float sumpressure1;
float pressure1avg;
float voltagessum1;
float voltage1;

float value2;
float Pressure2;
float a2;
float b2;
float c2;
float d2;
float error2 = 0;
float sumpressure2 = 0;
float pressure2avg;
float voltagessum2;
float voltage2;

setup_adc_ports(sAN1|sAN11|VSS_VREF);
setup_adc(ADC_CLOCK_DIV_64);
setup_spi(SPI_SS_DISABLED);
setup_timer_0(RTCC_INTERNAL|RTCC_DIV_1);
setup_timer_1(T1_DISABLED);
setup_timer_2(T2_DISABLED,0,1);
setup_comparator(NC_NC_NC_NC);// This device COMP currently not supported by the PICWizard
lcd_init();
delay_ms(1000);

input_a();
input_b();
input_c();

Error1 = 0;
Error2 = 0;

value1 = 0;
value2 = 0;

while (1){

//////////////////// zero pressure 1 via button press //////////////////////

if (input(PIN_C7)) // Test if P1 button is pressed
{
Error1 = voltage1 - 0.2; // Determine error through formula (P=0)
printf(LCD_PUTC, "\f P1 zeroed"); // Display on Text on LCD
while (input(PIN_C7) == 1) // Button de bounce
{
}
}
}
```

## Annexure A cont.

```
/////////////////////////////////////////////////////////////////
///////////////////////////////////////////////////////////////// zero pressure 2 via button press ///////////////////////////////////////////////////////////////////

if (input(PIN_B4))          // Test if P2 button is pressed
{
  Error2 = voltage2 - 0.2;    // Determine error through formula (P=0)
  printf(LCD_PUTC, "f P2 zeroed"); // Display on Text on LCD
  while (input(PIN_C7) == 1) // Button de bounce
  {
  }
}

/////////////////////////////////////////////////////////////////

/////////////////////////////////////////////////////////////////Reset variables/////////////////////////////////////////////////////////////////

pressure1 = 0;
pressure2 = 0;

voltage1 = 0;
voltage2 = 0;

sumpressure1 = 0;
pressure1avg = 0;

sumpressure2 = 0;
pressure2avg = 0;

/////////////////////////////////////////////////////////////////Determine pressures/////////////////////////////////////////////////////////////////

for (i=1;i<=250;++i)      // Determine average over 250 samples
{

  set_adc_channel(3);      // Set AD channel Pressure sensor 1
  delay_us(100);           // 100us Delay
  value1 = read_adc();     // Read AD input
  delay_us(100);           // 100us Delay

  a1 = (float)value1/511.5; // Determine AD input voltage
  voltagesum1 = voltagesum1 + a1;
  b1 = a1 - Error1;        // Error compensation
  c1 = (float)b1/5;        // Pressure formula
  d1 = c1 - 0.04;          // Pressure formula
  pressure1 = (float) d1/0.0012858; // Pressure formula
  sumpressure1 = sumpressure1 + pressure1; // Determine P1 pressure average

  ///////////////////////////////////////////////////////////////////

  set_adc_channel(11);     // Set AD channel Pressure sensor 2
  delay_us(100);           // 100us Delay
  value2 = read_adc();     // Read AD input
  delay_us(100);           // 100us Delay

  a2 = (float)value2/511.5; // Determine AD input voltage
  voltagesum2 = voltagesum2 + a2;
  b2 = a2 - Error2;        // Error compensation
  c2 = (float)b2/5;        // Pressure formula
  d2 = c2 - 0.04;          // Pressure formula
  pressure2 = (float) d2/0.0012858; // Pressure formula
  sumpressure2 = sumpressure2 + pressure2; // Determine P2 pressure average
}

}
```

## Annexure A cont.

```
pressure1avg = (float) sumpressure1 / 250; // Determine average pressure for P1
pressure2avg = (float) sumpressure2 / 250; // Determine average pressure for P2
voltage1 = (float) voltagesum1 / 250;
voltage2 = (float) voltagesum2 / 250;

/////////////////////////////////////////////////////////////////

/////////////////////////////////////////////////////////////////Prepare data for display/////////////////////////////////////////////////////////////////

if (pressure2avg < pressure1avg)
    pdiff = pressure2avg - pressure1avg;

if (pressure1avg < pressure2avg)
    pdiff = pressure1avg - pressure2avg;

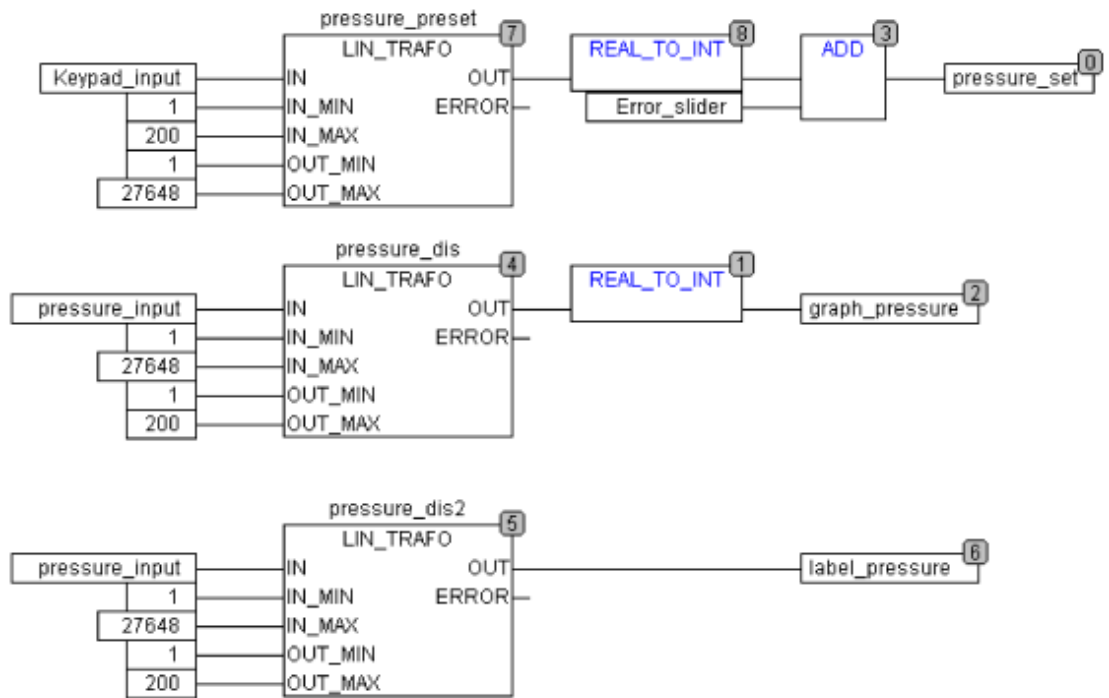
if (pressure2avg == pressure1avg)
    pdiff = 0;

printf(LCD_PUTC, "\\f%f %f", pressure1avg, pressure2avg);
printf(LCD_PUTC, "\\ndP = %fkPa", pdiff);
delay_ms(1000);

}

}
```

## Annexure B



## Annexure C

```
#include "flash trigger.h"
#include <lcd-flex.c>

#define Button_down    PIN_A0
#define Button_up     PIN_A1
#define Button_test   PIN_A2
#define Trigger_out   PIN_A3
#define Trigger_in    PIN_B0

int count = 3; // initial delay count (3us delay on opto coupler)
long d_var = 500; //debounce delay

//////////////////////////////////flash trigger//////////////////////////////////
void trigger_flash()
{
    output_high(Trigger_out);
    delay_ms(500);
    output_low(Trigger_out);
}

//////////////////////////////////Update lcd//////////////////////////////////
void Update_lcd()
{
    lcd_putc("\fDelay time us:");
    printf(lcd_putc, "\n%u ", count);
}

//////////////////////////////////increment delay//////////////////////////////////
void Up()
{
    {
        if (count >= 200)
        {
            break;
        }
        else{
            count = count + 1;
            Update_lcd();
            delay_ms(d_var);
        }
    }
}

//////////////////////////////////decrement delay//////////////////////////////////
void down()
{
    {
        if (count <= 3)
    }
```

## Annexure C cont.

```
{
    break;
}
else{
    count = count - 1;
    Update_lcd();
    delay_ms(d_var);
}
}

////////////////////////////////interrupt routine////////////////////////////////
#int_EXT
void EXT_isr(void)
{
    delay_us(count-3);
    trigger_flash();
    lcd_putc("\fTriggered press");
    lcd_putc("\ntest to reset");

    while (!(input(Button_test)))
    {
    }
    clear_interrupt(INT_EXT);
    delay_ms(500);
    Update_lcd();
    return;
    while (1){

    }
}
void main()
{
    setup_adc_ports(NO_ANALOGS|VSS_VDD);
    setup_adc(ADC_CLOCK_DIV_2|ADC_TAD_MUL_0);
    setup_spi(SPI_SS_DISABLED);
    setup_wdt(WDT_OFF);
    setup_timer_0(RTCC_INTERNAL);
    setup_timer_1(T1_DISABLED);
    setup_timer_2(T2_DISABLED,0,1);
    setup_ccp1(CCP_OFF);
    setup_comparator(NC_NC_NC_NC);
    setup_vref(FALSE);
    enable_interrupts(GLOBAL);
    enable_interrupts(INT_EXT);
    ext_int_edge( H_TO_L );
```

## Annexure C cont.

```
lcd_init();

delay_ms(100);
Update_lcd();

while(1){
if (input(Button_up))
{Up();
}
if (input(Button_down))
{Down();
}
if (input(Button_test))
{lcd_putc("\fTest");
trigger_flash();
Update_lcd();
delay_ms(d_var);
}
}
}
```

## Annexure D

### XY matrix plotter construction

The RPH system was installed and integrated into an XY table, which enabled the print head to move either in the X or the Y direction. A droplet was dispensed at multiple predefined X-Y coordinates. All of the XY table's components were initially assembled in Solid works CAD software and can be seen in Figure 85. Although many of the components were off the rack components, a lot of parts had to be designed and manufactured.

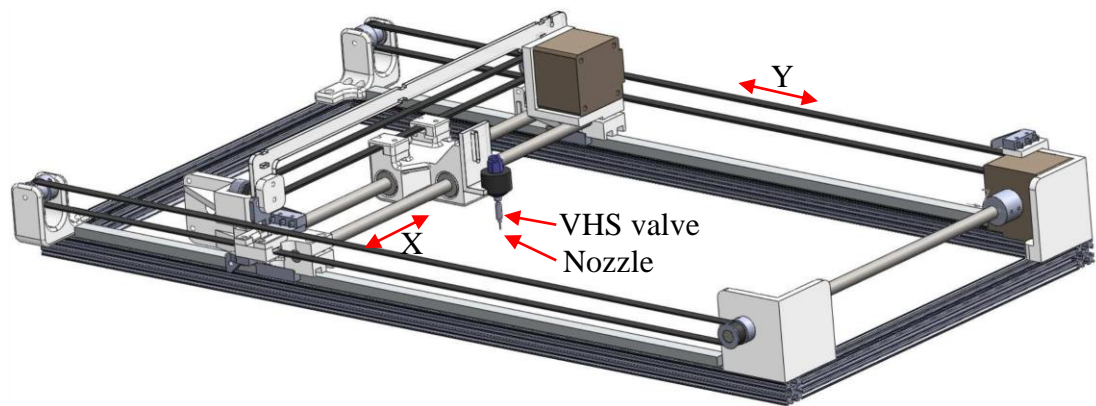


Figure 85. Isometric view of XY table

The XY table was designed in such a way that it could be used as a 3D printer by adding a Z axis. A photo of the complete XY table, with the integrated RPH, can be seen in Figure 86. The main components of the XY table were:

- OpenBeam bars
- Stepper motors
- Electronical components (Stepper driver and Cerebot MX4ck™ board)
- Linear guide rails, shafts and bearings
- ABS parts
- Timing belt pulleys and belts

## Annexure D cont.

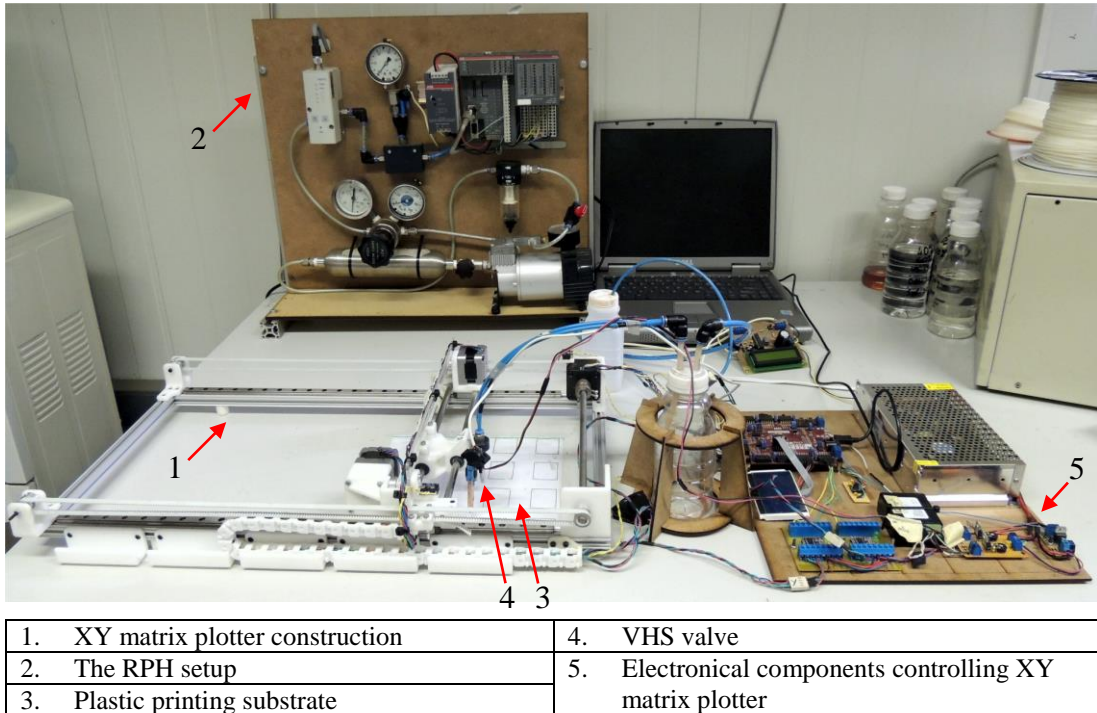


Figure 86. The XY table with the RPH system

All of the components mentioned above will be addressed below:

### OpenBeam bars

OpenBeam bars, shown in Figure 87, are 15 x 15 mm extruded aluminum bars, which are commonly used in industry for rapidly prototyping and building of machinery.



Figure 87. OpenBeam bars

## **Annexure D cont.**

One major advantage of the OpenBeam bar is it requires standard hardware components instead of proprietary and expensive fasteners. Each of the 4 slots is designed to capture a regular M3 bolt and nut. The time taken for the design and construction of the XY table was dramatically shortened by using OpenBeam bars.

### **Stepper motors**

A stepper motor is a digital electromechanical device that uses electrical impulses to move a rotor. The rotor can be moved by a discrete angle, also called a step angle. The rotor is linked to a shaft, which can then be connected to the required application (gears, wheels, etc.). Stepper motors are normally used in applications that require precise movements. The step angle of a stepper motor will depend on its specifications (type and model). At a step angle of  $1.8^\circ$  it will require the stepper motor to make 200 steps for 1 revolution ( $360^\circ$ ). Stepper motors offer the following advantages: high reliability, low cost, high torque at low speeds and simple construction that operates in almost every environment (Aranjo, Soori and Talukder, 2012).

The stepper motors used in the XY table were the hybrid type; the hybrid stepper motor consists of the combined characteristics of the Permanent Magnet (PM) and Variable Reluctance (VR) stepper motors. The hybrid stepper provides the best performance with respect to speed, torque and step resolution. The main components of the hybrid stepper motor are a multi-toothed rotor, which is axially magnetized, and a multi-toothed stator. The rotor is split in two halves, one end that is polarized south and the other north. The multi-teeth stator and rotor are aligned in various configurations during rotation. When current flows through the stator coils it will cause a magnetic field that will attract or repel the magnetic teeth on the rotor (NMB Minebea, 2010). This will enable the rotor to turn. A cross-sectional side view of a hybrid stepper motor is seen in Figure 88. The stepper motors were used to accurately control the X and Y movements.

## Annexure D cont.

### Electronical components

In order to move the VHS valve to certain pre-defined coordinates to dispense a droplet, the stepper motor and VHS valve had to be controlled using the following electronical components:

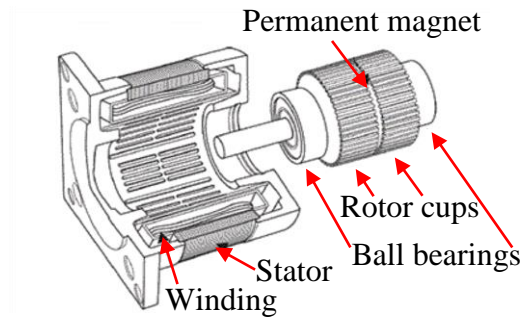


Figure 88. Hybrid stepper motor

### Stepper driver

The DRV8825 stepper driver breakout board, seen in Figure 89, was used to drive the stepper motors in the XY table.

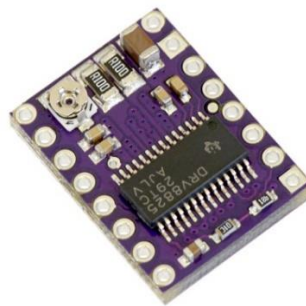


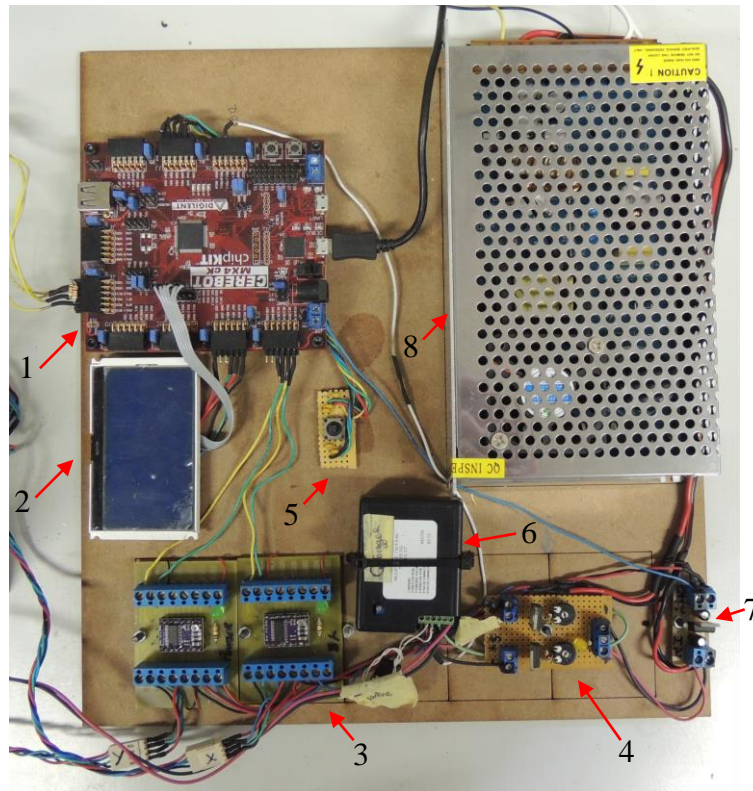
Figure 89. DRV8825 stepper driver

The driver board has the following features: adjustable current limiting, over current protection, a wide operating voltage, different micro step resolutions and has a compact design. Using the stepper driver break out board saved a lot of time on the design and assembly of the control circuitry. All the stepper motors used in the XY table were configured to the  $\frac{1}{32}$  step mode which resulted in a step angle of  $0.05625^\circ$ . By enabling micro-stepping the stepper motor's torque increased.

## Annexure D cont.

### Cerebot MX4cK™ board, graphical LCD and joystick

The Cerebot MX4cK™ board was used control the stepper drivers and spike and hold. The Cerebot MX4cK™ Board is a microcontroller development board based on the Microchip PIC32MX460F512L chip. The PIC32MX460F512L is a member of the 32 bit microcontroller family. The Cerebot MX4cK™ board is designed for embedded control and robotics control applications as well as general microcontroller experimentation. The development board comprises of 74 I/O pins that supports a number of peripheral functions, such as USB, UART, SPI, I<sup>2</sup>C, PWM and interrupt pins. A graphical LCD and joystick were used to serve as an interface between the development board and the user. A photo of the development board with the graphical LCD and joystick can be seen in Figure 90.



1. Cerebot MX4cK™ board	5. Joystick
2. Graphical LCD	6. Spike and hold unit
3. Stepper driver	7. Stepper driver 5V PSU
4. Spike and hold PSU	8. 12V 20A PSU

Figure 90. Electrical components for XY plotter

## **Annexure D cont.**

Using the joystick the following parameters could be adjusted:

- X and Y matrix size (number of points)
- Distance between points
- Valve pulse time

The size of the matrix could be adjusted in the x and y directions. The distance between the matrix points could also be adjusted in 0.1 increments. The valve pulse time was adjusted according to the results of the mathematical equation. The firmware was written in Microchip's XC 32 compiler.

### **Linear guide rails, shafts and bearings**

In the XY table design, two linear guide rails were used for the X axis and two linear shafts with Drylin linear bearings for the Y axis. A sample of the two bearings can be seen in Figure 91.

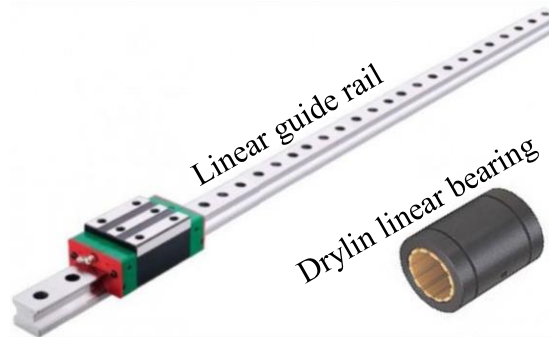


**Figure 91. Linear guide rail**

### **ABS parts**

All of the ABS parts were designed using Solid Works CAD program. The designed parts were then printed in the Idea 2 Product Lab, based at the Vaal University of Technology, using an UP plus FDM printer. All of the parts were printed with a layer thickness of 0.15 mm. All of the ABS printed parts can be seen in Figure 92.

## Annexure D cont.

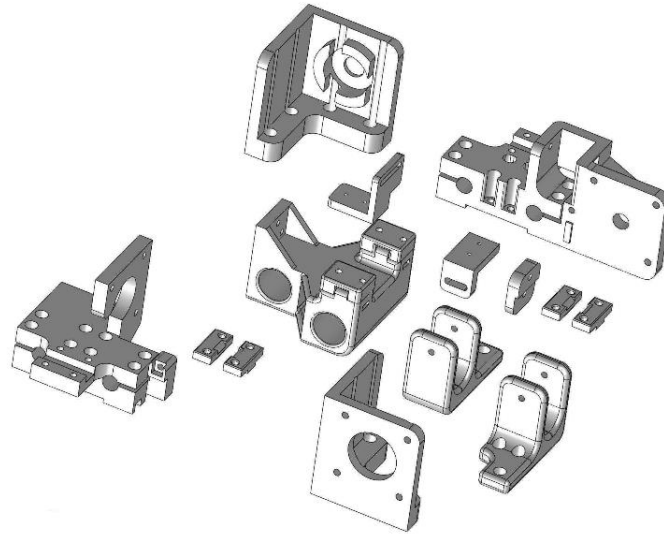


Figure 92. ABS printed parts

### Timing belt pulleys and belts

In order to obtain an accurate X-Y component movement, a timing belt and pulleys were used. T 2.5 timing belt and pulleys were used in this 3D printer chassis; the belt and pulley had a pitch of 2.5 mm. The timing pulley is connected to the stepper motor shaft. In order to calculate the distance (in mm) which the X-Y components will travel for 1 stepper motor step the following equation can be used:

$$x,y_{(\text{distance})} = \frac{\pi\theta d_{\text{pulley}}}{360} \quad \text{Eq. 42}$$

Where:

$x,y_{(\text{distance})}$   $\equiv$  x or y axis movement for 1 step (mm)

$d_{\text{pulley}}$   $\equiv$  Belt pulley diameter (mm)

$\theta$   $\equiv$  Stepper step angle ( ° )

The following calculation was done to determine the x and y movement for 1 step ( $\theta = 0.056^\circ$ , stepper pulley belt diameter = 12.3 mm):

**Annexure D cont.**

$$\begin{aligned} X, Y_{(\text{distance})} &= \frac{\pi \theta d_{\text{pulley}}}{360} \\ X, Y_{(\text{distance})} &= \frac{\pi(0.056)(12.3)}{360} \\ X, Y_{(\text{distance})} &= 0.006 \text{ mm} \end{aligned} \qquad \text{Eq. 43}$$